

FOUNDED 1977

DOE/BC/10841-15
(DE90000230)

**MODELING AND OPTIMIZING SURFACTANT STRUCTURE TO
IMPROVE OIL RECOVERY BY CHEMICAL FLOODING
AT THE UNIVERSITY OF TEXAS -- FINAL REPORT**

October 1987-September 1988

By
R. S. Schechter

April 1990

Performed Under Contract No. AC19-85BC10841

The University of Texas
Austin, Texas



**Bartlesville Project Office
U. S. DEPARTMENT OF ENERGY
Bartlesville, Oklahoma**

This report has been reproduced directly from the best available copy.

Available to DOE and DOE contractors from the Office Of Scientific and Technical Information, P.O. Box 62, Oak Ridge, TN 37831; prices available from (615)576-8401, FTS 626-8401.

Available to the public from the National Technical Information Service, U.S. Department of Commerce, 5285 Port Royal Rd., Springfield, VA 22161

Price: Printed A06
Microfiche A01

**MODELING AND OPTIMIZING SURFACTANT STRUCTURE TO
IMPROVE OIL RECOVERY BY CHEMICAL FLOODING
AT THE UNIVERSITY OF TEXAS**

**Final Report
October 1987-September 1988**

**By
R. S. Schechter**

April 1990

Work Performed Under Contract No. AC19-85BC10841

**Prepared for
U.S. Department of Energy
Assistant Secretary for Fossil Energy**

**Jerry F. Casteel, Project Manager
Bartlesville Project Office
P.O. Box 1398
Bartlesville, OK 74005**

**Prepared by
The University of Texas
Department of Engineering
Austin, TX 78712**

1998-1999

The following information is provided for the year ending 31/12/98. The figures are in thousands of dollars unless otherwise stated. The figures are unaudited and should be read in conjunction with the audited financial statements for the year ending 31/12/98.

The following table shows the results of operations for the year ending 31/12/98. The results are as follows:

Particulars	1998	1997
Revenue	1,234,567	1,123,456
Cost of sales	(567,890)	(543,210)
Gross profit	666,677	580,246
Operating expenses	(234,567)	(210,987)
Operating profit	432,110	369,259
Finance income	12,345	10,987
Finance expense	(8,765)	(7,654)
Profit before tax	435,690	372,592
Income tax	(12,345)	(10,987)
Profit after tax	423,345	361,605

The following table shows the financial position at the end of the year ending 31/12/98. The figures are in thousands of dollars unless otherwise stated. The figures are unaudited and should be read in conjunction with the audited financial statements for the year ending 31/12/98.

Particulars	1998	1997
Assets	1,234,567	1,123,456
Liabilities	(567,890)	(543,210)
Equity	666,677	580,246

The following table shows the cash flows for the year ending 31/12/98. The figures are in thousands of dollars unless otherwise stated. The figures are unaudited and should be read in conjunction with the audited financial statements for the year ending 31/12/98.

Particulars	1998	1997
Operating activities	123,456	110,987
Investing activities	(45,678)	(40,123)
Financing activities	(32,109)	(28,765)
Net change in cash	45,678	42,109

LIST OF CONTENTS

	Page
EXECUTIVE SUMMARY	1
DISCUSSION OF RESEARCH	4
A. Surfactant Adsorption	4
Introduction	4
Review of the Theory	5
Scope of Experimental Work	8
Original Experimental Procedure	8
Revised Experimental Procedure	10
Data Analysis	13
Results	15
Description of Modeling Procedure	16
Future Work	19
References	19
B. Thermodynamics of Solubilization	36
Theory	36
Results of Experimental Studies	43
References	50
C. The Permittivity of Microemulsions	61
Morphology of Microemulsions: A Very Brief Review	65
Results	68
Proposed Model	70
Conclusions	75
References	76
D. Microemulsion Structure: The Role of Alcohols	93
Tracer Diffusion and Partitioning of Components	94

Determination of Aggregation Number of DTAB Micelles Based on Electrical Conductivity and Degree of Micellar Dissociation	96
Results	97
Discussion	99
Conclusions	103
References	105

LIST OF TABLES

B.1	Parameter Values in Model Calculations for Alkyl Sulfates at 25°C	51
B.2	Values of $m_{S_{int}}^o - m_S^o$ (in kT) for the SDS Cases Studied	52
C.1	C_ℓ for Multiple Theory	79
C.2	Factors Inducing Type I to Type II Transition AOT/Water/Hydrocarbon Systems	80

LIST OF FIGURES

A.1	Sodium dodecyl sulfonate in NaCl at 30°C: surface charge density versus pH	21
A.2	Sodium dodecyl sulfonate in NaCl at 30°C: adsorption density versus pH	22
A.3	Sodium dodecyl sulfonate in NaCl at 30°C: equilibrium concentration versus pH	23
A.4	Sodium dodecyl sulfonate in NaCl at 30°C: zeta potential versus pH	24
A.5	Continuous potentiometric titration of TiO ₂ in aqueous NaCl solutions at 30°C: experimentally determined points	25
A.6	Continuous potentiometric titration of TiO ₂ in aqueous NaCl solutions at 30°C: lines calculated from CSBM parameters	26

A.7	Results of regression analysis for $C_{12}SO_3Na/30^\circ C/0.001$ M NaCl data set: measured points and corresponding points calculated from Eq. [A.8]	27
A.8	Results of regression analysis for $C_{12}SO_3Na/30^\circ C/0.001$ M NaCl data set: adsorption density as a function of C_{eq} at constant pH as calculated from Eq. [A.8]	28
A.9	Simulation of adsorption with $pK_S = pK_{Cl}$ and $\omega = 0$	29
A.10	Simulation of adsorption with $pK_S = (1 + pK_{Cl})$ and $\omega = 0$	30
A.11	Simulation of adsorption with $pK_S = (2 + pK_{Cl})$ and $\omega = 0$	31
A.12	Simulation of adsorption with $pK_S = (3 + pK_{Cl})$ and $\omega = 0$	32
A.13	Simulation of adsorption with $pK_S = (4 + pK_{Cl})$ and $\omega = 0$	33
A.14	Simulation of adsorption with $pK_S = pK_{Cl}$ and $\omega = 1.15$ kT*n with $n = 12$	34
A.15	Simulation of adsorption with $pK_S = (1 + pK_{Cl})$ and $\omega = 1.15$ kT*n with $n = 12$	35
B.1	Model of aggregate with solubilize core	53
B.2	Variation in solubility of alkanes with SDS concentration in micellar SDS solutions containing no added NaCl; \square = hexane, \blacklozenge = octane, \blacksquare = decane. Dashed lines indicate expected solubilities of SDS concentration and alkane solubility were linearly related	54
B.3	Variation in solubility of alkanes with SDS concentration in micellar SDS solutions containing 0.2 M NaCl; \square = hexane, \blacklozenge = octane, \blacksquare = decane	55
B.4	Variation in solubilize mole fraction of hexane with SDS concentration at 25°C. Solid lines refer to model predictions with $\mu_{S_{int}}^0 - \mu_S^0 = 0.18$ kT for the no-NaCl case and 0.14 kT for the 0.2 M NaCl case	56

B.5	Variation in solubilize mole fraction of octane with SDS concentration at 25°C. Solid lines refer to model predictions with $\mu_{S_{int}}^0 - \mu_S^0 = 0.28$ kT for the no-NaCl case and 0.20 kT for the 0.2 M NaCl case	57
B.6	Variation in solubilize mole fraction of decane with SDS concentration at 25°C. Solid lines refer to model predictions with $\mu_{S_{int}}^0 - \mu_S^0 = 0.32$ kT for the no-NaCl case and 0.22 kT for the 0.2 M NaCl case	58
B.7	Predicted variation in radius of solubilize core with SDS concentration for hexane solubilization at 25°C	59
B.8	Predicted variation in mole fraction of solubilize in interfacial region with SDS concentration for hexane solubilization at 25°C	60
C.1	Ratio of the dielectric constant of a suspension of conducting spheres to the dielectric constant of the continuous-phase versus disperse-phase volume fraction. van Dijk data for AOT/isooctane/water solutions at 35°C; $W_s = 25$, from Ref. C.13	81
C.2	Winsor phase diagrams showing the inversion zone (shaded area) and the conductivity percolation threshold (solid line)	82
C.3	Phase diagram for AOT/water/alkane systems showing the effect of the alkane carbon number on the boundary between the one and two-phase regions	83
C.4	The maximum water-to-AOT molar ratio (W_s^*) in a series of alkanes; ACN = 6 to ACN = 12	84
C.5	Dielectric constant versus volume fraction of water-plus-AOT for octane, decane, and undecane solutions at 25°C; $W_s = 25$ and $f_w = 0.536 \phi_d$	85
C.6a	Dielectric constant and conductivity versus temperature of AOT/water/decane solutions at 25°C; $\phi_d = 0.0781$ and $W_s = 24.7$. Note: the dielectric constants at 49 and 52°C are experimental artifacts and not the true values	86
C.6b	Permittivity versus frequency of AOT/water/decane solutions at 25°C; $\phi_w = 0.0781$ and $W_s = 24.7$	87

C.7	Diffusion coefficient of radioactively-tagged benzene sulfonate ion AOT/water/alkane solutions versus volume fraction of water-plus-AOT solutions at 25°C; $W_s = 25$ and $\phi_w = 0.536 \phi_d$	88
C.8a	Illustration of an oil-continuous domain (A) and a water-continuous domain (B) having the same compositions	89
C.8b	Model of microemulsion 25% water-continuous domains in a continuum of oil-continuous domains	90
C.9	Fraction of domains that are water continuous (β) versus volume fraction of water as determined from the model for the AOT/water/alkane experiment reported in Fig. C.5	91
C.10	Fraction of domains that are water continuous (β) versus temperature as determined from the model for the AOT/water/decane system reported in Fig. C.6a	92
D.1	Effect of solubilizates on electrical conductivity	106
D.2	Effect of solubilizates on viscosity	107
D.3	Effect of solubilizates on tracer diffusion coefficients	108
D.4	Change in micellar partitioning of phenol	109
D.5	Effect of solubilizates on the surfactant aggregation number	110
D.6	Calculated volumes of micellar core using two different methods; \square = calculated from aggregation number and known volume per surfactant and \blacklozenge = calculated from known surfactant tail length, assuming spherical shape	111

EXECUTIVE SUMMARY

Objectives of the Research Program

The objectives of this research program are (1) to characterize mineral oxide surfaces and to relate these parameters to surfactant adsorption, (2) to study chromatographic effects resulting from use of surfactant blends, (3) to understand the properties of microemulsions as they relate to surfactant structure, and (4) to develop a thermodynamic theory of microemulsions which includes surfactant structure, cosolvents, and surfactant blends as well as the properties of the system oil and water.

Abstract/Summary

Adsorption

Adsorption of surfactant from aqueous solutions is a complex function of a relatively large set of variables including the solution pH, electrolyte composition, temperature, and surfactant concentration as well as the surface characteristics of the mineral and surfactant molecular structure. Because of this complexity, one cannot hope to optimize a micellar system for enhanced oil recovery without the aid of an accurate model tying together all of the significant variables. It is the development of an adsorption theory that now occupies our attention. A model surface, titanium dioxide, has been selected for our initial studies. A particular sample of TiO_2 has been extensively studied (surface titration, ESCA, electrophoretic mobility, and electronmicroscopy) and is being used as a model system for comparison with predictions. The parameters describing naturally occurring minerals (clays, silica, etc.) will be incorporated into the theory once the titanium dioxide system is adequately modeled.

This year we have completed collecting a comprehensive suite of adsorption data for two surfactants--decyl and dodecyl sodium sulfonate. Isotherms over a wide range of pH, sodium chloride concentrations, and temperature are now

available. In addition, zeta potentials have been measured under conditions closely matching those which prevailed at points along the isotherm. These data taken together with those obtained in previous years will be used to test various theories including the one that we have proposed. Because of the range and diversity of the data available, it should be possible to distinguish between valid and invalid models.

The essence of our proposed model is also briefly described in this report and some preliminary calculations are reported. The results presented are merely for the purpose of demonstrating the trends that are anticipated. The best values of the parameters are yet to be determined and a comparison yet to be performed.

Thermodynamics of Solubilization

It is our contention that to properly optimize the surfactant system for micellar/polymer flooding, one must be able to model the influence of surfactant structure on adsorption, phase behavior, and interfacial tension. The modeling of phase behavior will require delineation of the number of phases which form and the microstructure of the surfactant-rich phases. This microstructure can vary over a wide range of possible configurations including oil drops in water forming an isotropic microemulsion phase to complex liquid crystalline phases which are highly viscous and certainly, therefore, undesirable. It seems to be a rather consistent observation that surfactants which exhibit high solvency and isotropic microemulsion phases at optimum often yield undesirable phase behavior over large portions of the phase diagram. Because of our need to understand both the structure of microemulsions and to delineate regions of undesirable behavior, thermodynamic modeling is crucial.

The free energy required to assemble a water-continuous microemulsion starting with molecularly-dispersed surfactant and excess solubilizate molecules is examined in some detail. The factors considered include the hydrophobic effect,

the free energy associated with mixing the surfactant's lipophile with solubilize molecules, the electrostatic free energy, and the free energy associated with the water-hydrocarbon contact area. When all of these contributions are considered simultaneously, then the shapes of the individual swollen micelles, the total solubilization surfactant monomer concentration (CMC) in equilibrium with the swollen micelles, can all be determined by minimizing the total free energy. The predictions of the theory have been confirmed by measuring the solubilization of hexane, octane, and decane in aqueous micellar solutions composed of sodium dodecyl sulfonate in various concentrations mixed with sodium chloride. The theory was found to fit moderately well when the activity of the counterions associated with the surfactant molecules was taken into account. To reconcile all of the experimental observations, it was found necessary to increase the free energy of that portion of the solubilize residing within the interfacial region. This was justified because the configuration of solubilize molecules in the interfacial region is constrained.

The Permittivity of Microemulsions

One probe that can be used to study the microstructure of a microemulsion is its dielectric properties. This measurement is complementary to the electrical conductivity of a microemulsion in the sense that the dielectric properties are only meaningful when the microemulsion is essentially nonconducting so that, depending on the microstructure, either the electrical conductivity or the dielectric constant will be instructive. The region of overlap is small.

To explain the unusual dielectric properties of microemulsions, a model which represents a microemulsion as a mosaic of water and oil-continuous regions has been adopted. Since the dielectric constant of an electrolyte solution (conductor) is infinite (zero frequency limit), then it is the proportion of water-continuous regions which contribute to make the dielectric constant of a

microemulsion large--much larger than that of a collection of mercury drops at the same volume fraction water as the microemulsion. There are two essential conclusions that stem from this work. The dielectric constant or its companion, the electrical conductivity, taken alone without any other measurements cannot define the state of a microemulsion. Two microemulsions can have the same dielectric constant but different water contents and visa versa.

The permittivity of a microemulsion is, however, very much related to the underlying phase behavior and measurement of both the water content and the dielectric constant does define the state of a microemulsion.

Microemulsion Structure: The Role of Alcohols

Alcohols are generally used in micellar solutions together with other surfactants to improve the phase behavior; that is, to reduce the tendency for liquid crystals to form and to adjust the optimum salinity of the surfactant system to match the one required by reservoir conditions. To further elucidate the mechanisms of surfactant-alcohol interaction, the partitioning of alcohol between an aqueous and a micellar phase has been studied and the specific sites at which alcohols bind to micelles considered. Until a stoichiometric ratio of one alcohol per surfactant in the micelle is reached, alcohols tend to bind exclusively within the palisade layer. Once all of these sites are filled, alcohols then appear to bind to the surface of micelles rather than partition into the interior.

DISCUSSION OF RESEARCH

A. Surfactant Adsorption

Introduction

This report contains the following: (1) a review of the theory of surfactant adsorption under development; (2) an outline of the scope of this investigation; (3) a description of the original and current experimental procedure and a discussion of the reasons for changing it; (4) a description of the method of data

analysis; (5) a set of typical experimental results, together with a description of results still to be obtained; (6) a brief outline of the modeling procedure, together with some preliminary results illustrating its use; (7) an outline of goals for the next period.

Review of the Theory

The basis of the theory of surfactant adsorption under development is the Complexation Site-Binding Model (CSBM) that has been widely accepted as a suitable description of the electrical double layer at the metal oxide/aqueous solution interface (see Refs. A.1 to A.6). The CSBM treats amphoteric sites on the surface as if they were chemical species in solution, "reacting" or complexing, with potential-determining and indifferent electrolyte ions subject to equilibrium constants. The constants are derived from potentiometric titration data from which surface charge density as a function of pH is determined for a range of electrolyte concentrations.

These constants are used in conjunction with a model of the double layer to characterize the behavior of the interface in aqueous solution. The double layer is modeled as three planes separated by layers of constant capacitance:

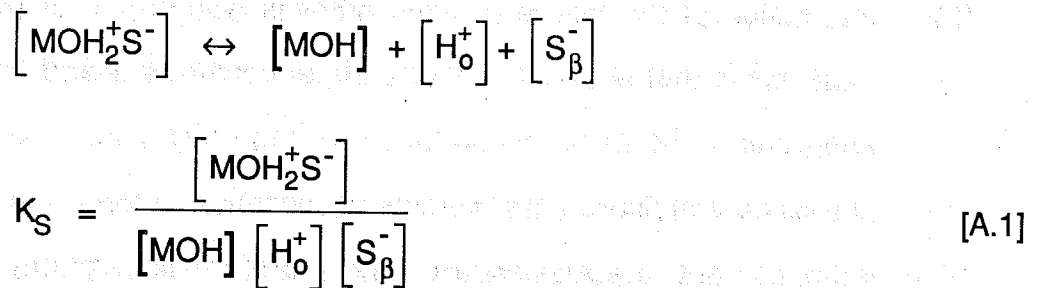
- (1) The surface (σ) plane where potential-determining ions are adsorbed.
- (2) The inner Helmholtz (β) plane where complexed indifferent ions are adsorbed.
- (3) The outer Helmholtz (d) plane where the diffuse layer begins.

Knowledge of the equilibrium constants, together with the values of the capacitances of the two layers (that in the CSBM are adjustable parameters), permits calculation of charge densities and potentials at all three planes as a function of pH and electrolyte concentration. The potential at the diffuse layer is assumed to be the same value derived from zeta-potential measurements.

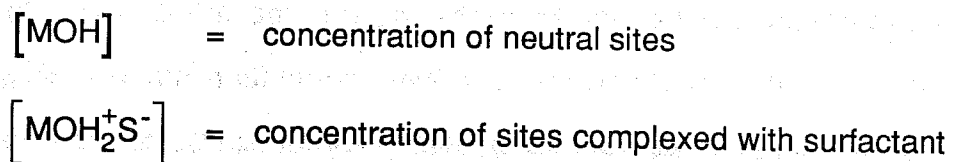
The CSBM is written mathematically as a set of 13 nonlinear equations with six parameters: four equilibrium constants and two capacitances. Due to their nonlinearity, the theoretical equations are not trivial to solve; but a computer program has been developed that, given a set of model parameters, solves the equations for all unknown values including charge densities, potentials, and site-type distribution.

To determine the correct values of the site-binding model parameters, the nonlinear equation solver is embedded in an optimization routine. This routine systematically changes values of the equilibrium constants subject to a set of specified constraints. The CSBM equations are then solved using those constants. The calculated values are compared with the experimentally determined values of surface charge density as a function of pH and salt concentration. The ultimate goal of the routine is to minimize the difference between the experimentally determined and theoretically calculated values.

To account for adsorption of surfactant, a new "reaction" is introduced to the model: the complexation of a surfactant molecule with a site on the surface subject to a complexation equilibrium constant (K_S):



where



$$= \frac{\text{adsorption density } (\Gamma_S)}{\frac{\text{surface area}}{\text{unit volume}}}$$

$$[H_o^+] = [H_{\text{bulk}}^+] \exp\left(\frac{-e\psi_o}{kT}\right)$$

$$[S_{\beta}^-] = [C_{\text{eq}}] \exp\left(\frac{+e\psi_{\beta}}{kT}\right) \exp\left(\frac{\omega\theta}{kT}\right)$$

with

$$\theta = \frac{\Gamma_S}{\Gamma_{\text{monolayer}}}$$

The special nature of the surfactant, namely the hydrophobic effect, is accounted for in two ways:

- (1) Interaction of the tail with the surface is accounted for through values of the equilibrium constant (K_S) that are greater than those for anions without hydrophobic moiety. The greater value means that surfactant ions are preferentially complexed at positive sites over other anions present in solution.
- (2) Interaction of the tails with each other is accounted for through the term $\exp(\omega\theta/kT)$ that is a function of surface coverage θ and lateral interaction energy ω of the tails. As surface coverage increases, the term increases; and since it multiplies the complex concentration term, the net effect is the enhancement of complexation (and therefore adsorption) with increasing surface coverage.

When surfactant is introduced to the system, the model expands to 17 nonlinear equations with 17 unknowns. The key assumption made is that the equilibrium constants determined for the system without surfactant do not change when surfactant is present. The only adjustable parameters to be determined in this

case are K_S and ω . The criteria used in determining the best values of these parameters in this case are the experimentally determined values of surface charge density, equilibrium surfactant concentration, and adsorption density.

Scope of Experimental Work

The ultimate goal of the experimental aspect of this investigation is to obtain an internally consistent set of data for each system under study that contains the following information: (1) surfactant bulk and surface concentration, (2) pH, (3) background electrolyte concentration, (4) surface charge density, and (5) zeta potential when possible.

The systems under investigation are summarized below.

Solid. Anatase form of titanium dioxide.

Surfactants. Sodium dodecyl and sodium decyl sulfonate at concentrations up to the solubility limit or the CMC, depending on the Krafft temperature of the system being studied.

Background Electrolyte. Sodium chloride at solution concentrations of 0.001, 0.01, and 0.1 M.

Temperature. 30° and 40°C.

Original Experimental Procedure

In the 1986-87 DOE Annual Report, hysteresis in the adsorption versus pH curves at pH values where the surface charge is neutral or negative was reported. This hysteresis was attributed to possible differences between adsorption and desorption kinetics. The focus of effort in the first part of this year was on determining the viability of fast potentiometric titration of TiO_2 in the presence of surfactant.

Under the conditions of fast titration, equilibrium with respect to pH is reached from 5 to 30 minutes after the addition of acid or base; but if adsorption or desorption equilibrium does not occur within that window, in time, fast titration is not

a viable technique. If, however, the titration were performed slowly enough that the hysteresis is eliminated, this would be an indication that true equilibrium with respect to adsorption had been reached.

Potentiometric titration was, therefore, performed with stability of surfactant activity rather than pH, the criterion for equilibrium. Under these conditions, up to three or four hours per individual point was required to reach equilibrium with respect to adsorption. Hysteresis was indeed eliminated but at the expense of efficiency. Under these conditions, a typical titration sequence would require three days rather than one day to complete. This extension in required time causes several problems:

- (1) Both the pH and surfactant-selective electrode calibrations drift with time. Their reliability after 12 to 15 hours continuously in solution is suspect. Unfortunately, recalibration requires removal of the probes from the sample with inevitable loss of the material clinging to the probes. A significant loss of solid and solution can be incurred over the course of the titration.
- (2) As humidified nitrogen is circulated through the system to prevent CO₂ contamination of the solution, some evaporation of the solution occurs. Over the course of three days, this loss, too, may become significant.
- (3) The observed behavior of metal oxides depends on whether fast or slow titration is performed.

Because of these problems, we decided that the method of slow continuous titration in the presence of surfactant was impractical for our purposes. The obvious alternative is a batchwise method in which a different sample is used for each individual point. In addition to avoiding problems with calibration drift and loss of material, this method does have the clear advantage of enabling us to make electrophoretic mobility measurements with the same particles for which pH and adsorption measurements are made. The surfactant-selective electrode is still

used to determine surfactant activity in solution but may be recalibrated as necessary throughout the measurement sequence. Surface charge density is the only parameter we have much difficulty measuring. The calculation depends on knowledge of pH both before and after addition of acid, base, or salt. Without detrimentally disturbing the sample, we cannot measure initial pH for each point; so, we instead used an average of pH values for samples to which no acid, base, or salt had been added. Details of the calculation method are described in the Data Analysis section.

Revised Experimental Procedure

The batchwise experimental procedure used to obtain data reported here is described below.

Solid Preparation. The titanium dioxide powder is dried at 110°C for one hour (nominal) and cooled in a desiccator. The sodium alkyl sulfonates and ultra-high-purity NaCl are used as received.

Solution Preparation. Surfactant solutions are prepared from distilled, deionized, degassed (DDD) water to minimize contamination from dissolved CO₂.

Suspension Sample Preparation. Approximately 44 g of surfactant solution is weighed into a clean, dry 50 ml-capacity polycarbonate centrifuge tube. To adjust the pH of the solution, the required amount of 0.1 M HCl or NaOH is added to the sample using an automatic burette. Approximately 1.32 g TiO₂ are weighed into the tube so that the final surface area/volume ratio is 1641 m²/liter. The tube is shaken vigorously by hand to disperse the solid in solution. The suspension is placed in a constant-temperature bath set at the desired temperature. For each surfactant/salt concentration combination, samples are made up so that the approximate range of equilibrium pH is between 3.5 and 7.

Electrode Assembly Description. The electrode assembly consists of the following probes: a reference electrode, a hydrogen ion-sensitive electrode, a

surfactant-sensitive electrode, a platinum resistance temperature compensation probe, and a Teflon stirrer. All probes fit into a polyethylene cap that clamps with an airtight seal onto the glass titration vessel containing the solution to be monitored. The stirrer is powered by a motor attached to the Teflon rotor.

pH Electrode Calibration. The reference electrode is a double-junction electrode. The inner filling solution is 3 M KCl. The outer filling solution is a NaCl solution at the same background NaCl concentration as that of the surfactant solution in the sample to be measured. The electrodes are calibrated at room temperature using manufacturer-supplied buffer solutions at pH = 4.0 and pH = 7.0. Temperature compensation for pH measurement at other temperatures is programmed into the microprocessor in the pH meter.

Surfactant-Selective Electrode Calibration. Surfactant activity is measured as a potential drop between the surfactant-selective electrode and the reference electrode. The measurement in mV is recorded at the same time the pH measurement is recorded.

The surfactant-selective electrode is calibrated by measuring the electrode response in solutions of known surfactant activity. A linear relationship has been found to exist between the logarithm of the surfactant activity and the response of the electrode.

In a typical measurement sequence, electrode response to the sample is first measured followed by response to two calibration solutions at concentrations that are expected to bracket that of the sample. Response to the next one or two samples in the sequence is measured; then the response to appropriate calibration solutions is measured. Surfactant activity of each sample is calculated from the calibration line given by the two bracketing calibration points. In this way, calibration errors due to slow drift of electrode response with time are minimized.

Sample Treatment. The suspensions are shaken vigorously by hand three times during the treatment process: at 0 hours elapsed time, at 18 hours (nominal) elapsed time, and at 42 hours (nominal) elapsed time from initial make-up of the sample.

After the nominal 42-hour period, the samples are centrifuged to reduce the solids content of the liquid and returned to the temperature bath. The pH and surfactant activity are then measured as described below.

Enough solid particles are redispersed in the solution to permit measurement of the electrophoretic mobility of the particles. The supernatant is then decanted from the remaining solid into a titration vessel.

The electrode assembly is placed on the titration vessel, that is then put back into the temperature bath. When the temperature of the solution in the vessel reaches equilibrium temperature, the pH and mV response of the surfactant-selective electrode is recorded.

Electrophoretic mobility measurements are limited to values of ionic strength less than about 0.01 M (at higher salt concentrations, Joule heating of the solution becomes a problem). For those samples for which measurement is possible, the following procedure is used.

The electrode assembly is removed from the solution and the titration vessel is capped. Using a disposable pipette, solution is withdrawn from the sample and put into the electrophoretic mobility cell. This solution is removed from the cell using a tube attached to an aspirator. This process is repeated again to wash out traces of DDD water used to rinse the cell between samples. Finally, a sample is put in the cell for measurement and blackened platinum electrodes are placed in the cell.

An electric field is imposed by applying a potential drop between the platinum electrodes. The migration of the particles is observed through a

laser-illuminated microscope. The velocity is recorded as a function of the potential drop across the cell. For each sample, measurements are conducted at potential drops varying from 30 to 80 volts across the cell.

Data Analysis

Activity Coefficient Calculation. Both the pH and surfactant selective electrodes measure the activity of an ion rather than its concentration. In order to calculate concentration, the activity coefficient for each ion is needed. Activity coefficients for H^+ , OH^- , and surfactant ions are calculated using the extended Debye-Hückel formula (Stumm and Morgan):^(A.7)

$$\log f_i = -Az_i^2 \frac{\sqrt{I}}{1 + Ba\sqrt{I}} \quad [A.2]$$

where

f_i = activity coefficient of ion i

I = ionic strength of solution

$$= 0.5 \sum_{i=0}^n C_i z_i^2$$

$$= 0.5(C_{Na}^{+1} + C_{Cl}^{-1} + C_S^{-1} + C_{Na(\text{surfactant counterion})}^{+1} + C_H^{+1} + C_{OH}^{-1})$$

z_i = magnitude of charge on ion i

$$A = 1.82 \cdot 10^6 (\epsilon T)^{-3/2}$$

$$B = 50.3 (\epsilon T)^{-1/2}$$

ϵ = dielectric constant

T = absolute temperature

a = ion-size parameter

The ion-size parameter is an adjustable parameter corresponding to the size of the ion in angstroms. For H^+ and OH^- , values of a as a function of temperature are

available in the literature (Kielland),^(A.8) but for surfactant ions, they must be estimated. Kielland notes that, according to Brüll,^(A.9) "the ion-size parameter may be regarded as the effective diameter of the hydrated ion." Given the ionic conductance (λ) of an ion in solution, the effective diameter may be calculated from Stokes's law and the ionic frictional coefficient (f) as follows:

$$f = \frac{|z|eF}{\lambda} \quad [A.3]$$

where

$$\begin{aligned} e &= \text{elementary charge} \\ &= 1.60219 \cdot 10^{-19} \text{ C} \end{aligned}$$

$$\begin{aligned} F &= \text{Faraday's constant} \\ &= 96,484.6 \text{ C mol}^{-1} \end{aligned}$$

$$\begin{aligned} \lambda &= \text{ionic conductance} \\ [&=] \Omega^{-1} \text{cm}^2 \text{mol}^{-1} \end{aligned}$$

According to Stokes's Law,

$$f = 6\pi\eta r \quad [A.4]$$

where

$$\eta = \text{viscosity of bulk solution}$$

$$[&=] \text{mNsm}^{-2}$$

$$r = \text{hydrated radius of ion}$$

An expression for r is obtained by equating these expressions for f and rearranging

$$r = \frac{|z|eF}{6\pi\eta\lambda} \quad [A.5]$$

Inserting the constants with the units as shown above results in

$$r = 82.0107 \frac{|z|}{\eta\lambda} \quad [\text{A.6}]$$

[=] Å

Using the values of λ for alkyl sulfonates that are available in the literature (Lange's Handbook of Chemistry),^(A.10) the following ion-size parameters were calculated:

Sodium decyl sulfonate:

$$30^{\circ}\text{C}: a = 7.88 \text{ \AA}$$

$$40^{\circ}\text{C}: a = 9.55 \text{ \AA}$$

Sodium dodecyl sulfonate:

$$30^{\circ}\text{C}: a = 8.54 \text{ \AA}$$

$$40^{\circ}\text{C}: a = 10.34 \text{ \AA}$$

Results

Typical results for sodium dodecyl sulfonate at 30°C in NaCl with initial surfactant concentration of 500 μM are displayed in Figs. A.1 to A.5:

Figure A.1. Relative surface charge density as a function of pH.

Figure A.2. Adsorption density as a function of pH.

Figure A.3. Equilibrium surfactant concentration as a function of pH.

Figure A.4. Zeta potential as a function of pH.

Gaps in all data sets still remain due to the difficulty of predicting the final equilibrium pH, surfactant bulk concentration (C_{eq}), and adsorption density (Γ_s) levels from a given set of initial solution conditions. For sodium dodecyl sulfonate, data are still required near the solubility limit at both 30 and 40°C for all NaCl concentrations. Unfortunately, solubility limits are not available in the literature and must be experimentally determined. Likewise, CMC values for sodium decyl sulfonate must also be experimentally determined at the NaCl

concentration/temperature combinations of interest. A detailed discussion of results is deferred until complete data sets may be presented.

Description of Modeling Procedure

Although it is not complete, the $C_{12}SO_3Na/30^\circ C/0.001\text{ M NaCl}$ data set does contain enough points to permit illustration of the modeling procedure.

Modeling of the data involves three steps:

- (1) Optimization using potentiometric titration data without surfactant to determine CSBM parameters to be used in the model.
- (2) Smoothing of adsorption density data in the form $\Gamma_S = \Gamma_S(C_{eq}, pH)$ via regression analysis.
- (3) Simulation of $\Gamma_S = \Gamma_S(C_{eq}, pH)$ using the CSBM model with assumed values of K_S and lateral interaction energy and comparison of simulated results with results from regression analysis of the experimental data.

A description of each step follows.

Optimization. Figure A.5 shows the results of continuous potentiometric titration of TiO_2 in 0.001, 0.01, and 0.1 M NaCl at $30^\circ C$. Surface charge density as a function of pH and salt concentration was calculated as described in the Data Analysis section.

The optimization routine was run using the data shown in Fig. A.5. The constants determined by the routine are used to calculate the lines shown in Fig. A.6 that also shows the experimental data. The calculated values compare well with the experimental data except at low pH and high salt concentration and low salt concentration and high pH. The optimization routine may have found constants that are actually at a local minimum due to the original set of constraints used. Improvement might be effected by rerunning the optimization routine with a broader set of constraints. This will be checked in the next period.

Smoothing of Data. Since the data is scattered in the three-dimensional data space $\Gamma_S = \Gamma_S(C_{eq}, pH)$, it is difficult to compare experimental results with those generated by the model. For this reason, a functional relationship that permits calculation of Γ_S at desired values of C_{eq} and pH is required. A Taylor-series expansion of the form

$$\Gamma_S = a_{i,j} \sum_{j=0}^3 \sum_{i=0}^3 C_{eq}^i pH^j \quad [A.7]$$

is assumed to fit the data. A stepwise regression analysis [using the statistical analysis software package Statview 512+ (1986, Abacus Concepts, Inc.)] is then performed on the data that first determines which terms may be deleted from the equation without significantly affecting the results and then calculates the values of the leading coefficients for the remaining terms. The resulting equation has no theoretical significance, of course; it is merely a device to allow convenient representation of the data. It does have the added advantage of smoothing the data with respect to experimental error.

For the incomplete $C_{12}SO_3Na/30^\circ C/0.001 \text{ M NaCl}$ data set used here for illustrative purposes, the following equation was generated:

$$\begin{aligned} \Gamma_S = & 0.014 + 5250.3 C_{eq} - 1971.2 C_{eq} pH + 235.6 C_{eq} pH^2 \\ & - 9.2 C_{eq} pH^3 + 13009.038 C_{eq}^2 - 15589386.2 C_{eq}^3 \end{aligned} \quad [A.8]$$

The correlation coefficient between measured and fitted values is $R^2 = 0.914$. Both measured and fitted values of adsorption density are displayed in Fig. A.8.

Figure A.8 shows results of using Eq. [A.8] to calculate Γ_S at constant pH for various values of C_{eq} . Results are displayed only in the areas for which data is

available since extrapolation of this equation is not valid. No conclusions should be drawn from these results since the data set is not yet complete; they are presented only to illustrate the method used to regress the data.

Upon completion of the $C_{12}SO_3Na/30^\circ C/0.001\text{ M NaCl}$ data set, Eq. [A.8] will be recalculated to reflect the addition of new data points. As other data sets are completed, their corresponding regression equations will also be calculated.

Simulation. Given the complete set of CSBM parameters determined by the optimization routine from potentiometric titration data for TiO_2 in aqueous $NaCl$ solutions at $30^\circ C$, simulations of adsorption were possible. The computer program containing the extended version of the CSBM, that includes the equations accounting for surfactant adsorption, was run for various combinations of K_S and ω .

First, only K_S was varied to see the effect on calculated levels of adsorption density; the $\omega\theta$ term was omitted. Figures A.9 to A.13 show the results of these simulations. Clearly, as the value of K_S increases by orders of magnitude over that of K_{Cl} , adsorption density increases, since the surfactant ion is competing more and more successfully with Cl^- for positive sites on the surface.

Next, K_S was fixed and ω was set to 1.15 kT per methyl group. Figures A.14 to A.15 show the results of a simulations run using $n = 12$ methyl groups. For $K_S = K_{Cl}$ (see Fig. A.14), inclusion of the lateral interaction energy term also results in higher adsorption levels than those shown in Fig. A.9, where $\omega\theta$ was omitted. For $pK_S = 1 + pK_{Cl}$ ($K_S = 10 \cdot K_{Cl}$), the same trend is seen (see Fig. A.15); but the calculation becomes unstable at low pH values for higher levels of C_{eq} . Apparently a phase transition is being mathematically reached. This instability in the isotherm requires a more thorough investigation and will be explored in the next period.

Future Work

Goals for the next period include:

- (1) Measurement of solubility limit values for $C_{12}SO_3Na$ at 30 and 40°C for 0.001, 0.01, and 0.1 M NaCl and of CMC values for $C_{10}SO_3Na$ at 30°C for 0.001, 0.01, and 0.1 M NaCl.
- (2) Extension of data sets to include results with surfactant concentrations near the solubility limit or the CMC.
- (3) Regression analysis of all data sets to obtain suitable smoothing equations.
- (4) Rerun of optimization using a broader set of constraints on parameters to determine the best set of CSBM parameters.
- (5) Investigation of instability induced in simulation of adsorption density when the $\omega\theta$ term is included in model equations.
- (6) Determination of values of K_S and ω that matches theoretically calculated and experimental data.

References

- (A.1) Davis, J. A., James, R. O., and Leckie, J. O., J. Colloid Interface Sci. **63**, 480 (1978).
- (A.2) Davis, J. A., James, R. O., and Leckie, J. O., J. Colloid Interface Sci. **67**, 90 (1978).
- (A.3) James, R. O., and Healy, T. W., J. Colloid Interface Sci. **40**, 42 (1972).
- (A.4) James, R. O., Davis, J. A., and Leckie, J. O., J. Colloid Interface Sci. **65**, 331 (1978).
- (A.5) James, R. O., and Parks, G. A., in Surface and Colloid Sci. (E. Matijevic, Ed.), Vol. 12, Wiley Interscience, New York, 119 (1982).
- (A.6) Yates, D. E., Levine, S., and Healy, T. W., J. Chem. Soc. Faraday Trans. **70**, 1807 (1974).

- (A.7) Stumm, W., and Morgan, J. J., Aquatic Chemistry: An Introduction Emphasizing Chemical Equilibria in Natural Waters, John Wiley & Sons, New York, 134 (1981).
- (A.8) Kielland, J., "Individual Activity Coefficients of Ions in Aqueous Solutions," J. Am. Chem. Soc. **59**, 1675 (1937).
- (A.9) Brüll, L., "Considerazioni sul raggio ionico nelle soluzioni acquose di elettroliti," Gazzetta Chimica Italiana **64**, 624 (1934).
- (A.10) Lange's Handbook of Chemistry, citation incomplete.

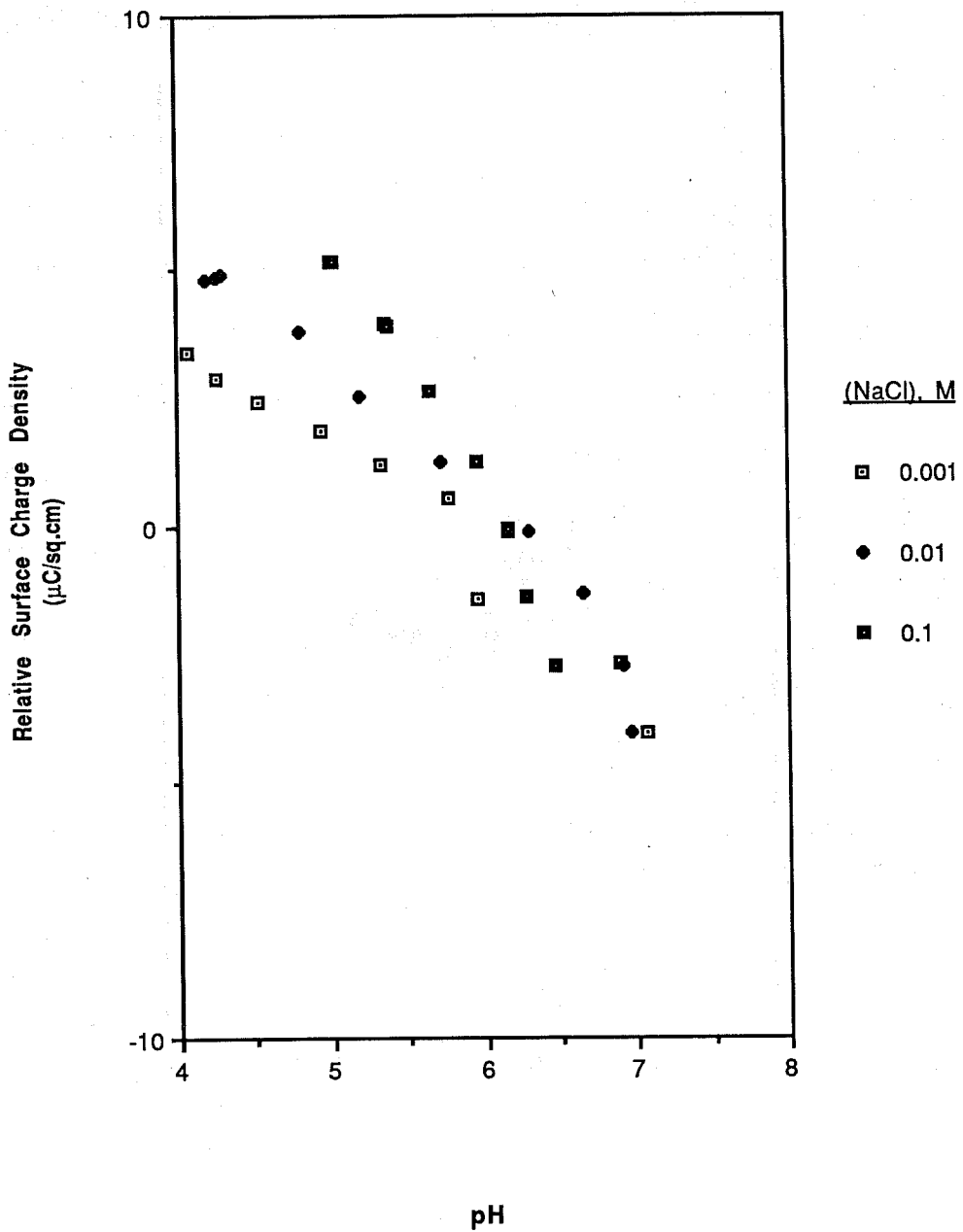


Fig. A.1. Sodium dodecyl sulfonate in NaCl at 30°C: surface charge density versus pH.

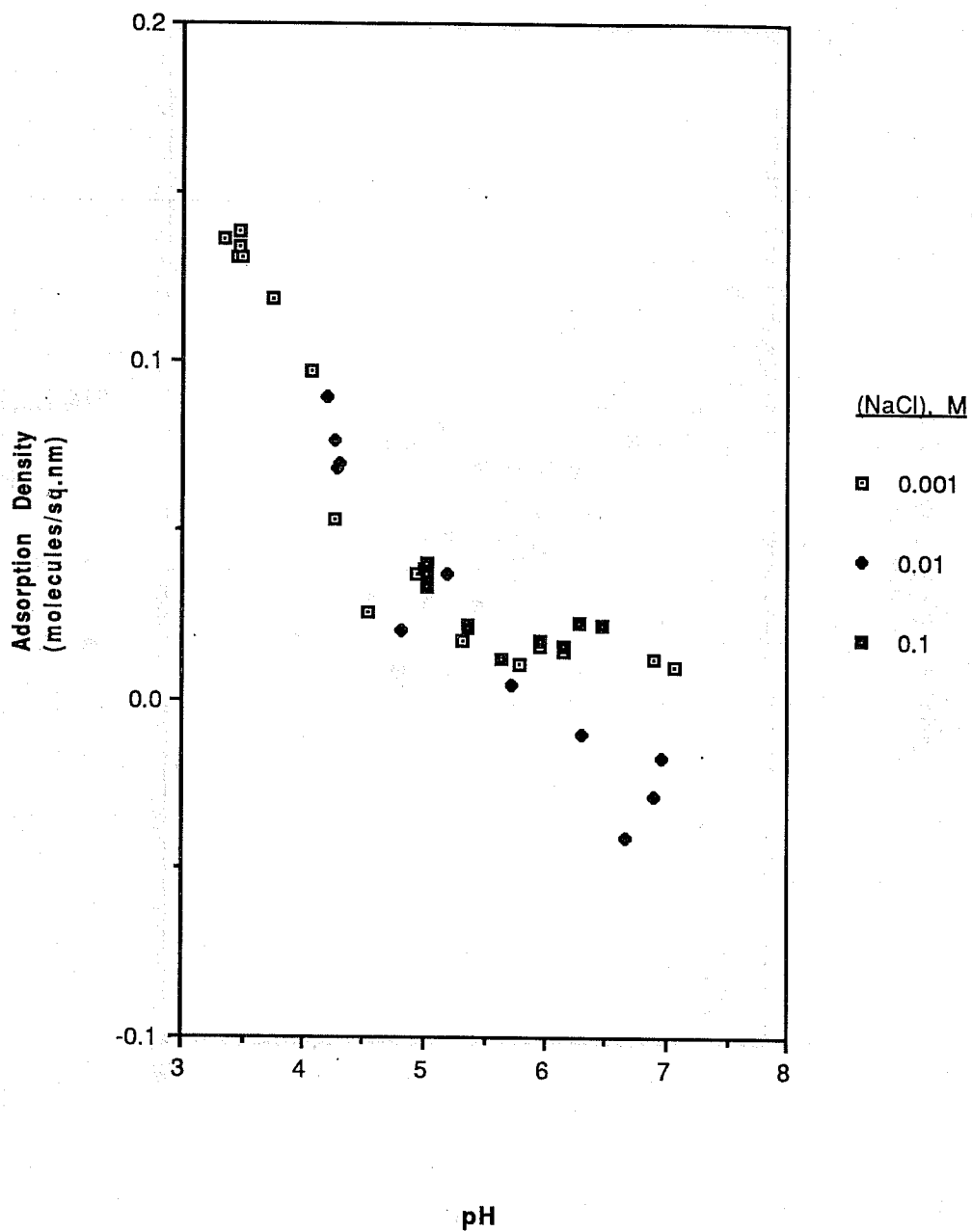


Fig. A.2. Sodium dodecyl sulfonate in NaCl at 30°C: adsorption density versus pH.

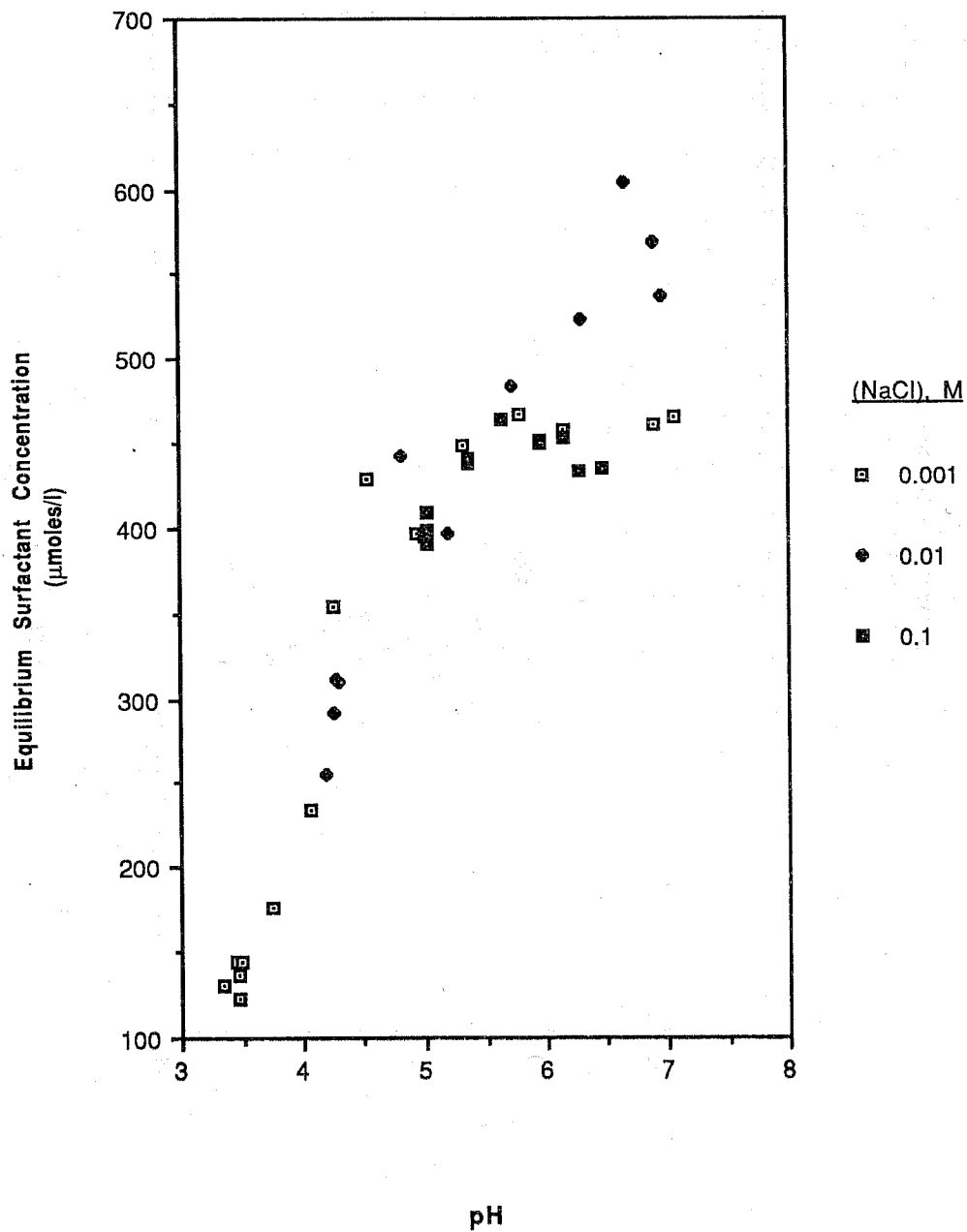


Fig. A.3. Sodium dodecyl sulfonate in NaCl at 30°C: equilibrium concentration versus pH.

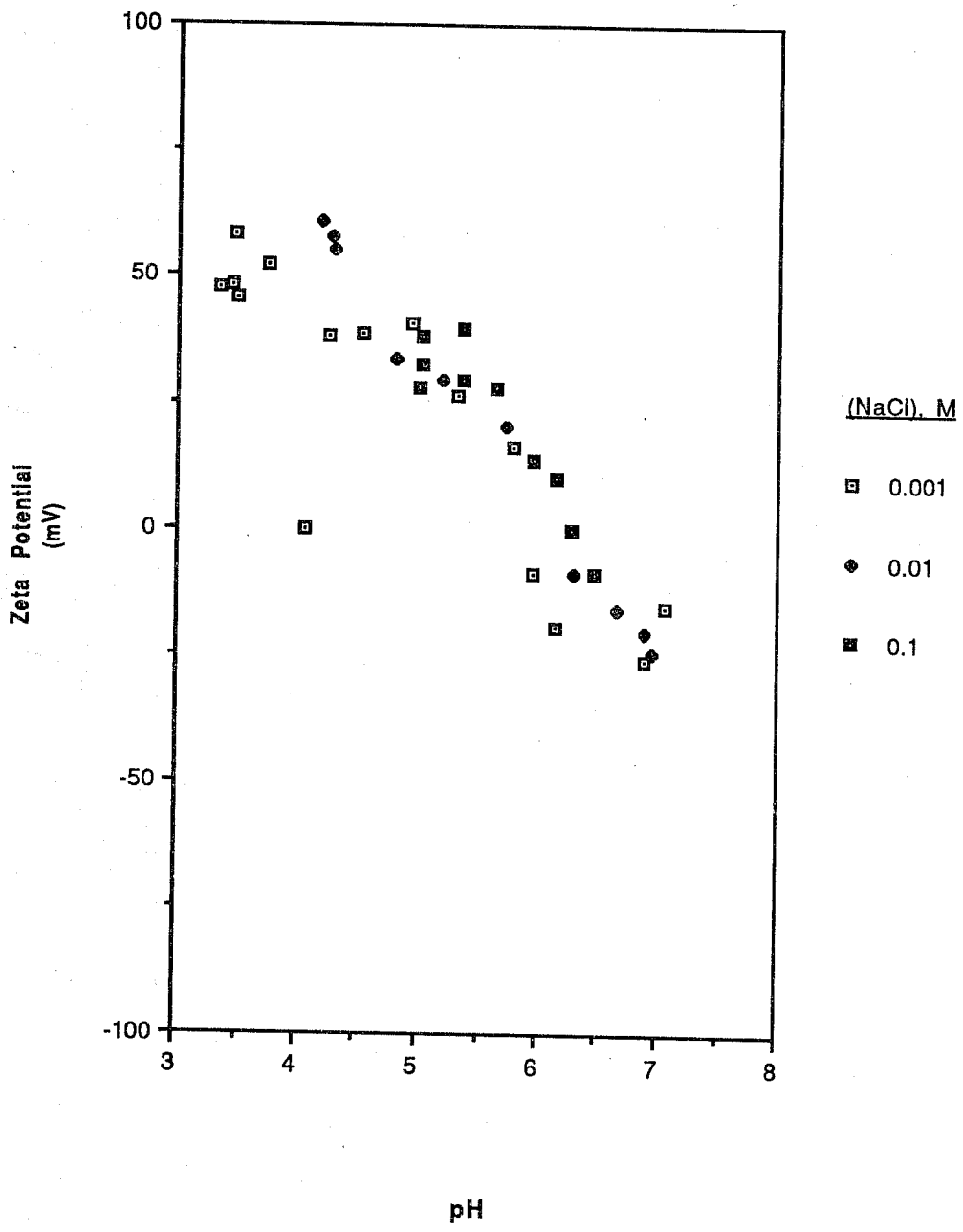


Fig. A.4. Sodium dodecyl sulfonate in NaCl at 30°C: zeta potential versus pH.

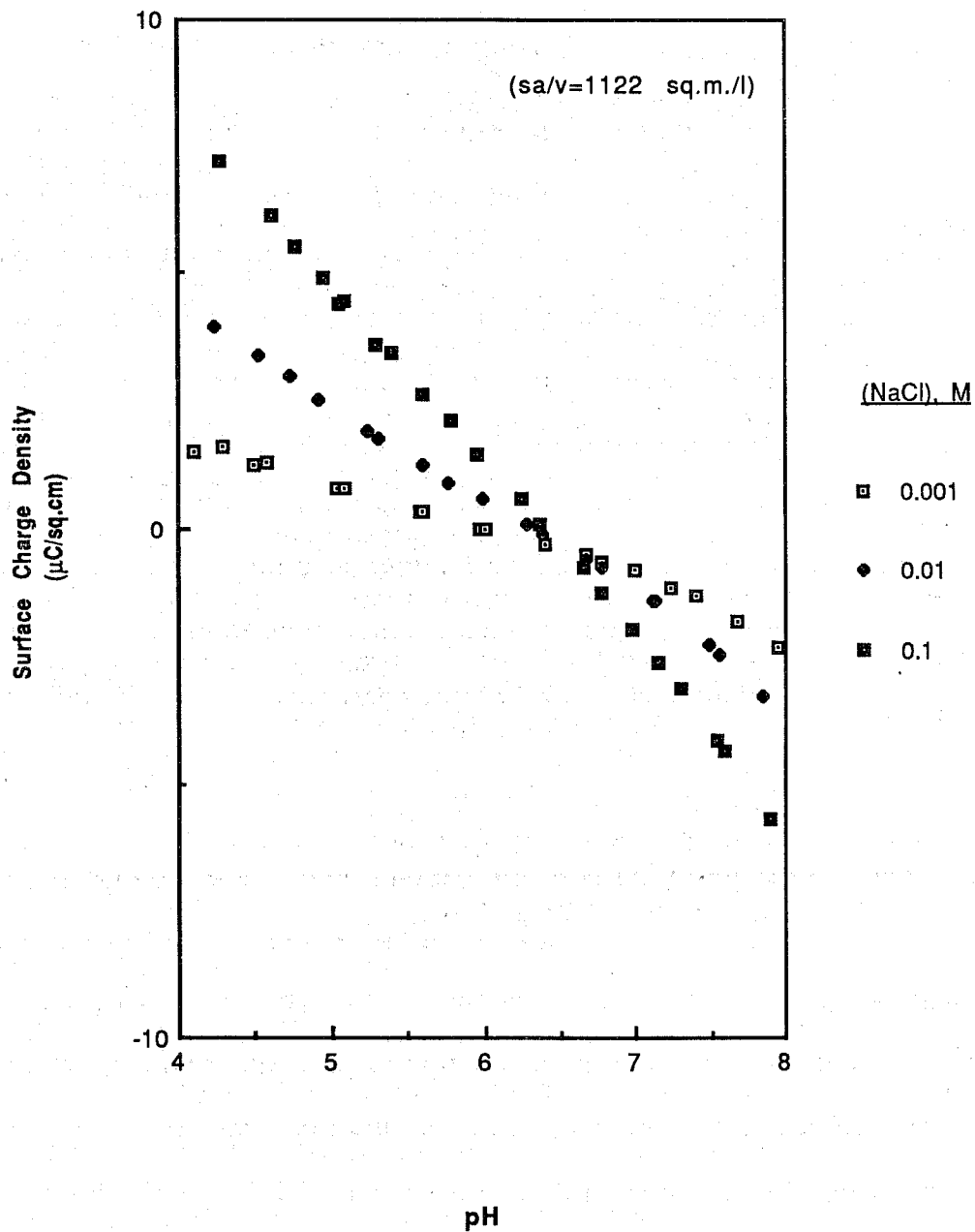


Fig. A.5. Continuous potentiometric titration of TiO_2 in aqueous NaCl solutions at 30°C : experimentally determined points.

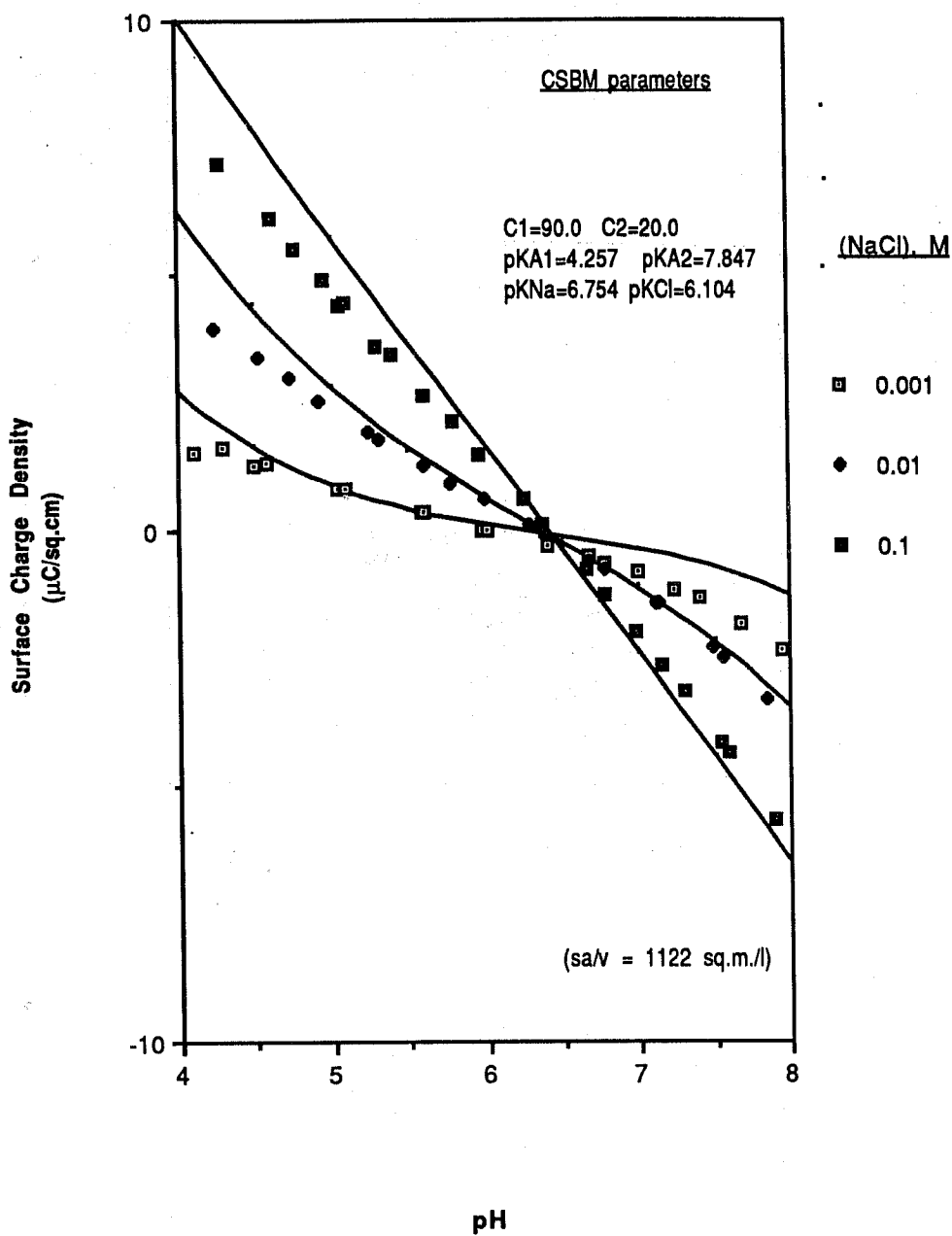


Fig. A.6. Continuous potentiometric titration of TiO_2 in aqueous NaCl solutions at 30°C : lines calculated from CSBM parameters.

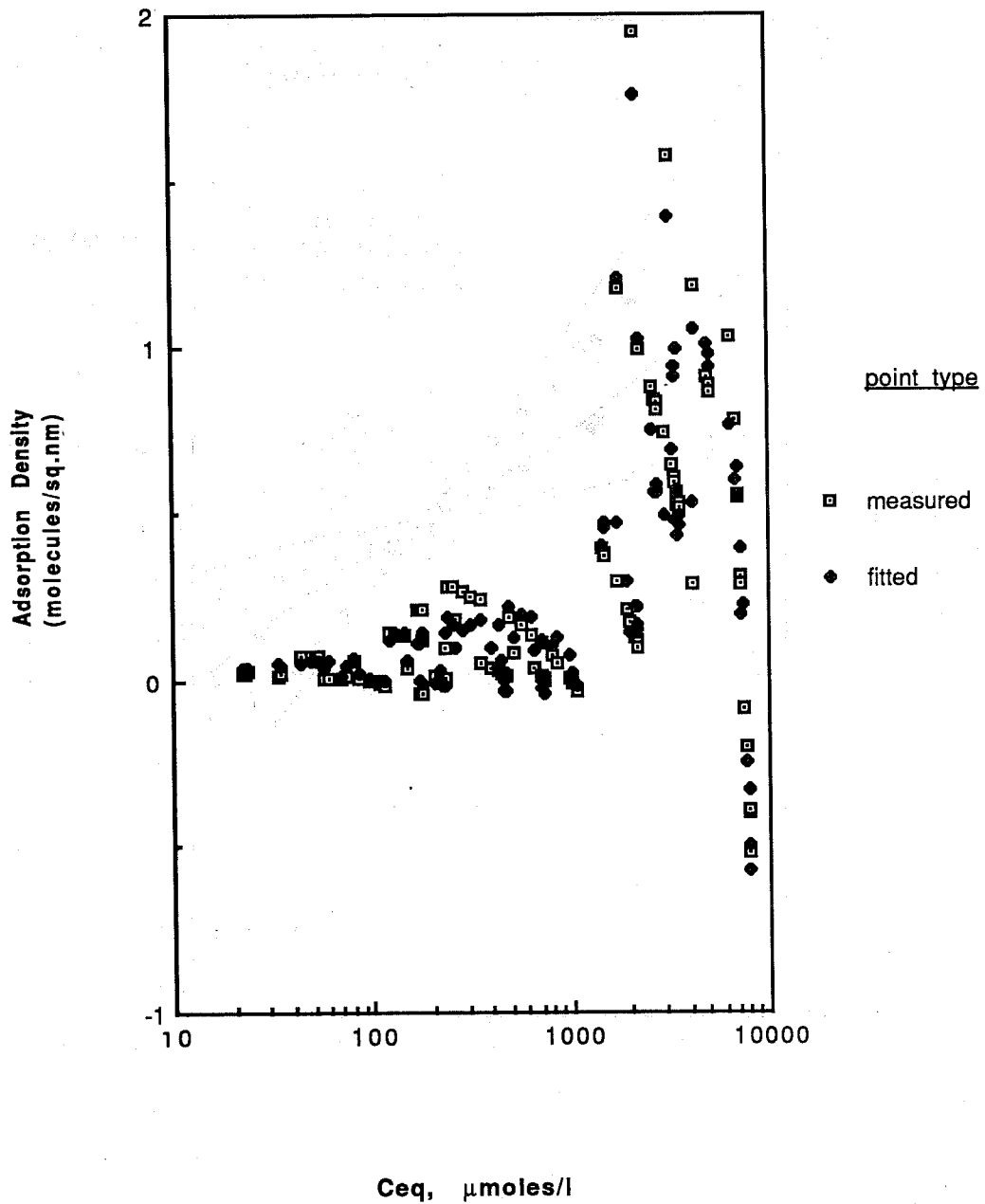


Fig. A.7. Results of regression analysis for $C_{12}SO_3Na/30^\circ C/0.001\text{ M NaCl}$ data set: measured points and corresponding points calculated from Eq. [8].

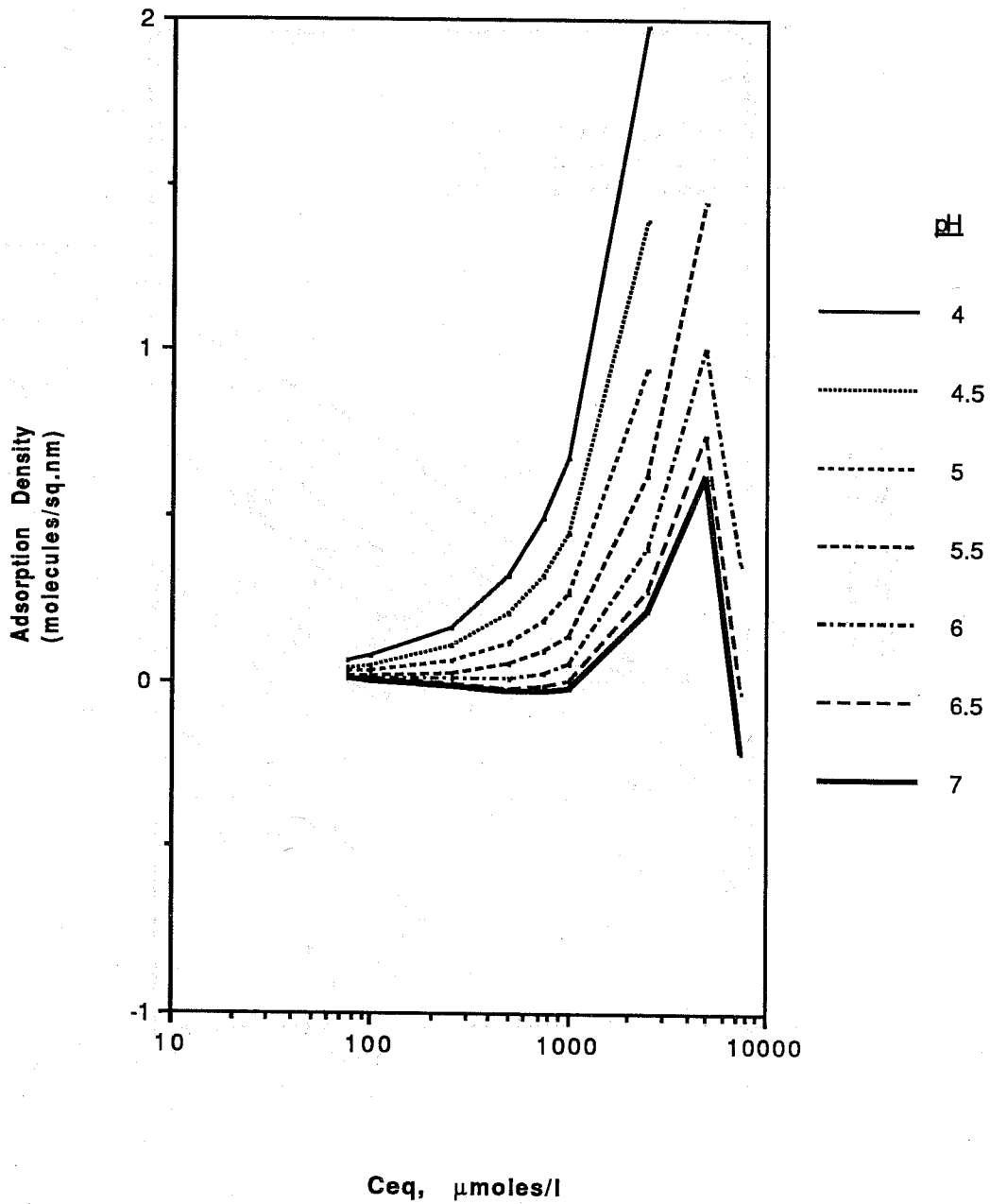


Fig. A.8. Results of regression analysis for $C_{12}SO_3Na/30^\circ C/0.001 M NaCl$ data set: adsorption density as a function of C_{eq} at constant pH as calculated from Eq. [8].

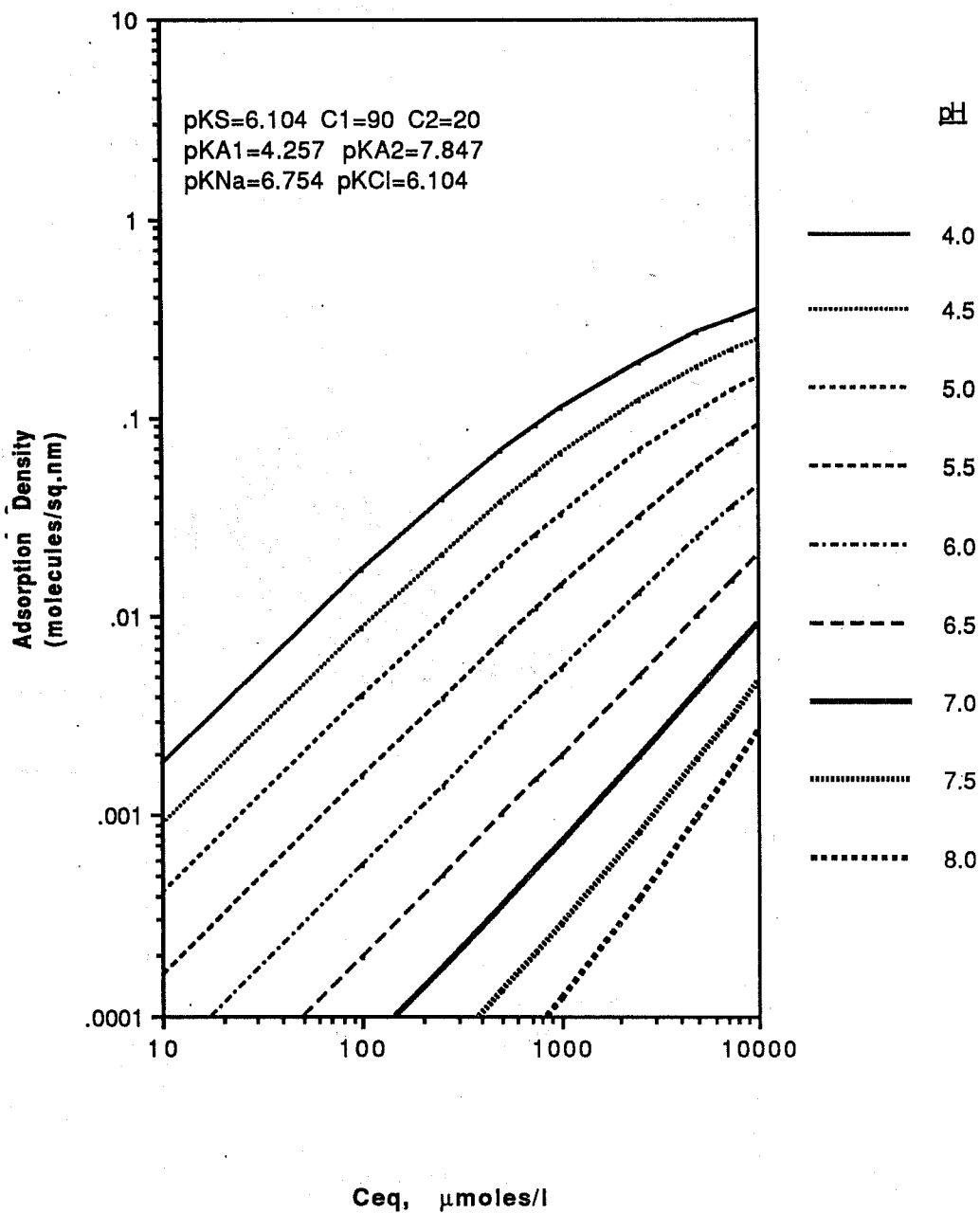


Fig. A.9. Simulation of adsorption with $pK_S = pK_{Cl}$ and $\omega = 0$.

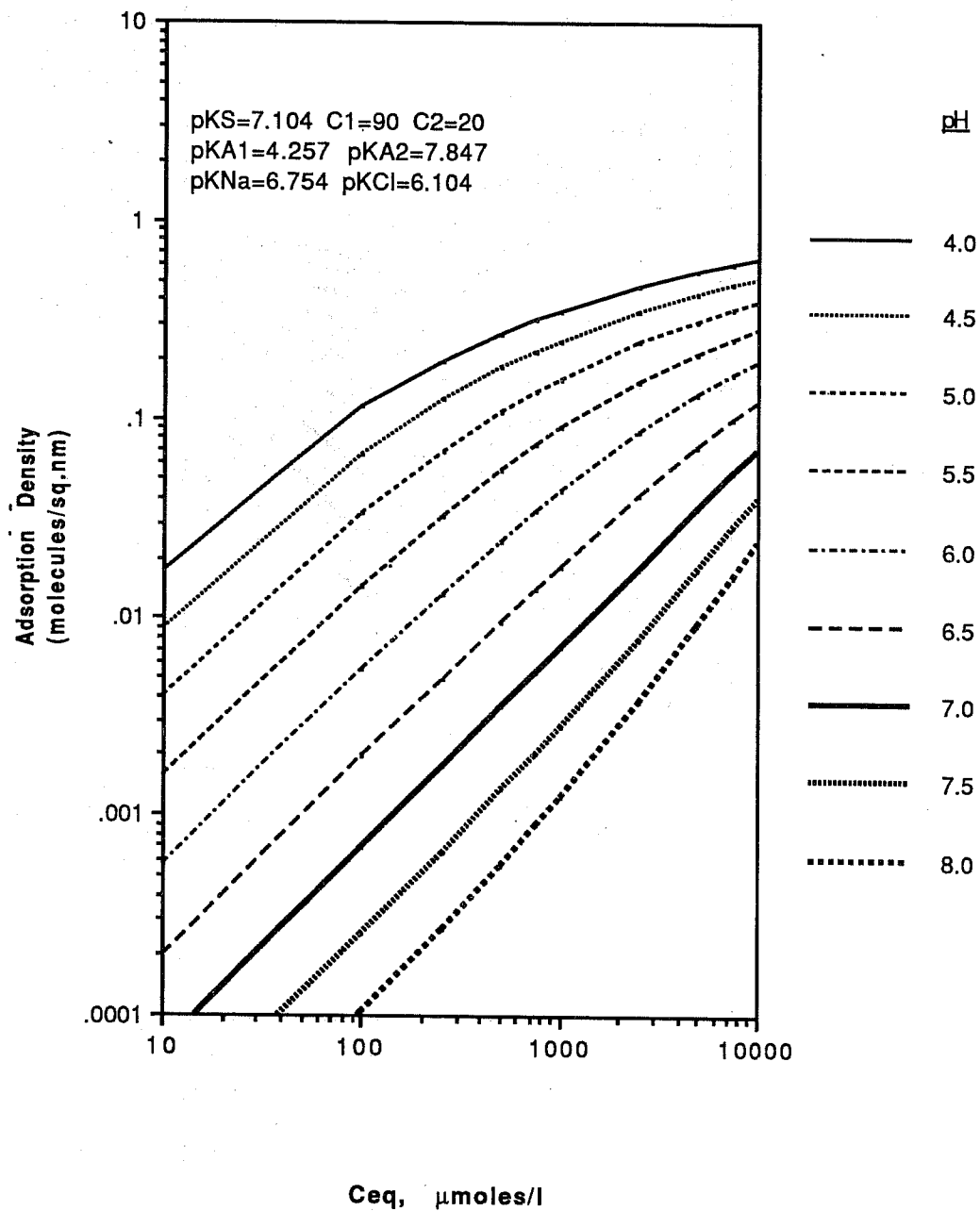


Fig. A.10. Simulation of adsorption with $pK_S = (1 + pK_{Cl})$ and $\omega = 0$.

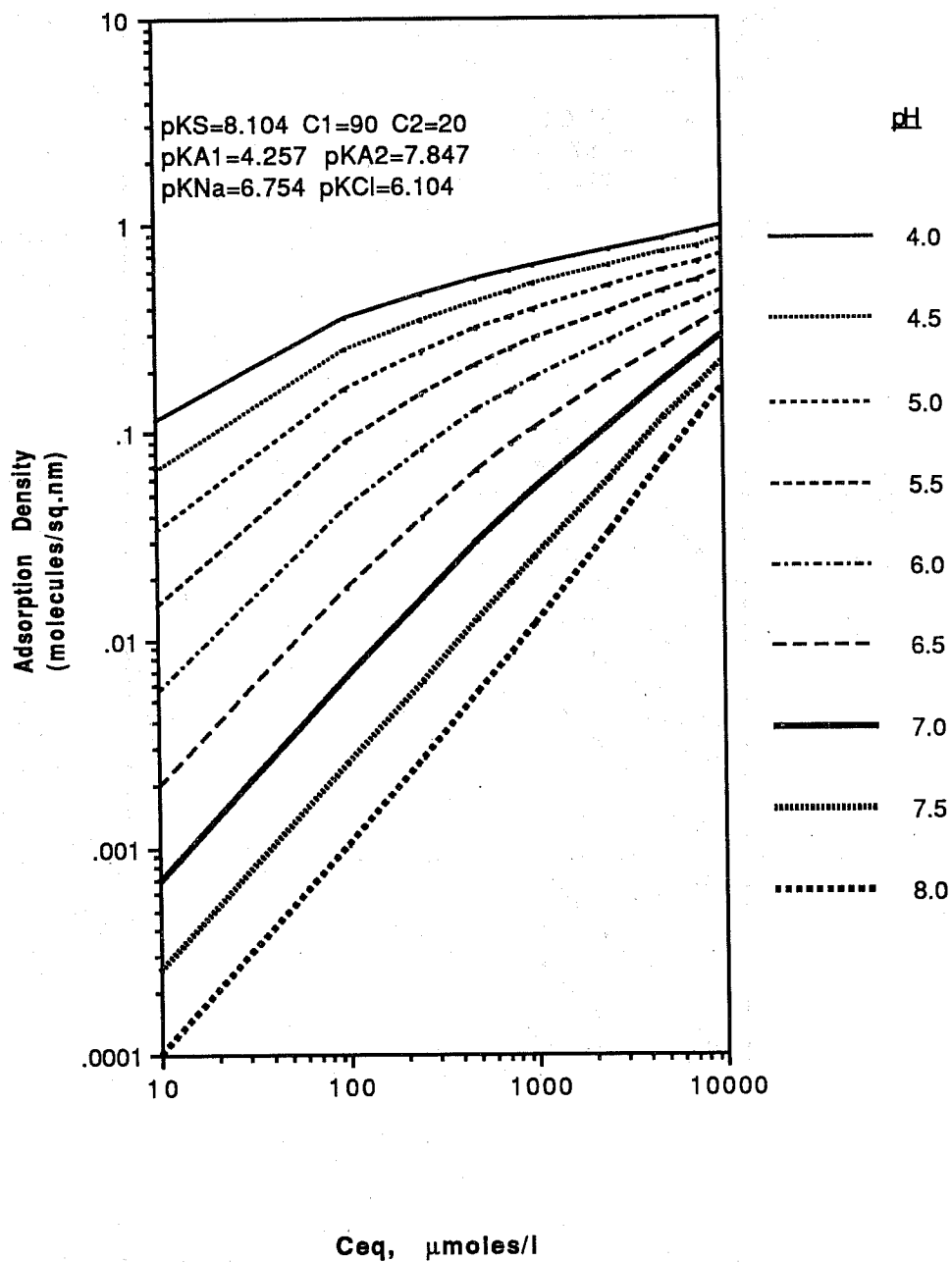


Fig. A.11. Simulation of adsorption with $pK_S = (2 + pK_{Cl})$ and $\omega = 0$.

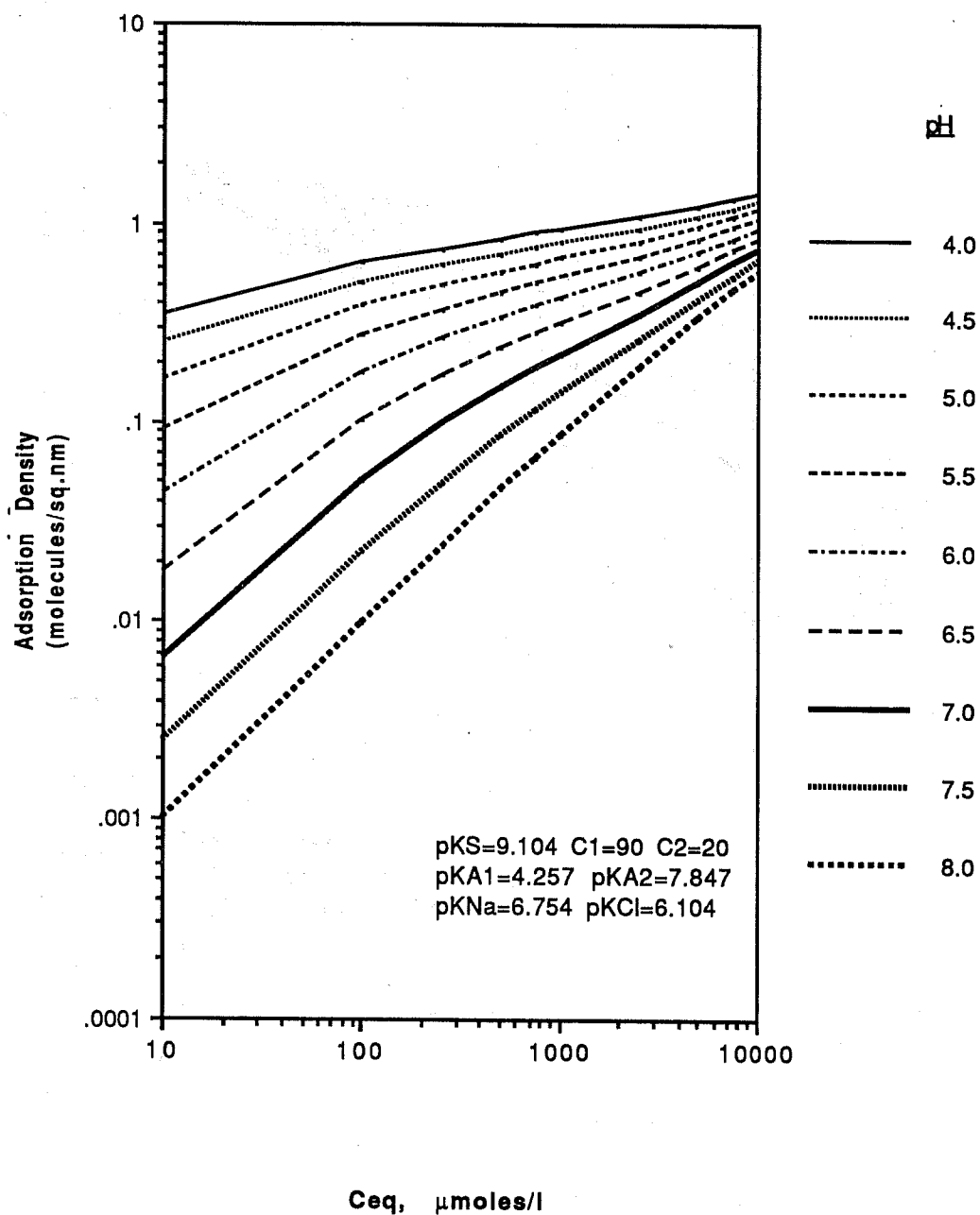


Fig. A.12. Simulation of adsorption with $pK_S = (3 + pK_{Cl})$ and $\omega = 0$.

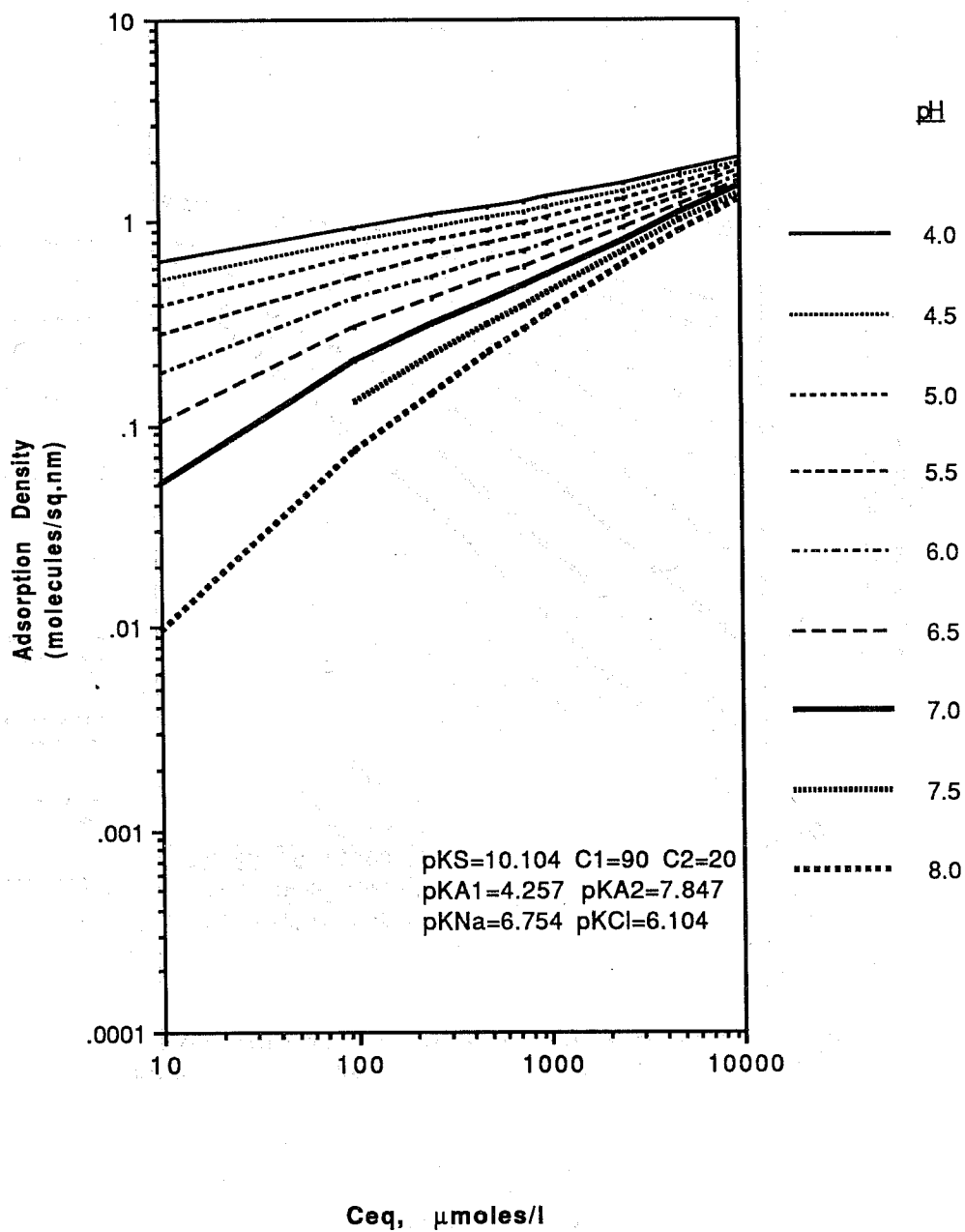


Fig. A.13. Simulation of adsorption with $pK_S = (4 + pK_{Cl})$ and $\omega = 0$.

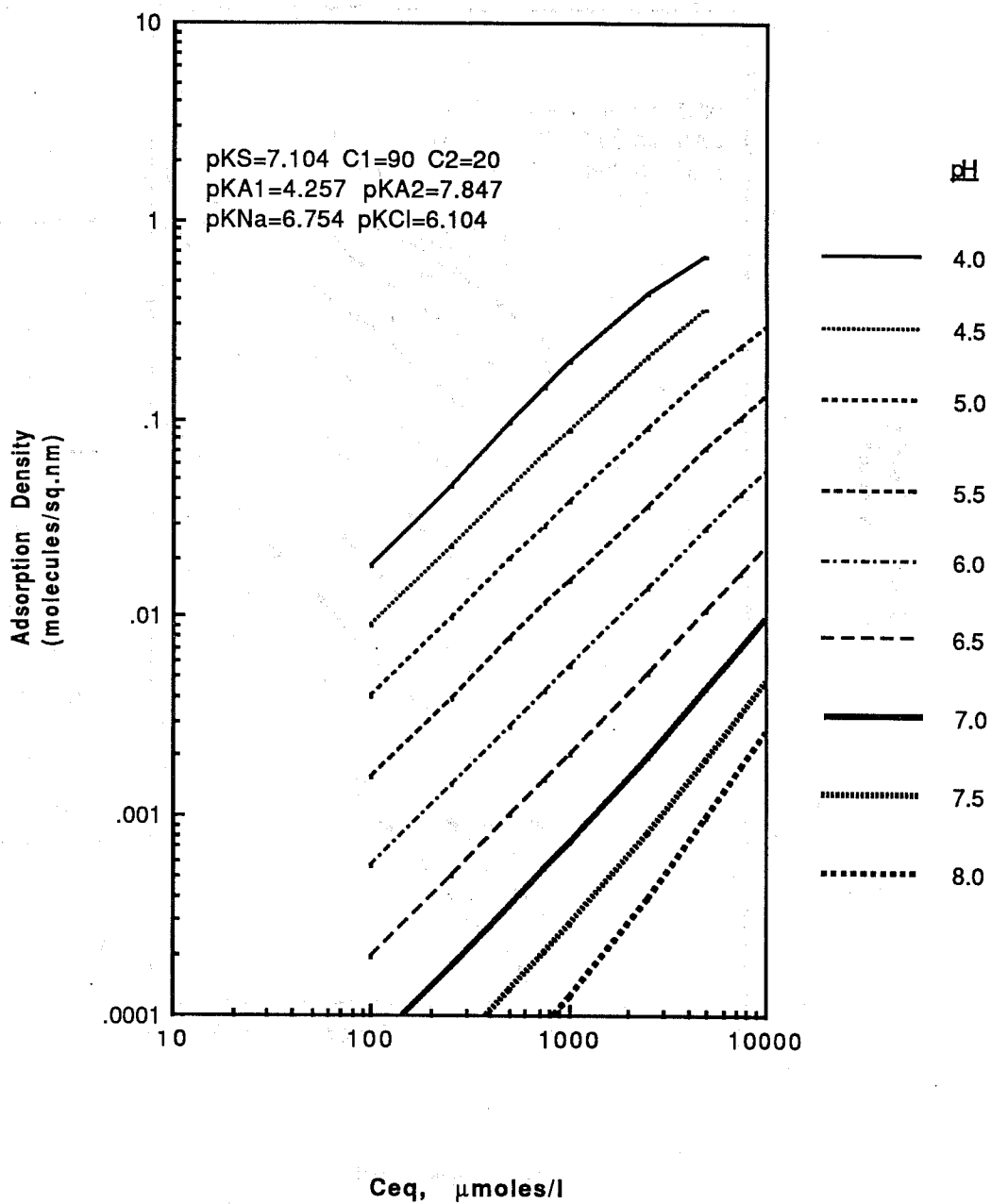


Fig. A.14. Simulation of adsorption with $pK_S = pK_{Cl}$ and $\omega = 1.15 kT \cdot n$ with $n = 12$.

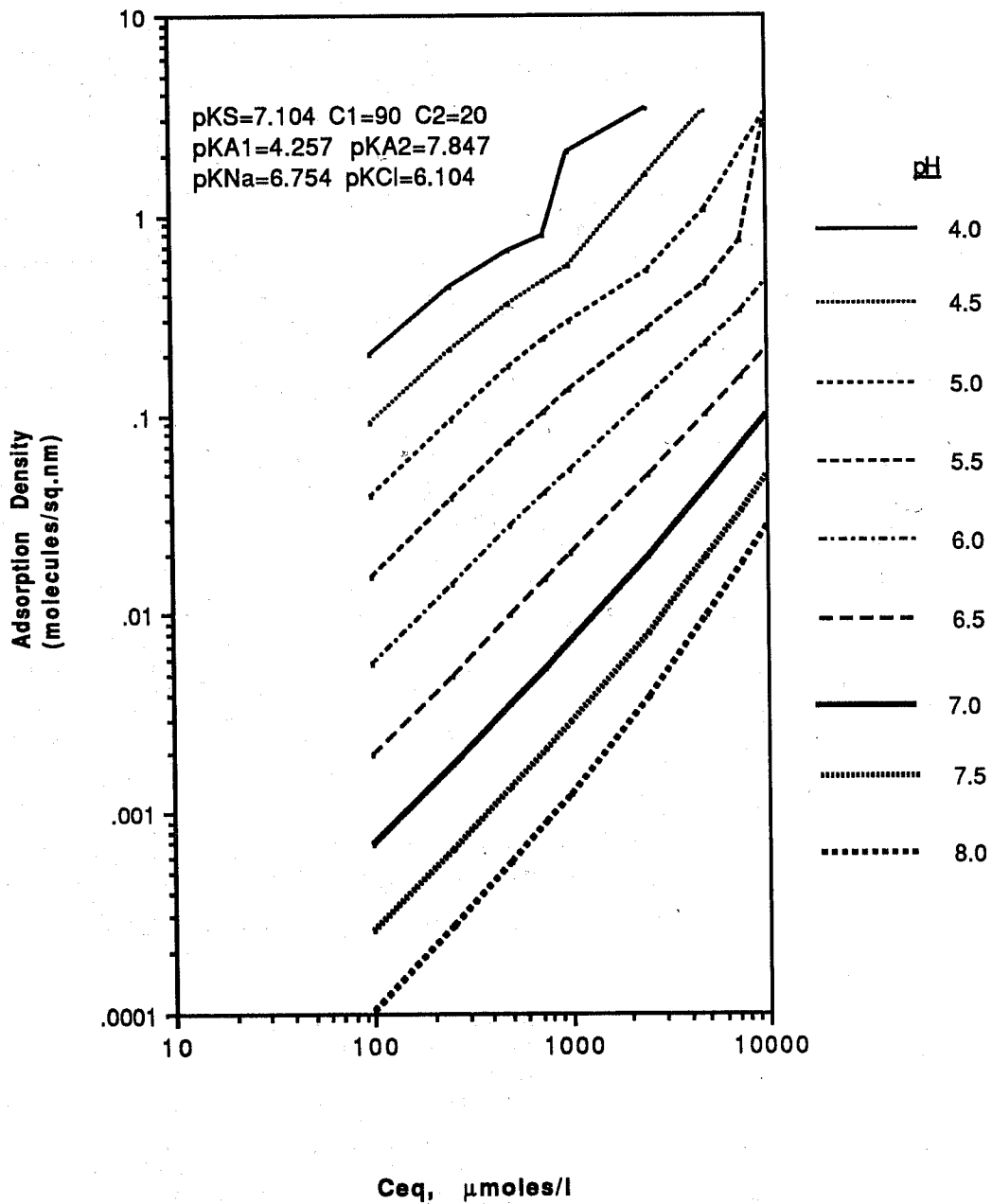


Fig. A.15. Simulation of adsorption with $pK_S = (1 + pK_{Cl})$ and $\omega = 1.15 kT \cdot n$ with $n = 12$.

B. Thermodynamics of Solubilization

Theory

The solvency of an aqueous micellar solution is intimately related to its effectiveness as an oil recovery agent. Those solutions that form three-phase systems at reservoir conditions in the presence of crude oil and that have large surfactant phase volumes have been generally found to yield essentially complete displacement of residual oil when sufficiently large slugs of micellar solution are injected at reasonable rates. This research is intended to elucidate the relationship that exists between the surfactant structure and the solvency of micellar or inverted micellar solutions and to predict the phase behavior of these solutions. Two parallel approaches are being followed. One approach considers the energy required to bend an interface from its natural radius of curvature as an additional contribution to the free energy of the system, and this will partly, but not entirely, determine the equilibrium radius of the drops. In this approach, a micellar solution is modeled as a dispersion of drops in a continuous phase.

A second approach, and the one detailed in this section, focuses on water-continuous systems and itemizes the contributions to the free energy of formation of drops starting with surfactant and oil in their standard states. The drop radius of an isolated drop is then found. This is the natural radius. The standard state for the oil is considered to be an excess bulk phase that for simplicity is assumed to be free of water. The standard state of the surfactant is an infinitely dilute aqueous phase. These are assembled to form an entity such as the one illustrated by Fig. B.1. In this model, the solubilize forms a central core and is also comingled among the amphiphilic tails. The chemical potential of the solubilize must evidently be the same whether it resides in the core, comingled with the tails, or in the excess bulk phase.

The microemulsion droplet is formed from i dispersed amphiphiles and j solubilize molecules so that symbolically one can write



It is assumed that the system is dilute, with minimal interactions among the amphiphiles, solubilize molecules, and droplets in solution. The free energy for this reaction can be represented as

$$\mu_A^{\circ} + RT \ln X_A + \left(\frac{j}{i}\right) \left(\mu_S^{\circ}\right) = \mu_{\text{mic}}(i,j) + \frac{RT}{i} \ln X_{\text{mic}} \quad [\text{B.2}]$$

where μ_A° and μ_S° are the standard states of the amphiphile and the solubilize, respectively, $\mu_{\text{mic}}(i,j)$ is the standard free energy per amphiphile of an aggregate containing i amphiphiles and j solubilize molecules, and X_A and $X_{\text{mic}}(i,j)$ are the mole fractions of amphiphile and aggregates or droplets, respectively, in the system. Equation [B.2] can be rearranged to yield an expression for the mole fraction of aggregates

$$X_{\text{mic}}(i,j) = X_A^i \exp \left[- \left(\frac{i\mu_{\text{mic}}^{\circ}(i,j) - i\mu_A^{\circ} - j\mu_S^{\circ}}{RT} \right) \right] \quad [\text{B.3}]$$

The mass balance in this case is

$$X_{A,\text{tot}} \equiv X_A + \sum_{i=1}^{\infty} \sum_{j=1}^{\infty} j X_{\text{mic},i,j} \quad [\text{B.4}]$$

where $X_{A,\text{tot}}$ is the specified total mole fractions of amphiphile.

In applying Eq. [B.3], the main challenge is accurately evaluating the chemical potential of the aggregate ($\mu_{\text{mic}}(i,j)$) as a function of i and j . Mallikarjun and Dadyburjor^(B.1) presented a model that used a statistical thermodynamic

approach to evaluate the translational, rotational, and configurational contributions to the micelle free energy. However, they did not consider the presence of a core that is an essential part of a model for microemulsions.

Nagarajan and Ruckenstein^(B.2) have presented a free energy model that identifies the major forces promoting and limiting solubilization. Solubilization is shown to be promoted by the negative free energy of the mixing of the solubilizates and amphiphiles in the swollen micelles and by the lower head-head repulsion that results as the heads move further apart. The major factor opposing solubilization is the increase in interfacial free energy as the surface area per amphiphile increases. Their analysis considered two cases, neither of which corresponded to the one depicted by Fig. B.1.

The standard free energy of the swollen micelle is divided into bulk and surface terms. The bulk terms relate to the free energy of the lipophile and solubilizate dissolved in the palisade layer of the swollen micelle and that of the solubilizate in the central core. The free energy of the solubilizate within the palisade layer is calculated assuming that lipophile and solubilizate form an ideal solution evaluated at the temperature and pressure of the system. This is equivalent to assuming that the interfacial layer of the micelle is indeed liquid-like and precisely mimics a bulk phase composed of a mixture of solubilizate and lipophile at the same conditions. The bulk-phase free energy of the core assumed to be composed of solubilizate only is therefore equivalent to that of the excess bulk hydrocarbon phase.

The surface terms include a repulsive component arising from the interaction of the ionic groups (here, ionic surfactants are considered) and an interfacial free energy term associated with the hydrocarbon-water surface.

Following this approach, the free energy of the above aggregate per amphiphile can be written as

$$\begin{aligned} \mu_{mic_{i,j}} = & \mu_{A_{hc}} + \frac{j_{int}}{i} \mu_{S_{hc}} + F_{rep} + \frac{j - j_{int}}{i} \mu_S^{\circ} \\ & + \sigma(A_C - A_H) + \frac{kT}{i} \ln X_{mic_{i,j}} \end{aligned} \quad [B.5]$$

where $\mu_{A_{hc}}$ and $\mu_{S_{hc}}$ are the free energies of the lipophile and solubilize when dissolved in the interfacial layer of the swollen micelle, j_{int} is the number of the solubilize molecules in the interfacial layer (note, $j \geq j_{int}$), F_{rep} is the repulsive surface term due to head group interaction, σ is the free energy per unit area of the hydrocarbon interface, A_C is the surface area of the micelle core per amphiphile, A_H is the surface area of the core shielded by the surfactant head group and not part of the core-water interface, and $X_{mic_{i,j}}$ is the aggregate mole fraction in the aqueous phase.

The free energies of the lipophile and solubilize contained in the core can be written as

$$\mu_{A_{hc}} = \mu_{A_{hc}}^{\circ} + kT \ln X_{A_{hc}} \quad [B.6]$$

$$\mu_{S_{int}} = \mu_{S_{int}}^{\circ} + kT \ln X_{S_{int}} \quad [B.7]$$

where $\mu_{A_{hc}}^{\circ}$ is the standard state chemical potential of the lipophile in the micelle taken in the absence of solubilize, $\mu_{S_{int}}^{\circ}$ is the standard state chemical potential of the solubilize in the interfacial region at infinite dilution, and $X_{A_{hc}}$ and $X_{S_{int}}$ are the mole fractions of the lipophile and solubilize in the interfacial region. Equations [B.5], [B.6], and [B.7] substituted into Eq [B.2] yields

$$\begin{aligned}
\Delta G_{agg}^{\circ} &= kT \ln X_{A_w} = \left(\mu_{A_{hc}}^{\circ} - \mu_{A_w}^{\circ} \right) \\
&+ \frac{j_{int}}{i} \left(\mu_{S_{int}}^{\circ} + kT \ln X_{S_{int}} - \mu_S^{\circ} \right) \\
&+ kT \ln X_{A_{hc}} + \frac{kT}{i} \ln X_{mic_{i,j}} + \sigma(A_C - A_H) + F_{rep}
\end{aligned} \tag{B.8}$$

The first term on the right is the standard free energy of transfer of the amphiphile tail from water to a micelle containing no solubilize. This free energy change is due to the hydrophobic effect. For linear alkyl surfactants, $(\mu_{A_{hc}}^{\circ} - \mu_{A_w}^{\circ})$ is estimated to be -2000 cal/gmole for the terminal CH_3 group and -700 cal/gmole per CH_2 group incorporated in the micelle.^(B.3) Here, we assume, as Tanford does,^(B.3) that the CH_2 group closest to the head group lies outside the micelle core and does not contribute to $(\mu_{A_{hc}}^{\circ} - \mu_{A_w}^{\circ})$. The expression for free energy of transfer of the lipophile is then

$$\mu_{A_{hc}}^{\circ} - \mu_{A_w}^{\circ} = - (2000 + (N_T - 2) (700)) \frac{\text{cal}}{\text{gmole}} \tag{B.9}$$

where N_T is the number of carbons in the surfactant tail.

The above expression gives the values of $(\mu_{A_{mic}}^{\circ} - \mu_A^{\circ})$ in pure water. The following expression is used to adjust $(\mu_{A_{hc}}^{\circ} - \mu_{A_w}^{\circ})$ for variations in ionic strength:^(B.4)

$$\begin{aligned}
\left(m_{A_{hc}}^{\circ} - m_{A_w}^{\circ} \right)^{salt} &= \left(m_{A_{hc}}^{\circ} - m_{A_w}^{\circ} \right)^{water} \\
&- (0.129 + 0.0645 N_T) kT C_{salt}
\end{aligned} \tag{B.10}$$

where C_{salt} is the total molarity of CMC and added sodium chloride.

The second term in Eq. [B.8] refers to the change in free energy of the solubilize as it is transferred to the micelle interface. μ_S° is the chemical potential of the bulk solubilize phase, and $\mu_{S_{int}}^{\circ}$ is the standard free energy of the solubilize in the interfacial region. Since the liquid alkanes are very similar in structure to the surfactant tails, the solubilize molecules and the tails should mix ideally in the absence of packing constraints. Therefore, the activity coefficients of the amphiphile and the solubilize in the interfacial region are assumed to be unity. The micelle packing constraints are included in the standard free energy of the solubilize as it moves from the bulk solubilize liquid to the micelle $\mu_{S_{int}}^{\circ} - \mu_S^{\circ}$. Because of the constraints on the amphiphiles, the solubilizes located between the tails are slightly more constrained than in the bulk. A positive value of $\mu_{S_{int}}^{\circ} - \mu_S^{\circ}$ is expected, with the value expected to increase as the chain length of the solubilize increases. The values used for $\mu_{S_{int}}^{\circ} - \mu_S^{\circ}$ are discussed in subsequent sections.

The third term in Eq. [B.8] represents the entropy of the mixing of the aggregates per amphiphile. The solution is assumed to be dilute in micelles and the interaction between micelles is neglected. The CMC is often defined as the monomer concentration at which half the total amphiphile molecules in the system exist as monomer and half are contained in the micelles. This definition is used to evaluate the aggregate mole fraction ($X_{mic,i,j}$) at each value of the CMC.

The fourth term in Eq. [B.8] represents the interfacial energy of the micelle core-water surface. The surface area of the water/hydrocarbon contact per amphiphile (A_C) depends on the micelle volume and geometry, which are evaluated here as follows.

The existence of a solubilize core relaxes the geometrical constraints on packing the surfactant within the palisade layer. Those micellar aggregates having a solubilize core will be assumed to be spherical, as this shape has the smallest

area per amphiphile for a given core volume and aggregation number. This assumption appears justified, since it is the increase in the interfacial energy of the aggregate that ultimately limits the amount solubilized.

The model of the aggregate used to analyze the extent of solubilization in the presence of a solubilize core is shown in Fig. B.1. The aggregate volume is divided into two volumes: (1) a spherical solubilize core at the center of the micelle with radius (r_S) and (2) an interfacial volume near the surface of the aggregate that contains both the solubilize and the surfactant tails. The thickness of the interfacial region is assumed to be the length of a fully extended amphiphile tail (again, one carbon on the tail is excluded from the aggregate volume). The radius of the swollen micelle with a central core is, therefore,

$$r_m = 1.5 + 1.265(N_T - 1) + r_S \quad [B.11]$$

The surface area is $4\pi r_m^2$ and

$$A_C = \frac{4\pi r_m^2}{i} \quad [B.12]$$

For the alkyl surfactants, A_H is the cross-sectional area of the alkyl chain, roughly 21 \AA^2 .

The fifth term in Eq. [B.8] also involves σ , the interfacial free energy per unit area of core-water interface. Here, σ is obtained by forcing Eq. [B.8] to represent the CMC and the aggregation number measured when the surfactant under consideration is present in water but the solubilize is absent. Thus, the calculations force the model to fit observations in the absence of solubilize.

Since there are two variables to be fixed, the CMC and the aggregation number, then two parameters in Eq. [B.8] must be adjusted. The last term (F_{rep}),

the repulsive free energy between the head groups, is the second variable that is fit. Since, as Tanford^(B.3) argues, F_{rep} is inversely proportional to A_C , the proportionality constant can be fixed together with σ to give the proper CMC and aggregation number in the absence of solubilize.

The model is now complete. The extent of solubilization is determined by finding the minimum free energy aggregate. The search is conducted over two dimensions. The solubilize mole fraction in the interfacial zone ($X_{S_{int}}$) and the solubilize core radius (r_S) are varied. The values of ($X_{S_{int}}$) and (r_S) corresponding to the minimum free energy aggregate establish the number of amphiphile and solubilize molecules in the aggregate and the extent of solubilization of the surfactant solution.

Results of Experimental Studies

Measurements of the CMC and the solubilization have been obtained and are compared to the predictions of the free energy model. All the parameters used follow directly from independent measurements of micelle size and CMC in the absence of solubilize. The surfactant used in the studies reported here is sodium dodecyl sulfate (SDS) and the values of σ and F_{rep} are given in Table B.1. It will be shown that the model predictions are in good agreement with the experimental results and that the model accurately describes the observed changes in solubilization as the surfactant, solubilize, surfactant concentration, and salinity are varied. In applying the model to the solubilization results with the liquid alkanes, the free energy of transfer of the alkane from the bulk liquid alkane to the interfacial zone of the aggregate is not known and is assigned a value that best matches the experimental results. As will be seen, the assigned values in this case are reasonable and the trends in the values are consistent.

Besides predicting CMC and the extent of solubilization under various conditions, the model also predicts other aspects of solubilization, including the

average aggregate size and how the various contributions to the aggregate free energy vary with the extent of solubilization. Although no experiments were performed to confirm these predictions, they are also presented.

The results indicate that the extent of solubilization, when a core is present, increases markedly with the addition of electrolyte. The extent of solubilization also increases slightly with increasing surfactant concentration. It will be shown that both of these phenomena are due to an increase in counterion concentration that lowers the monomer concentration and increases micelle size.

A systematic study was made to determine the effect that surfactant and electrolyte concentrations have on the extent of solubilization of hexane, octane, and decane in aqueous solutions of sodium dodecyl sulfate. SDS was chosen for this study for two reasons. First, relative to other surfactants there is an extensive amount of data available on the CMC and aggregation number of SDS as a function of NaCl concentration. These data permit testing of the hypothesis that the extent of solubilization can be predicted from CMC and aggregation number data in the absence of solubilizate. Second, SDS is one of the very few surfactants for which the monomer and counterion activities have been measured as functions of surfactant concentration.^(B.5) These activity data can be used to estimate the monomer concentration and the surfactant aggregation number at different concentrations of SDS.

The results of the experiments measuring the solubilization of normal hexane, octane, and decane in SDS solutions with no added NaCl are shown in Fig. B.2. For each alkane, the total concentration of alkane present in the micellar solution is plotted as a function of SDS concentration. Note that hexane, the alkane with the smallest molar volume, is solubilized the most and that decane, with the greatest molar volume, is solubilized the least. This result largely reflects the fact that a greater number of small molecules can enter the micelle before the

$\sigma(A_C - A_H)$ term reaches an unfavorable level. However, there are other contributing factors, including a greater entropy of mixing and fewer packing constraints on the solubilize when the smaller molecule is solubilized.

Also shown in Fig. B.2 are lines drawn through the solubilization data at the two lowest SDS concentrations. These lines represent the expected solubilization if the rate of increase in solubilization with surfactant concentration remained constant. The divergence of the data above these lines indicates that, as the SDS concentration increases, each added SDS molecule is capable of solubilizing more alkane. It is true that, as the SDS concentration increases, the monomer concentration decreases, leaving more SDS in micelle form and capable of solubilization. However, this accounts for only a small fraction of the observed divergence from linear behavior.

It is known that an increase in surfactant concentration above the CMC results in an increase in the concentration of free counterion.^(B.5) To determine whether the nonlinear solubilization behavior shown in Fig. B.2 is due to a variation in the free counterion concentration, similar solubilization experiments were performed with a relatively high concentration of added electrolyte (0.2 M NaCl). The addition of electrolyte increases the overall counterion concentration and tends to overwhelm or "swamp out" the effect of changes in counterion concentration with surfactant concentration.

Figure B.3 shows the variation in hexane, octane, and decane solubilization with SDS concentration at 0.2 M NaCl. With the counterion effect "swamped out," there is a nearly linear variation in solubilization with SDS concentration for each of the alkanes. This finding indicates that the nonlinear increase in solubilization with increasing SDS concentration observed in the absence of electrolyte is due to an increase in the free counterion concentration. The effect that counterion concentration has on solubilization is also seen by comparing the amount of

solubilization in the no-NaCl cases (Fig. B.2) to solubilization in the 0.2 M NaCl cases (Fig. B.3). Solubilization is significantly greater in the 0.2 M NaCl cases in which the counterion concentration is relatively high.

An understanding of the effect of surfactant concentration on solubilization can be developed by investigating how the counterion concentration, monomer concentration, and aggregation number vary with surfactant concentration. Table B.1 shows the effect of added NaCl on the parameters and F_{rep} . These data plus knowledge of the sodium ion activity as a function of surfactant concentration can be used to predict the micellar shape as well as intermediate values of σ and F_{rep} .^(B.6) These calculations permit σ and F_{rep} to vary with both the salt and the surfactant concentrations.

For example, to determine the monomer concentration and aggregation number for the SDS solutions containing 0.2 M NaCl, the concentration of free counterion due to the added SDS is estimated based on measured sodium activities.^(B.5) The total free counterion concentration is then found by adding 0.2 M to this value, since essentially all the NaCl is dissociated. This total free counterion concentration is then used to determine the proper σ and F_{rep} .

In addition to knowing the total sodium ion concentration, one more term is required to apply the proposed model to the case of alkane solubilization. This is the free energy of transfer of the alkane from the bulk liquid to the region between the tails, written as $\mu_{S_{int}}^o - \mu_S^o$ in Eq. [B.8]. Since the heads of the amphiphiles are essentially pinned at the surface of the micelle, the freedom of the amphiphile tails is slightly restricted as is the freedom of the solubilize molecules located between the tails. The constraints on the solubilize molecule cause $\mu_{S_{int}}^o - \mu_S^o$ to be positive. Here, $\mu_{S_{int}}^o - \mu_S^o$ will be selected to match the experimental data, and the manner in which the value of $\mu_{S_{int}}^o - \mu_S^o$ changes with aggregate size and composition will be examined.

A convenient measure for representing solubilization results is the mole fraction of solubilize in the micellar aggregate. The solubilize mole fraction ($X_{S_{agg}}$) is evaluated as follows:

$$X_{S_{agg}} = \frac{C_{S_{tot}}}{(C_{S_{tot}} - C_{S_w}) + (C_{A_{tot}} - C_{A_w})}$$

where $C_{S_{tot}}$ and $C_{A_{tot}}$ are the total concentrations of solubilize and amphiphile in the surfactant solution, respectively, and C_{A_w} is the calculated CMC. C_{S_w} is the solubility of solubilize in the electrolyte solution.

The solubilize mole fractions of n-hexane, n-octane, and n-decane are shown in Figs. B.4 to B.6 as functions of the SDS concentration. In each figure, the lower set of squares shows the solubilize mole fraction in the absence of electrolyte while the upper set of circles shows the solubilize mole fraction at 0.2 M NaCl. Note that the solubilize mole fraction changes considerably more rapidly with SDS concentration in the absence of NaCl than when the NaCl concentration is 0.2 M. As previously noted, the extent of solubilization is more sensitive to increases in the counterion with increasing SDS concentration when no-NaCl is present, since the overall counterion concentration is lower.

Also included in Figs. B.4 to B.6 are solid lines that show the model predictions when the free energy of transfer of the solubilize from the bulk liquid to the interfacial region ($\mu_{S_{int}}^{\circ} - \mu_S^{\circ}$) is held constant at the value that fits the experimental data at 0.1 M SDS. It can be seen that, with a constant value of $\mu_{S_{int}}^{\circ} - \mu_S^{\circ}$, the model consistently overpredicts solubilization at SDS concentrations below 0.1 M SDS and underpredicts solubilization above 0.1 M SDS. However, a constant value of $\mu_{S_{int}}^{\circ} - \mu_S^{\circ}$ is not appropriate for two reasons. First, at lower SDS concentrations there is less solubilization and, as will be seen, a smaller solubilize core and a smaller total aggregate size. With a smaller aggregate

radius, the tails must converge more in packing, reducing the freedom of the interspersed solubilize molecules. Increased constraints on the solubilize molecules increase $\mu_{S_{int}}^o - \mu_S^o$ and reduce the expected extent of solubilization. Second, since there is less solubilization at lower SDS concentrations, the mole fraction of solubilize in the interfacial region is reduced. A higher percentage of the molecules in the interfacial region are constrained amphiphiles. Since it is the pinned amphiphiles that restrict the movement of the solubilize molecules, a higher value of $\mu_{S_{int}}^o - \mu_S^o$ is expected.

To investigate the variation in $\mu_{S_{int}}^o - \mu_S^o$ with SDS concentration (and, therefore, solubilize mole fraction) the value of $\mu_{S_{int}}^o - \mu_S^o$ was adjusted to fit the data in Figs. B.4 to B.6. The resulting values of $\mu_{S_{int}}^o - \mu_S^o$ are shown in Table B.2. There are several points to be noted here. First, for a given solubilize and electrolyte concentration, $\mu_{S_{int}}^o - \mu_S^o$ is seen to decline regularly as the SDS concentration and solubilize mole fraction increase. This finding is consistent with the idea that, as solubilization increases, there are fewer constraints on the solubilize molecules. Second, the values of $\mu_{S_{int}}^o - \mu_S^o$ for a given solubilize and surfactant concentration are considerably lower for the 0.2 M NaCl cases than for the no-NaCl cases. Again, this is related to the extent of solubilization, since the aggregates formed at 0.2 M NaCl have a higher solubilize mole fraction and are larger in size. It can also be seen that, at the same concentrations of surfactant and electrolyte, the value of $\mu_{S_{int}}^o - \mu_S^o$ increases as the solubilize chain length increases. This is a reasonable result, since a longer-chained solubilize is expected to have more difficulty fitting between the amphiphile tails. Finally, it should be noted that the magnitudes of $\mu_{S_{int}}^o - \mu_S^o$ listed for each alkane are quite small in comparison to the magnitude of the hydrophobic effect. The values of the free energy of transfer from water to a bulk alkane phase are approximately -13.1, -16.1, and -19.1 kT for hexane, octane, and decane, respectively.

The free energy model was used to predict, for each case studied, the radius of the solubilize core, the mole fraction of solubilize in the interfacial region, and the total number of amphiphile and solubilize molecules in the aggregate. These predictions were generated using the $\mu_{S_{int}}^o - \mu_S^o$ values listed in Table B.2. Figure B.7 shows the variation in solubilize core radius with SDS concentration for the solubilization of hexane. This result is typical. Figure B.8 shows the variation with SDS concentration of the mole fraction of solubilize in the interfacial region of the aggregate. The solubilize core radius and interfacial mole fraction are higher in the presence of added NaCl and increase more rapidly with SDS concentration when no NaCl is present. Both the core size and the interfacial solubilize mole fraction have been found to be inversely related to the length of the solubilize chain. (B.6)

Thus, when organic liquids are solubilized, a distinct solubilize core will often form. These swollen micelles are precursors of microemulsion solutions for which both water and oil-continuous regions simultaneously exist. To properly account for solubilization when a core forms, it is necessary to also consider the presence of solubilize molecules located between the tails of the amphiphile in the interfacial region.

The solubilization of hexane, octane, and decane by solutions of SDS has been investigated over a range of conditions. In modeling the results, the free energy of the solubilize in the interfacial region has to be adjusted to account for packing constraints imposed by amphiphile tails. The values of these free energy adjustments are consistent and reasonable with the constraints on packing the solubilize molecules. They decrease as the solubilize mole fraction and aggregate size increase.

The results also support the free energy model prediction that, for a given surfactant/solubilize combination, the mole fraction of solubilize depends

primarily on counterions in the solution. It is, however, necessary to account for both counterions contributed by the surfactant as well as those contributed by simply adding electrolyte. Once this is done, solubilization can be predicted.

References

- B.1. Nallikarjun, R., and Dadyburjor, D. B., J. Colloid Interface Sci. **84**, 73 (1981).
- B.2. Nagarajan, R., and Ruckenstein, E., Separations. Sci. Technol. **16**, 1429 (1981).
- B.3. Tanford, C., The Hydrophobic Effect: Formation of Micelles and Biological Membranes, 2nd Ed., John Wiley, New York City (1980).
- B.4. Stigter, D., J. Phys. Chem. **79**, 1015 (1975).
- B.5. Cutler, S. G., Meares, P., and Hall, D. G., J. Chem. Soc., Faraday Trans. 1 **74**, 1758 (1978).
- B.6. Oates, J. D., Ph.D. Dissertation, The University of Texas at Austin (1988).

Table B.1. Parameter Values in Model Calculations for Alkyl Sulfates at 25°C.

Surfactant	Literature CMC value	Aggregation Number Used in Calculation	σ (ergs/cm ²)	Value of F_{rep} With No Solubilize (kT)
C ₁₂ SO ₄ Na	8.1x10 ⁻³ (5)	62(6)	41.3	2.86
C ₁₂ SO ₄ Na, 0.20 M NaCl	9.0x10 ⁻⁴ (6)	101(6)	34.5	1.84
C ₁₂ SO ₄ Na, 0.50 M NaCl	5.2x10 ⁻⁴ (6)	142(6)	34.7	1.80

Table B.2. Values of $m_{S_{int}}^o - m_S^o$ (in kT) for the SDS Cases Studied.

(A) No NaCl

<u>SDS Concentration (M)</u>	<u>Solubilizate</u>		
	<u>Hexane</u>	<u>Octane</u>	<u>Decane</u>
0.025	0.24	0.33	0.37
0.050	0.22	0.29	0.35
0.100	0.18	0.28	0.32
0.150	0.16	0.26	0.30
0.200	0.15	0.25	0.28

(B) 0.2 M NaCl

<u>SDS Concentration (M)</u>	<u>Solubilizate</u>		
	<u>Hexane</u>	<u>Octane</u>	<u>Decane</u>
0.025	0.15	0.20	0.23
0.050	0.15	0.20	0.22
0.100	0.14	0.20	0.22
0.150	0.14	0.19	0.22
0.200	0.13	0.19	0.21

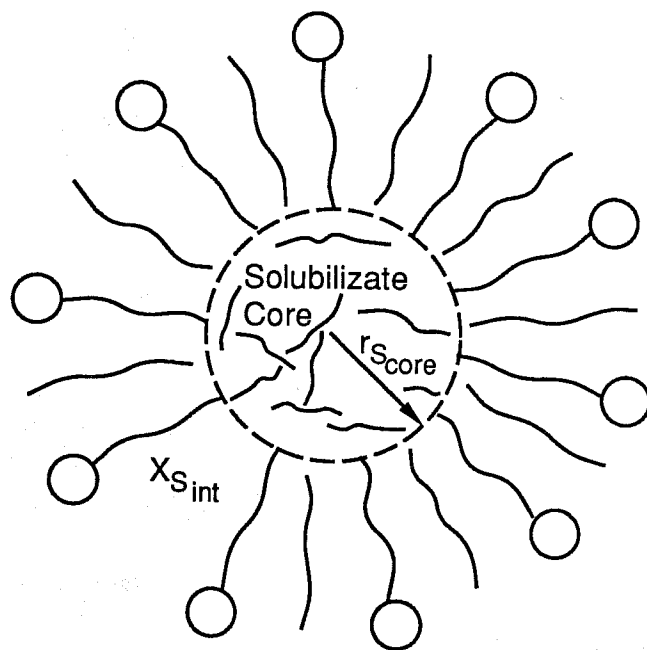


Fig. B.1. Model of aggregate with solubilize core.

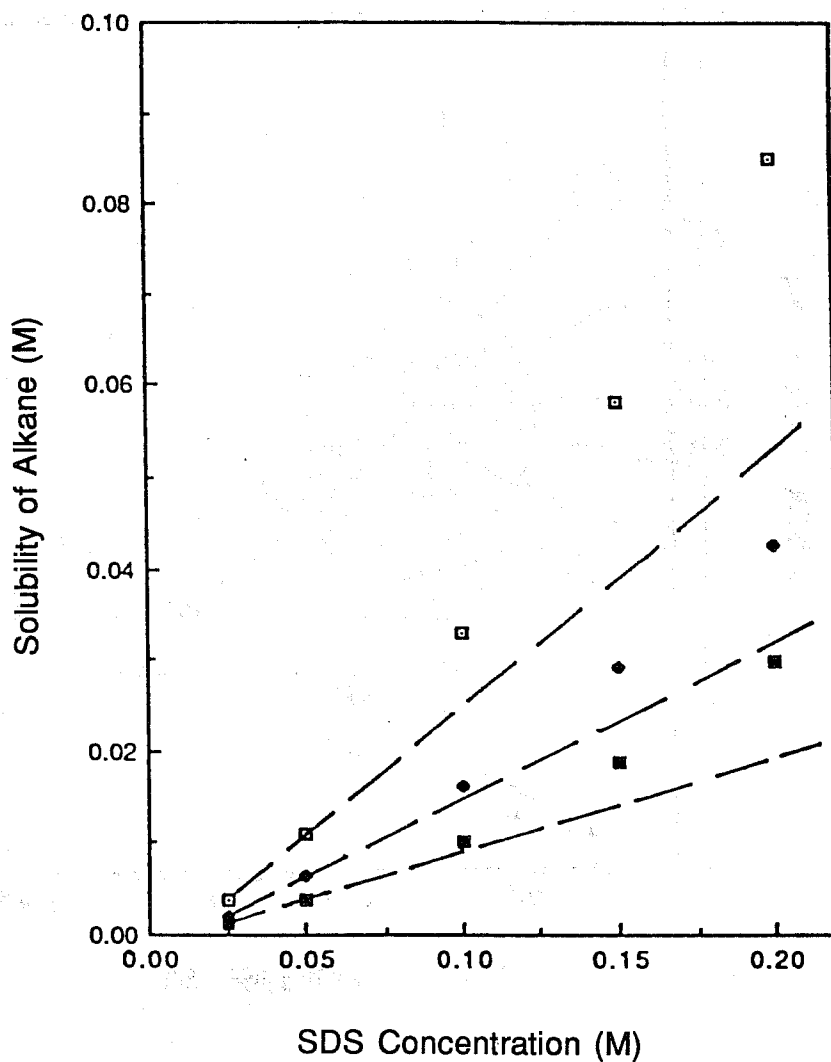


Fig. B.2. Variation in solubility of alkanes with SDS concentration in micellar SDS solutions containing no added NaCl; \square = hexane, \blacklozenge = octane, \blacksquare = decane. Dashed lines indicate expected solubilities if SDS concentration and alkane solubility were linearly related.

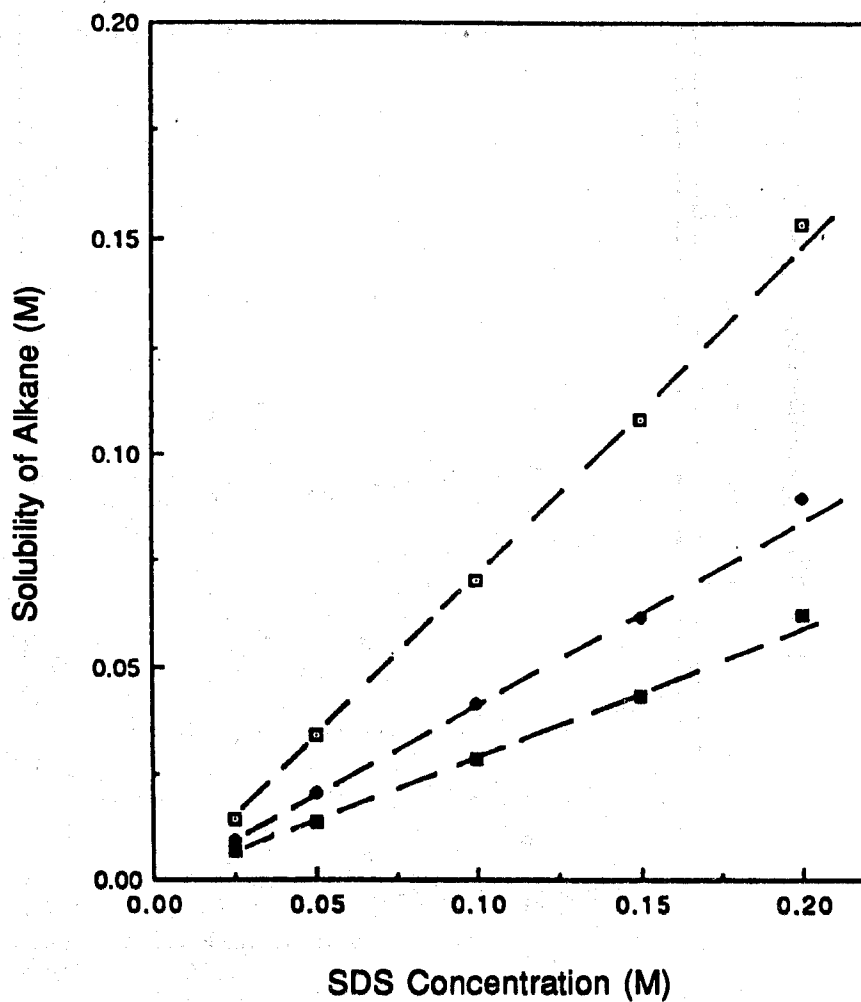


Fig. B.3. Variation in solubility of alkanes with SDS concentration in micellar SDS solutions containing 0.2 M NaCl; □ = hexane, ◆ = octane, ■ = decane.

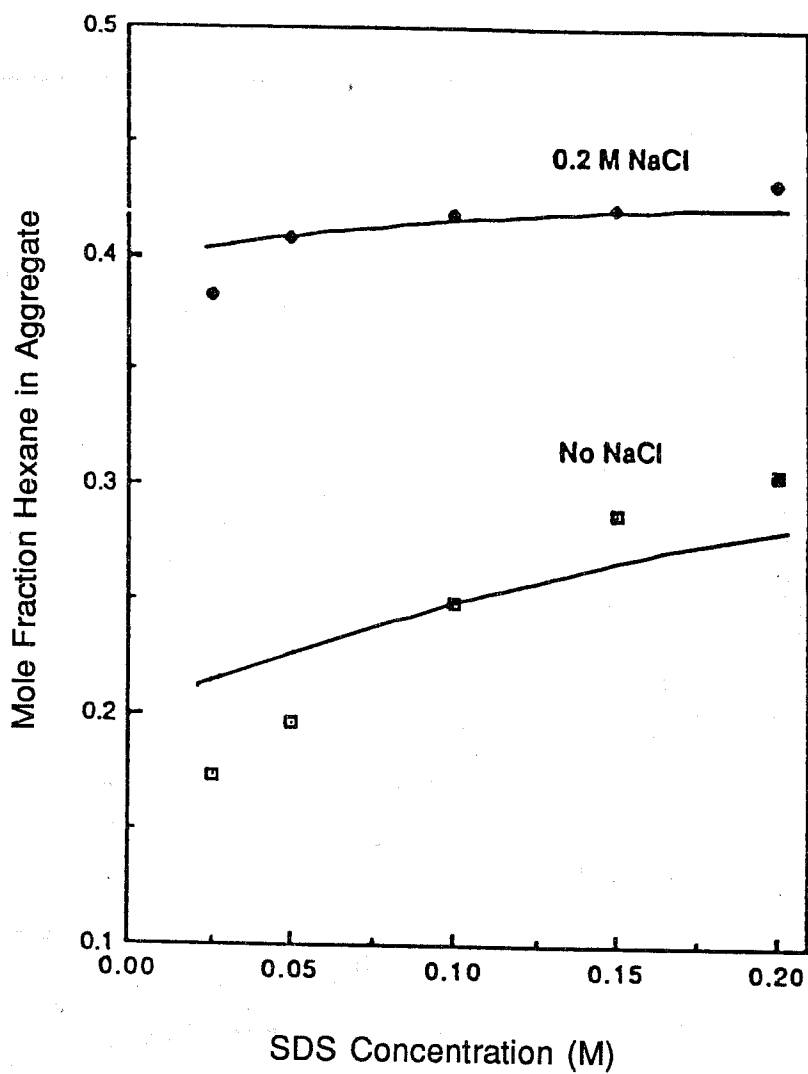


Fig. B.4. Variation in solubilizate mole fraction of hexane with SDS concentration at 25°C. Solid lines refer to model predictions with $\mu_{\text{int}}^{\circ} - \mu_{\text{S}}^{\circ} = 0.18 \text{ kT}$ for the no-NaCl case and 0.14 kT for the 0.2 M NaCl case.

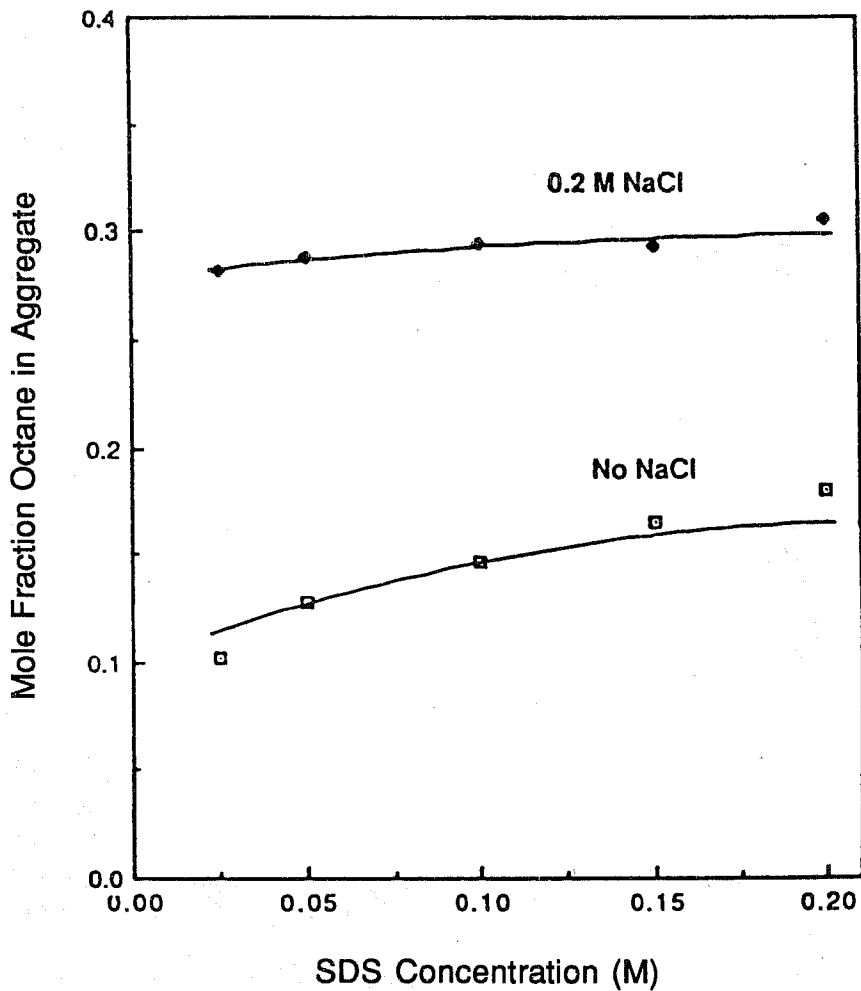


Fig. B.5. Variation in solubilize mole fraction of octane with SDS concentration at 25°C. Solid lines refer to model predictions with $\mu_{S_{int}}^o - \mu_S^o = 0.28 \text{ kT}$ for the no-NaCl case and 0.20 kT for the 0.2 M NaCl case.

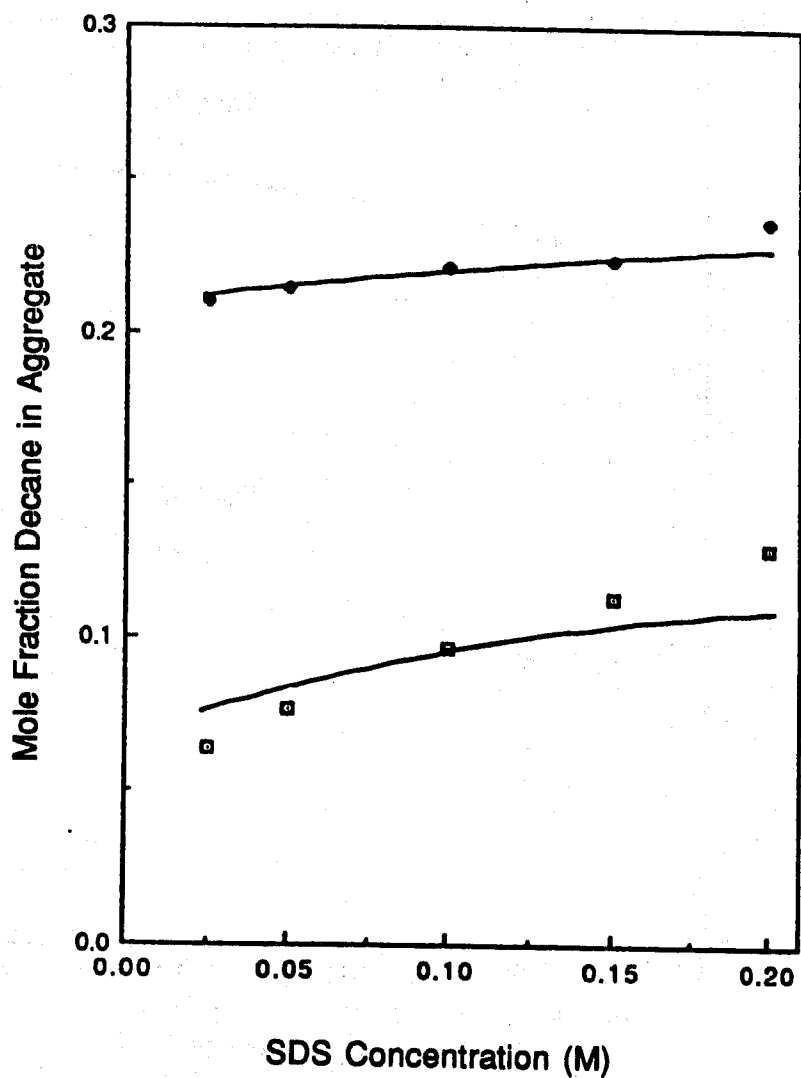


Fig. B.6. Variation in solubilize mole fraction of decane with SDS concentration at 25°C. Solid lines refer to model predictions with $\mu_{S_{int}}^{\circ} - \mu_S^{\circ} = 0.32 \text{ kT}$ for the no-NaCl case and 0.22 kT for the 0.2 M NaCl case.

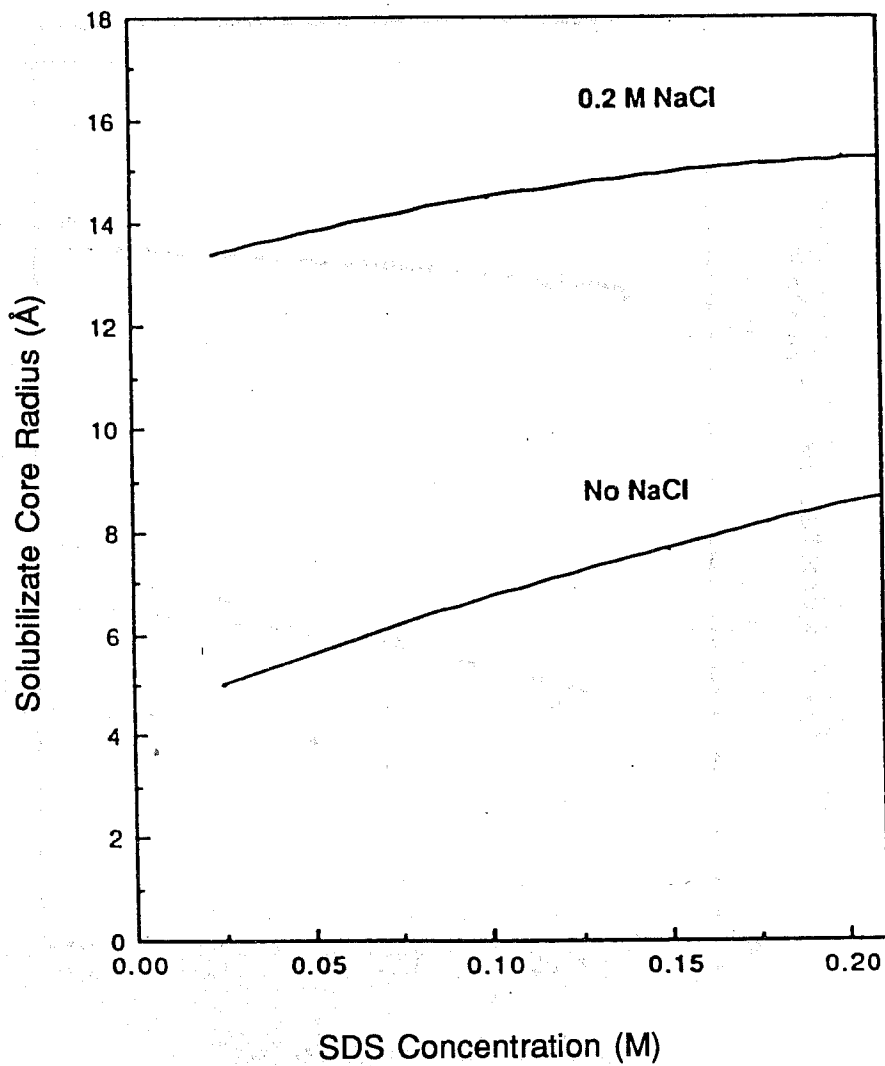


Fig. B.7. Predicted variation in radius of solubilize core with SDS concentration for hexane solubilization at 25°C.

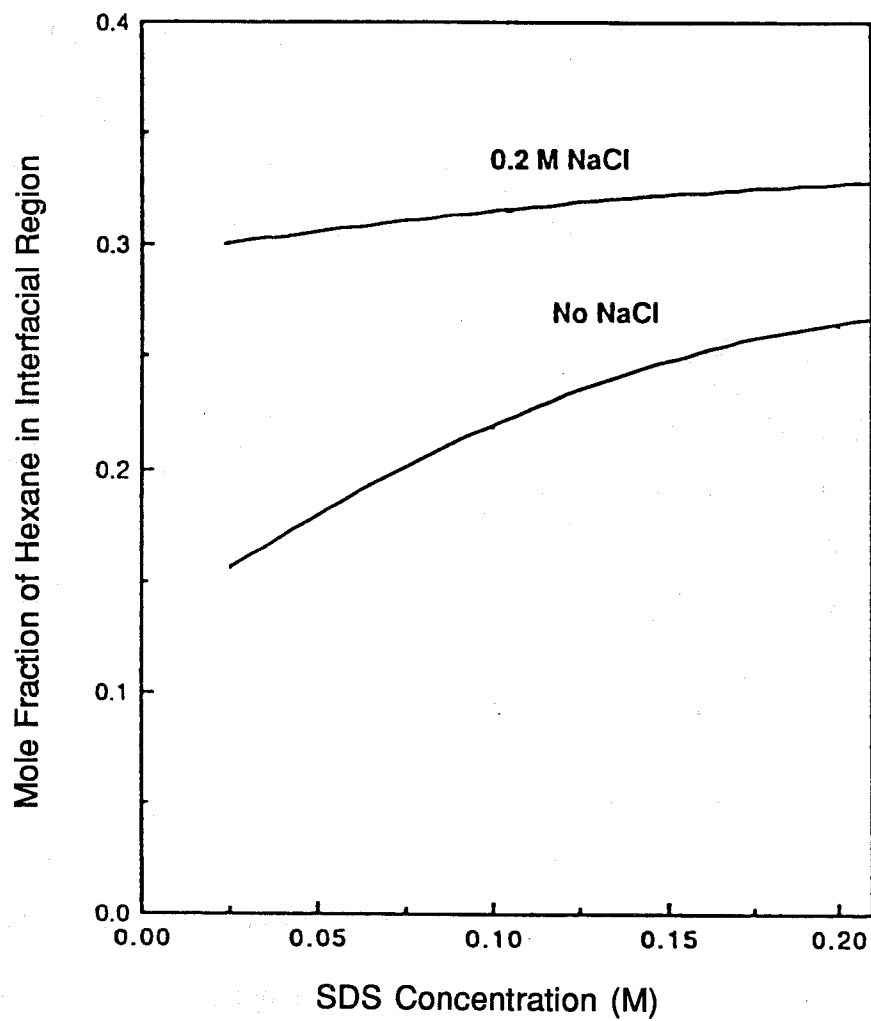


Fig. B.8. Predicted variation in mole fraction of solubilize in interfacial region with SDS concentration for hexane solubilization at 25°C.

C. The Permittivity of Microemulsions

The permittivity behavior of microemulsions has been the subject of some study. Comparison of the reported experimental results indicates considerable consistency among the values attesting to their basic reliability. The overwhelming bulk of the data relate to systems composed of anionic surfactants, water, and hydrocarbon at compositions below the conductivity percolation threshold. Thus, in a sense, the systems can be considered water-in-oil (W/O) microemulsions. While many researchers have investigated essentially the same systems and obtained wide agreement in the experimental trends, fundamental differences persist in the interpretation of trends.

A common interpretation involves calculating dielectric constants of equivalent heterogeneous materials.^(C.1-C.4) The Maxwell-Wagner equation predicts the dielectric constant of a composite of noninteracting spherical particles dispersed in a continuum.^(C.1,C.2) One can also include the effect of particle shape or the effect of conductivity that causes interfacial polarization and gives rise to an additional dielectric relaxation at a frequency different than those characteristic of the components. The theories for dispersions of one discontinuous phase in another continuous phase cannot model the observed permittivity behavior of many microemulsion systems.

Some researchers explain the permittivity behavior in purely qualitative terms. Boned et al.^(C.5) have reported using conductivity and dielectric constant data to detect structural transitions in a potassium oleate/hexanol/water/hexadecane system. They investigated the one-phase region of the phase diagram and have hypothesized that, within this region, there exist three different solubilization modes of water. No attempt was made to model the data quantitatively, but the proposal of structural transitions is an important one.

Eicke et al.^(C.6) have recently suggested that fractal clusters form that create an effective volume fraction of reverse micelles larger than the actual micelle volume fraction. Van Dijk et al.^(C.7) have also proposed a clustering model. They have modeled data from an AOT/water/isooctane system in which the dielectric constant and conductivity of a microemulsion increases with temperature. To explain this result, van Dijk et al. postulate that there is an energy barrier to clustering that must be overcome. This is not intuitive, since attractive forces become less and less important as temperature is raised. In addition, we have found that the dielectric constant and conductivity decreases with increasing temperature in nonionic microemulsions.^(C.8) This is exactly opposite to the anionic case, but it does follow well-known trends in phase behavior for the differing systems.

Not all researchers subscribe to the above-outlined view of clustering. Some recognize that the inversion from water-in-oil to oil-in-water cannot occur suddenly.^(C.9-C.13) Robbins^(C.9) has proposed a model that postulates the coexistence of water and oil-continuous domains. In a similar fashion, Lam^(C.13) has proposed that a microemulsion may be viewed as a mosaic of oil and water-continuous domains. It is, in fact, Lam's model that is adopted to model the permittivity results reported here.

A model is proposed for the permittivity of W/O microemulsions that explains all the observed phenomena, the high values of the dielectric constant, and the dielectric relaxation. Furthermore, we show that it is possible to estimate roughly the sizes of reverse micelles provided accurate permittivity measurements can be made in the appropriate frequency range. The experimental data reported here show clearly that the basic trends in the dielectric constants of sodium di-2-ethylhexylsulfosuccinate(AOT)/water/hydrocarbon systems are correlated with the trends of the underlying microemulsion phase behavior.

The equation that will be used extensively in this report has been derived by Günther and Heinrich based on the premise that any distribution of charge can be represented by a system of multipoles.^(C.14) Their result for the dielectric constant of a monodisperse system of spherical particles randomly distributed in a dielectric medium is

$$\epsilon = \epsilon_2 \frac{(1-k) \left[3 + 2 \left(\frac{\epsilon_2}{\epsilon_1} - 1 \right) \right] - 2\phi_1 \left(\frac{\epsilon_2}{\epsilon_1} - 1 \right)}{(1-k) \left[3 + 2 \left(\frac{\epsilon_2}{\epsilon_1} - 1 \right) \right] + \phi_1 \left(\frac{\epsilon_2}{\epsilon_1} - 1 \right)} \quad [\text{C.1}]$$

where

$$k = \frac{1}{3} \frac{\left(\frac{\epsilon_2}{\epsilon_1} - 1 \right)^2}{3 + 2 \left(\frac{\epsilon_2}{\epsilon_1} - 1 \right)} \sum_{\ell=1}^{\infty} \frac{\ell(\ell+1)C_{\ell}}{1 + \frac{\ell+1}{2\ell+1} \left(\frac{\epsilon_2}{\epsilon_1} - 1 \right)} \quad [\text{C.2}]$$

and C_{ℓ} 's are related to the radial distribution function. For a random distribution, the values of the C_{ℓ} 's calculated by Günther and Heinrich are given in Table C.1. The dielectric constant given by Eq. [C.1] is in general agreement with the Bruggeman equation at small to moderate disperse-phase volumes (see Fig. C.1). This equation is expected to be highly accurate because of the few assumptions imposed in its derivation. It shows that the dielectric constant depends only on the dielectric constants of the disperse and continuous phases, respectively, and the disperse-phase volume fraction. There are no other parameters.

The concept of accounting for the presence of the counterions inside reverse micelles and their effect on the permittivity behavior of W/O microemulsions was

introduced by Chou and Shah.^(C.15) They have incorporated Schwarz's theory of double-layer polarization^(C.16) into the Maxwell-Wagner theory, considering the interfacial double-layer within the reverse micelle as a thin shell and calculating two relaxation times. De Rozieres et al.^(C.17) adopted this view and have calculated both the polarizability and the critical frequency of an isolated reverse micelle in an oscillating electric field. They find that micelles are highly polarizable due to the mobility of the counterions in the micelle interior. Thus, the value of the dimensionless polarizability (Q) defined by

$$\alpha = 4\pi\epsilon_0 a^3 Q \quad [C.3]$$

where α is the polarizability, ϵ_0 is the permittivity of vacuum, and a , the radius of the reverse micelle, is close to unity. The polarizability of a conducting sphere corresponds to $Q = 1$. The critical frequency reported by de Rozieres et al.^(C.17) represents the point at which the diffusion rate of the ions through the aqueous interior becomes a limiting process.

Since swollen reverse micelles are highly polarizable, it might be thought that the dielectric constant of the system will be comparable to a random dispersion of highly conducting spheres. The dielectric constants of an Aerosol-OT/water/isooctane system with a water-to-AOT molar ratio of 25 and temperature of 35°C^(C.7) are shown as a function of the particle volume fraction (f_{water} for a W/O microemulsion) in Fig. 1 and compared with predictions of the three different theories. This comparison is typical. Except for very small volume fractions, the measured values of the dielectric constant are substantially larger than predicted by the equations. Also shown in Fig. C.1 are the data for a dispersion of mercury drops in castor oil.^(C.18) Notice that the dielectric constant of the dispersion of mercury drops is less than that of a microemulsion containing the

same volume fraction of water. This is a striking result. The Günther and Heinrich equation predicts permittivities that compare well with the experiment for a dispersion of conductors but underestimate the dielectric constant of microemulsions even though it has been shown that reverse micelles are essentially conducting spheres. It seems, therefore, that the model of a microemulsion composed of a dispersion of spherical drops must be rejected except for very small disperse-phase volumes.

The inadequacy of the theories has been recognized by Peyrelasse and Boned.^(C.19) They have used an extension of the Bruggeman equation that allows for ellipsoidal drops^(C.19,C.20) and introduces into the equation a parameter related to the axial ratio of the ellipsoids.^(C.20,C.21) The procedure is strictly empirical; the ellipsoidal shape has not been confirmed by any independent experiment and, furthermore, thermodynamic considerations suggest that spheres, not ellipsoids, are preferred. Thus, while it may be possible to fit dielectric constants using an ellipsoidal model, it seems unlikely that the shapes so obtained are real.

Morphology of Microemulsions: A Very Brief Review

Many previous studies of the permittivity of microemulsions have involved sophisticated experimental techniques and very reliable data have been obtained for the effects of temperature, salinity, hydrocarbon media, and composition. But, the results have generally been interpreted without serious consideration as to the influences of these variables on changing microstructure. Peyrelasse and Boned^(C.19) report results from an experiment with AOT, water, and several hydrocarbons in which the differences in the dielectric constants caused by simply changing the hydrocarbon medium is remarkable. These systems are presumed to be oil-continuous solutions of reverse micelles, yet the dodecane system exhibits a dielectric constant ($\epsilon = 31.8$) nearly seven times larger than the cyclohexane system ($\epsilon = 4.85$) with the same water-to-surfactant molar ratio ($W_s = 6$) and

disperse-phase volume fraction [$\phi_d = 0.3$ ($\phi_d = \phi_{AOT} + \phi_{water}$; $\phi_{water} = 0.065$)]. This evidence clearly demonstrates the importance of knowing the phase behavior to understanding the permittivity of microemulsions.

There is as yet no coherent theory relating the morphology of the microstructure of microemulsions to their physical properties.^(C.22) At the extreme of either large volume-fraction or small volume-fraction water are found oil-swollen micelles or water-swollen reverse micelles, respectively. Under certain conditions it is possible to continuously vary the water-to-oil ratio while maintaining a single-phase isotropic thermodynamically stable microemulsion. This continuous variation may extend from one side of the phase diagram to the other, as shown by Fig. C.2. Thus, in some cases there exists a continuity of states each differentially different from the preceding one that extends from micelles to reverse micelles. This implies that there are intermediate states for which the classifications water and oil continuous are meaningless. Neither term can adequately describe the microstructure of these microemulsions. Scriven has called these intermediate states bicontinuous.^(C.23) They can also be thought to represent an inversion zone. In Fig. C.2, those states that are neither water nor oil continuous are depicted as shaded regions.

The position of the inversion zone will change depending on the underlying phase behavior as depicted by Fig. C.2. For a Winsor Type I system, the inversion zone is positioned near the surfactant-oil leg of the ternary diagram. The inversion zone shifts toward the surfactant-water leg of the triangle as the system is varied from Type I to Type II. This change can be accomplished by altering any one of a number of formulation variables.^(C.22) These are listed in Table C.2.

The extent of the inversion zone is not now known. Figure C.2 depicts it as roughly a rectangular region, but this should not be accepted as correct since its extent should certainly depend on a number of factors.^(C.24) Furthermore, several

different types of measurements will be required to define its extent. It is contended, however, that the portion of the inversion zone to the right of the conductivity percolation threshold (shown as a vertical line) can be mapped using dielectric measurements. As a corollary, the deviation of the dielectric behavior of microemulsions from that exhibited by a collection of conducting spheres is due to the onset of bicontinuous behavior. Thus, our model presumes, as did Lam et al.,^(C.24) that a microemulsion at compositions within the inversion zone consists of a mosaic of oil and water-continuous regions. If β is defined as the fraction of the microemulsion volume that is water continuous, then β will increase at a given phase volume of water whenever the alkane carbon number and the temperature are increased or the electrolyte concentration and surfactant lipophile are decreased, since according to Table C.1, these factors yield a Type II \rightarrow Type I transformation.

In this work, we study the effect of changing the alkane carbon number (ACN) and temperature in AOT/water/alkane solutions. The dielectric constants of octane, decane, and undecane microemulsions with varying disperse-phase volume fractions are reported. One decane solution was selected for studying the temperature dependence of the permittivity. The relative sizes of the reverse micelles in dilute solution are determined using a Taylor-dispersion experiment with a radioactive tracer.^(C.13) Partial phase diagrams are constructed from solubilization experiments. We conclude that, as the disperse-phase volume fraction is increased, the microemulsions transform slowly from a microstructure that is oil continuous to one that is bicontinuous, as the compositions enter the inversion zone. Additionally, as the temperature or the ACN are increased for a given composition, the inversion zone and conductivity percolation threshold move toward the surfactant-oil leg of the phase diagram. These transitions can be

observed by measuring the changing permittivity behavior and conductivities of the solutions.

Results

A typical partial phase diagram for AOT/water/alkane systems is shown in Fig. C.3. In the center region of the phase diagram, solutions are clear and very viscous. To better understand the effect of ACN on the phase behavior, we determined the maximum water solubilized at 25°C by solutions of 10 wt% AOT in the series ACN = 6 to ACN = 12. The results are plotted in Fig. C.4. Octane is the optimum alkane, solubilizing the greatest amount of water; therefore, on its phase diagram, the border between the one and two-phase regions that extend from the oil vertex toward the surfactant-water leg will be down closest to the oil-water leg.

The dielectric constants of the octane, decane, and undecane microemulsions are plotted versus water-plus-AOT volume fraction ($\phi_w = 0.536 \phi_d$) in Fig. C.5. For given fractions of water, the octane system exhibits the lowest dielectric constant, while the undecane system exhibits the highest. In all cases, the specific conductivities were lower than 2 mmho/cm and did not show any trend.

Figures C.6a and C.6b show the results of varying the temperature on the AOT/water/decane sample with $\phi_d = 0.15$ ($\phi_w = 0.078$). The solution remains clear throughout the experiment and does not have the bluish tint of a middle-phase microemulsion. In Fig. C.6a, the dielectric constants at 0.1 MHz are plotted versus the temperature. We see that, as temperature increases, both the conductivity and the permittivity increase. However, for the highest two temperatures, the dielectric constant plateaus and then decreases. This same type of behavior was also observed by van Dijk^(C.25,C.26) in his extensive series of experiments with AOT/water/isooctane and by Peyrelasse and Boned.^(C.19) Van Dijk also observed similar trends in permittivity and conductivity when the disperse-phase volume fraction was raised to very large values, $\phi_d = 0.40$ at constant temperature.^(C.7,C.26)

In both our case and van Dijk's case, the apparent maxima are spurious artifacts of the experimental method. Because the conductivities are so large, the measuring circuit is dominated by the inductance and the susceptance is no longer capacitive. The practical conductivity limit of the apparatus is 50 $\mu\text{micromho/cm}$. As conductivity rises above 50 $\mu\text{micromho/cm}$, the dielectric constants measured are increasingly underestimated. Van Dijk^(C.27) mentions this limitation when describing his experimental set-up but reports dielectric constants for solutions with conductivities three times greater than the limiting conductivity of his apparatus (500 $\mu\text{micromho/cm}$), including those exhibiting a maximum. This also explains why Peyrelasse and Boned observed apparent maxima in the critical frequencies of dielectric relaxation.^(C.19)

In Fig. C.6b, the permittivity is plotted versus frequency. Dielectric relaxation appears in the frequency range 0.1 to 1 MHz for temperatures greater than 44°C. For both the 49 and 52°C solutions, the observed permittivities are decreasing at the lowest frequencies scanned. This is a clear indication of electrode polarization and shows that the solutions are water continuous; ions in the solution are sufficiently mobile to polarize oppositely-charged electrodes. The steep increase in the conductivity and the onset of electrode polarization leads us to conclude that continuous paths through water-continuous regions extend from one electrode to the other at about 49°C, the percolation threshold.

The diffusion coefficients of the radioactively-tagged SDBS* are plotted versus the disperse-phase volume fraction in Fig. C.7. For the dilute system, far from the bicontinuous region of the phase diagram, the diffusion coefficients are greatest in the octane-based microemulsion and smallest in the undecane-based microemulsion. If we assume that the reverse micelles in these dilute solutions are spherical and monodisperse, we can use the Stokes-Einstein equation to calculate

the reverse micelle radii. The diffusion coefficients indicate that the reverse micelle size increases with increasing ACN.

The diffusion coefficients decrease as the disperse-phase volume fraction goes from 0.05 to 0.10. We need to be very careful about how we interpret these data. There are at least three possible reasons for this trend. First, the size of the drops may increase. Also, interactions between particles can cause a decrease in the measured diffusion coefficient. Finally, it is possible that some structural changes occur, as ϕ increases, that cause a decrease in the measured diffusion coefficient.

Proposed Model

As was discussed above, investigators have proposed attractive interactions between micelles to explain light-scattering spectra but this cannot fully explain the dielectric behavior. Furthermore, we have found that the dielectric constant of nonionic microemulsions decreases with increasing temperature.^(C.8) This finding leads us to conclude that submicroscopic changes in the structural morphology, not strong interactions between reverse micelles, is the origin of the dielectric phenomena observed.

It has been assumed previously that the disperse phase consists only of reverse micelles and that all the water is contained in an oil-external domain. However, the data indicate an apparent water fraction that is much larger than the fraction of water actually in the microemulsion. This paradox may be understood by taking into account the possibility of water-external domains containing large amounts of oil. Figure C.8 illustrates the proposed idea. The domains A and B contain X_w volume fraction of water. Domain A is oil continuous and will exhibit a low dielectric constant while domain B is water continuous (of as yet undefined morphology) and will exhibit a high dielectric constant. Suppose that B domains comprise 25% of a solution and A domains the other 75% as pictured in Fig. C.8b.

The solution is macroscopically oil continuous; however, the large water domains (B) are dispersed in a continuum that is not 100% oil. The overall dielectric constant of the solution will be affected by this change in morphology.

The dielectric constant of the background phase in Fig. C.8b is precisely determined by Eq. [C.1]. Using the dielectric constant calculated for the background, the dielectric constant of the whole system can be found by substituting $\beta = 0.25 (= \phi_1)$ and $\epsilon_2 = \epsilon_{\text{cont}}$ into the appropriate theory. The macroscopic dielectric constant is a measure of the volume fraction of O/W domains that coexist with W/O domains in oil-continuous microemulsions. This gives an estimate of how far into the phase-inversion zone a particular system is. At some point in the phase-inversion zone, the conductivity percolation threshold will be crossed. The value of β at this transition may vary but is expected to be between about 0.3 and 0.6.

The experimental evidence shows that, as the temperature, alkane carbon number, and the water-plus-AOT fraction increase, these microemulsions become bicontinuous exhibiting properties of both W/O and O/W systems. This transition to bicontinuity does not occur suddenly. Instead, a microemulsion transforms gradually from being a dispersion of reverse micelles in oil to a distribution of water and oil-continuous domains as the inversion zone moves toward the oil-surfactant leg of the phase diagram or as the compositions move into the inversion zone. In cases when the microemulsions become conducting, they have crossed the conductivity percolation threshold, which is a distinct boundary within the inversion region.

Two features of Figs. C.6a and C.6b appear significant. At temperatures above 47°C, the dielectric constant displays large low-frequency values that decrease rapidly with frequency and level off at frequencies above 100 kHz. This is the result of electrode polarization, indicating the sample is at least partially

water continuous. Secondly, the dielectric constant drops abruptly after reaching a maximum value, although the conductivity is still increasing, indicating a fundamental change in the geometry of the system.

We now analyze the data using this new picture of the possible microemulsion microstructure. Systems with low conductivities will be considered macroscopically oil continuous; so many more W/O domains exist than O/W domains that no conduction occurs across the solution. The number of O/W domains is below the percolation threshold. Secondly, the O/W domains will be considered perfectly polarizable--that is, conducting. Finally, we consider the O/W domains to be approximately spherical. Using a theory for the dielectric constant of a heterogeneous material of spheres in a nonconducting medium, we determine the dielectric constant of the oil continuum [$\epsilon_{\text{cont}} = \epsilon(\phi_1 = \phi_w, \epsilon_1, \epsilon_{\text{oil}})$] and then, using this value and the measured dielectric constant of the solution, back-calculate from the equation [$\epsilon_{\text{micro}} = \epsilon(\phi_1 = \beta, \epsilon_1, \epsilon_{\text{cont}})$] the volume fraction of O/W domains β .

Using Eq. [C.1] as the basis and assuming that the water-continuous domains are conductive ($\epsilon_1 \rightarrow \infty$), the dielectric constants of the oil continua and the volume fractions of water-continuous domains (β 's) are calculated using the experimental data in Figs. C.5 and C.6. The β 's are plotted in Figs. C.9 and C.10. Notice in Fig. C.9 that the β 's are very small for $\phi_w = 0.025$ and increase with increasing ϕ_w . The β for the dodecane system increases most rapidly. In Fig. C.10, β is plotted versus temperature for the AOT/water/decane experiment with $\phi_w = 0.078$. It appears to be approaching an asymptote at 44°C and β is quite large, equal to 0.6. Values of β for the higher temperatures were greater than unity. The onset of bicontinuity is reflected in this result.

We now consider dielectric relaxation in microemulsions. The critical frequency for dielectric relaxation is related to the time it takes to fully polarize a

material. The polarizability of the water domains is due to the presence of ions in solution. The ions have finite mobility and a limited space in which to travel. At low frequencies, the ions can travel all the way across a water domain, fully polarizing the domain, before the direction of the imposed field changes. At high frequencies, the ions cannot respond fast enough to keep up with the oscillations in the field. In this latter case, the polarization of the water domain is due only to the field's effect on the water molecules. The critical frequency is that intermediate frequency where the ions move continuously back and forth across the domain, causing maximum energy dissipation (due to friction). The larger the distance the ions can travel, that is the larger the water domain, the longer it takes to polarize the domain and the lower the critical frequency will be.

De Rozieres et al.^(C.17) have derived an equation for the critical frequency, which is a linear function whose slope (m) depends on the ratio of the permittivities ϵ_1/ϵ_2 .

$$\frac{2\pi a^2}{D_{\text{ion}}} f_c = b + m \left(\frac{N_{\text{agg}} e^2}{4\pi a \epsilon_0 \epsilon_w kT} \right) \quad [\text{C.4}]$$

where N_{agg} is the number of surfactant head groups on the reverse micelle surface, D_{ion} is the diffusion coefficient of the counterions, e is the elementary unit of charge, and b is the intercept. From the plot for $\epsilon_1/\epsilon_2 = 35$, we find $b \approx 8$ and $m \approx 2$. We know that the AOT head group covers approximately 69 Å of interfacial surface area at 25°C.^(C.22) Using the value $D = 2 \cdot 10^{-9} \text{ m}^2/\text{sec}$ and substituting appropriate values for the constants, we find

$$f_c \approx \frac{2.5 \cdot 10^{-8}}{a^2} + \frac{9.1}{a} \quad [\text{C.5}]$$

where f_c has units of Hz and a has units of meters.

Assuming that the relation holds approximately for the water domains, then the critical frequency characterizes the average distance across the water domains. In our model, as the system becomes bicontinuous, more and more domains are water continuous and the likelihood of O/W domains being adjacent increases so the observable size of the O/W regions increases. Therefore, we expect decreasing critical frequencies with increasing disperse-phase volume fraction and with increasing temperature because these changes in the formulation variables induce phase inversion. This is what is found.

For the AOT/water/dodecane($W_S = 10$) system, Peyrelasse and Boned^(C.19) report that the critical frequency decreases precipitously as the fraction of water increases. They were apparently unable to determine the critical frequencies for the lowest volume fractions ($\phi_w < 0.024$), but the values span a two-decade range from 2 to 105 MHz. Applying Eq. [C.5], we can estimate the sizes of the O/W domains. For $\phi_w = 0.024$ ($\epsilon = 3.84$), the average size of the O/W domains is about 900 Å. For $\phi_w = 0.030$ ($\epsilon = 7.68$), the size of the domains has increased to 1600 Å. For $\phi_w = 0.041$ ($\epsilon = 19.5$), the size increases to almost 10^{-1} cm at the percolation limit. Because Eq. [C.4] was derived by considering a single inverted micelle in an electric field, it is not known what errors are incurred in applying Eq. [C.5] to determine the domain size; however, the values found here appear quite reasonable. It is desirable to confirm these values by some independent experimental means.

At very low volume fractions, where β is nearly zero, one may expect to find no relaxation in the frequency region (< 400 MHz) examined by Peyrelasse and Boned,^(C.19) and, indeed, none is reported for ϕ_w less than 0.024. If dielectric loss could be measured accurately in the frequency range 0.1 to 10 GHz, dielectric relaxation, due to the reverse micelles, should be observed. In that case, it would be possible to determine the micelle size, provided one used proper values of the

surface area covered by a surfactant head group, the water dielectric constant, and the counterion diffusion coefficient.

Independent experimental confirmation of our model is required. Recently, Jahn et al.^(C.28) published freeze-fracture electron micrographs of nonionic and AOT microemulsion systems. The pictures of the nonionic systems reveal a definite transition from water-continuous to bicontinuous to oil-continuous structures as the oil fraction is increased. Unfortunately, the experiment on the AOT system was performed at 15°C with D₂O instead of H₂O. Both low temperature and substitution of D₂O promote Type II behavior, moving the inversion zone to the left on the phase diagram; and the micrographs show what appear to be densely-packed reverse micelles.

Conclusions

Permittivity experiments can be used to study the structure of oil-continuous microemulsions. However, it is of utmost importance to recognize that formulation variables strongly affect the underlying phase behavior and, thus, the permittivity behavior observed. The dielectric constant plotted versus variables, such as temperature or alkane carbon number, gives an indication of the proximity of the microemulsion system to the phase-inversion region and the conductivity percolation threshold. Previous attempts to model dielectric constants of W/O microemulsions have been unsatisfactory because investigators have ignored these effects of phase behavior. With anionic surfactant systems, only when the formulation variables are adjusted to move the inversion zone away from the surfactant-oil leg of the phase diagram and the composition of interest is it correct to describe an oil-continuous microemulsion simply as reverse micelles dispersed in an oil continuum. As long as the dielectric constant of a microemulsion is roughly equal to that of an equivalent mercury-in-oil system, the microemulsion can be pictured as a dispersion of polarizable reverse micelles, the model parameter β

being equal to zero. But, when the dielectric constant is larger than that of a mercury-in-oil system, fluctuations in structure caused by the onset of phase inversion must be considered and the β is no longer zero. Critical frequency quantifies the size of the water domains. When β is zero, only the dielectric relaxation due to the reverse micelles may be observed; the critical frequencies should be in the range of 1 GHz. With the onset of phase inversion, a critical frequency will be observed in the 1 to 100 MHz range, indicating the presence of extended water domains.

The model presented explains the experimental trends in dielectric constants and critical frequencies in detail. Additional experimental confirmation of the model will require the independent observation of large water domains present simultaneously with reverse micelles in oil-continuous microemulsions. Experiments that may confirm our model include viscosity, freeze-fracture microscopy, and spectroscopy experiments. Spectroscopic data, in particular, should be carefully analyzed. It is possible that previous results have been misinterpreted and unusually large micelle-micelle interaction energies postulated because the presence and effect of the inversion zone has been ignored.

References

- (C.1) Maxwell, J. C., A Treatise on Electricity and Magnetism, Vol. 1, 3rd Ed., Clarendon Press, Oxford (1892).
- (C.2) Wagner, K. W., Arch. Elektrotech. **2**, 371 (1914).
- (C.3) Clause, M., "Dielectric Properties of Emulsions and Related Systems," in Encyclopedia of Emulsion Technology (Paul Becher, Ed.), Marcel Dekker, Inc., New York (1983).
- (C.4) Dukhin, S. S., "Dielectric Properties of Disperse Systems," in Surface and Colloid Sci. (Egon Matijevic, Ed.), Vol. 3, Wiley-Interscience, New York (1971).

- (C.5) Boned, C., Clause, M., Lagourette, B., Peyrelasse, J., McClean, V.E.R., and Sheppard, R. J., J. Phys. Chem. **84**, 520 (1980).
- (C.6) Eicke, H. F., Geiger, S., Sauer, F. A., and Thomas, H., Ber. Bunsenges. Phys. Chem. **90**, 872 (1986).
- (C.7) van Dijk, M. A., Broekman, E., Joosten, J.G.H., and Bedeaux, D., J. Physique **47**, 727 (1986).
- (C.8) Middleton, M. A., Schechter, R. S., and Johnston, K. P., Langmuir, accepted for publication.
- (C.9) Robbins, M. L., in Micellization. Solubilization. and Microemulsions (K. L. Mittal, Ed.), Vol. 2, Plenum Press, New York (1977).
- (C.10) Kaler, E., Bennett, K. E., Davis, H. T., and Scriven, L. E., J. Chem. Phys. **79**, 5673 (1983).
- (C.11) Chang, N. J., and Kaler, E., Langmuir **2**, 184 (1986).
- (C.12) Robbins, M. L., and Bock, J., J. Colloid Interface Sci. **124**, 462 (1988).
- (C.13) Lam, A. C., Ph.D. Dissertation, The University of Texas at Austin (1986).
- (C.14) Günther, K., and Heinrich, D., Zeitschrift für Physik **185**, 345 (1965).
- (C.15) Chou, S. I., and Shah, D. O., J. Phys. Chem. **85**, 1480 (1981).
- (C.16) Schwarz, G., J. Phys. Chem. **66**, 2636 (1962).
- (C.17) de Rozieres, J., Middleton, M. A., and Schechter, R. S., J. Colloid Interface Sci. **124**(2), 407 (1988).
- (C.18) Guillien, R., Annales de Physique, **16**, 205 (1941).
- (C.19) Peyrelasse, J., and Boned, C., J. Phys. Chem. **89**, 370 (1985).
- (C.20) Reynolds, J. A., and Hough, J. M., Proc. Phys. Soc. **70B**, 769 (1957).
- (C.21) Boned, C., and Peyrelasse, J., J. Phys. D: Appl. Phys. **16**, 1777 (1983).
- (C.22) Bourrel, M., and Schechter, R. S., Microemulsions and Related Systems, Marcel Dekker, Inc., New York (1988).
- (C.23) Scriven, L. E., Nature **263**, 123 (1976).

- (C.24) Lam, A. C., Falk, N., and Schechter, R. S., J. Colloid Interface Sci. **120**(1), 30 (1988).
- (C.25) van Dijk, M. A., Casteleijn, G., Joosten, J.G.H., and Levine, Y. K., J. Chem. Phys. **85**(1), 626 (1986).
- (C.26) Dijk, M. A., Phys. Rev. Lett. **55**(9), 1003 (1985).
- (C.27) van Dijk, M. A., Ph.D. Dissertation, University of Utrecht, The Netherlands (1986).
- (C.29) Jahn, W., and Strey, R., P. Phys. Chem. **92**, 2294 (1988).

Table C.1. C_ℓ for Multiple Theory.

ℓ	C_ℓ
1	$0.2258 \phi_r (1 - \phi_r)$
2	$0.0500 \phi_r (1 - \phi_r)$
3	$0.01002 \phi_r (1 - 0.7518 \phi_r)$
4	$0.002962 \phi_r (1 - \phi_r)$
5	$0.000736 \phi_r (1 + 2.677 \phi_r)$
6	$0.0001835 \phi_r (1 - \phi_r)$
7	$0.00004583 \phi_r (1 + 1.078 \phi_r)$
8	$0.00001145 \phi_r (1 - \phi_r)$
9	$0.000002862 \phi_r (1 - 0.9994 \phi_r)$

Note: $\phi_r = \phi/\phi_m$ where $\phi_m = 0.7405$.

Table C.2. Factors Inducing Type I to
Type II Transition AOT/Water/
Hydrocarbon Systems.

Decreasing alkane carbon number.

Decreasing temperature.

Increasing electrolyte composition.

Increasing surfactant lipophile length.

Increasing branching of surfactant.

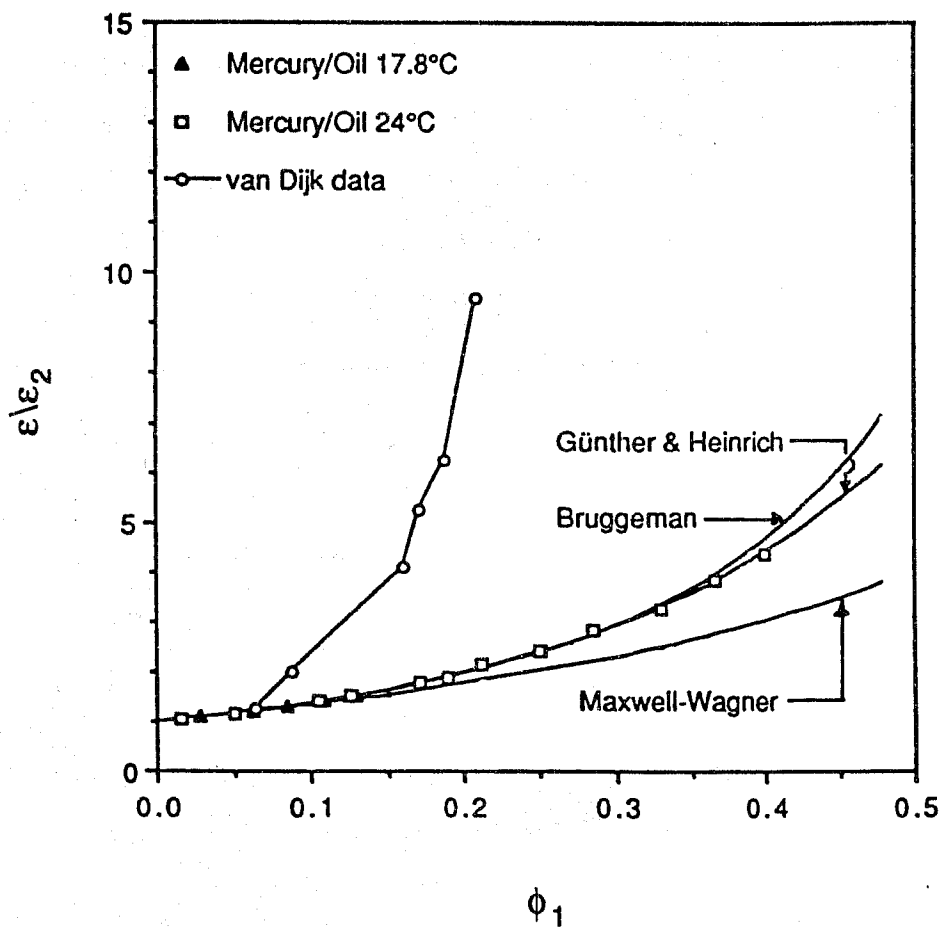
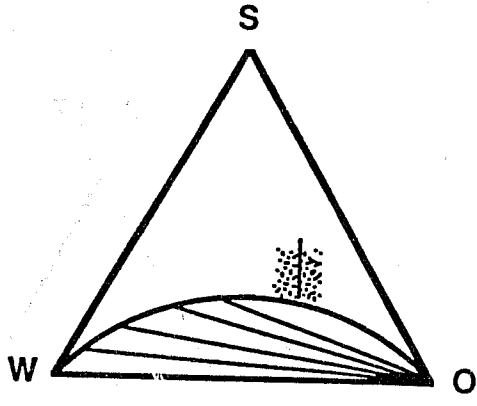
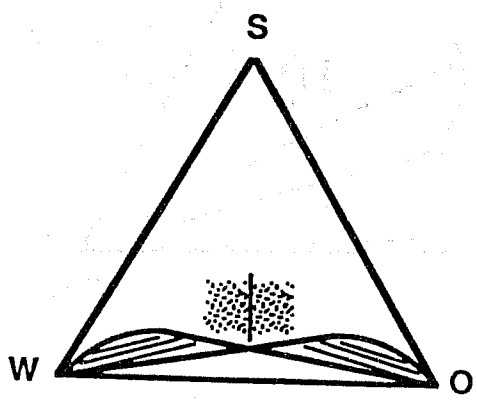


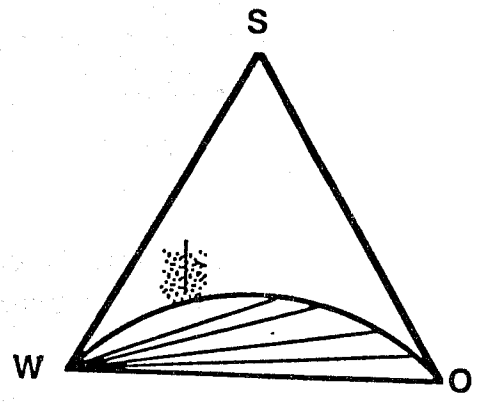
Fig. C.1. Ratio of the dielectric constant of a suspension of conducting spheres to the dielectric constant of the continuous-phase versus the disperse-phase volume fraction. van Dijk data for AOT/isooctane/water solutions at 35°C; $W_s = 25$, from Ref. C.13.



(a) Type I System



(b) Type III System



(c) Type II System

Fig. C.2. Winsor phase diagrams showing the inversion zone (shaded area) and the conductivity percolation threshold (solid line).

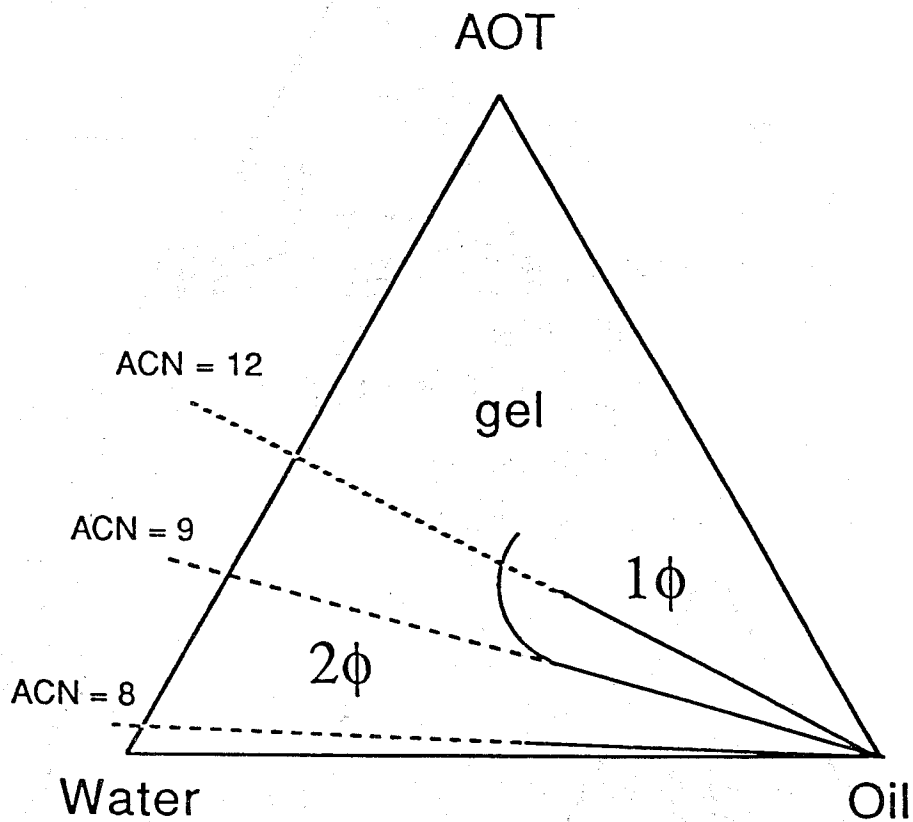


Diagram showing effect of alkane chain number on phase behavior

Fig. C.3. Phase diagram for AOT/water/alkane systems showing the effect of the alkane carbon number on the boundary between the one and two-phase regions.

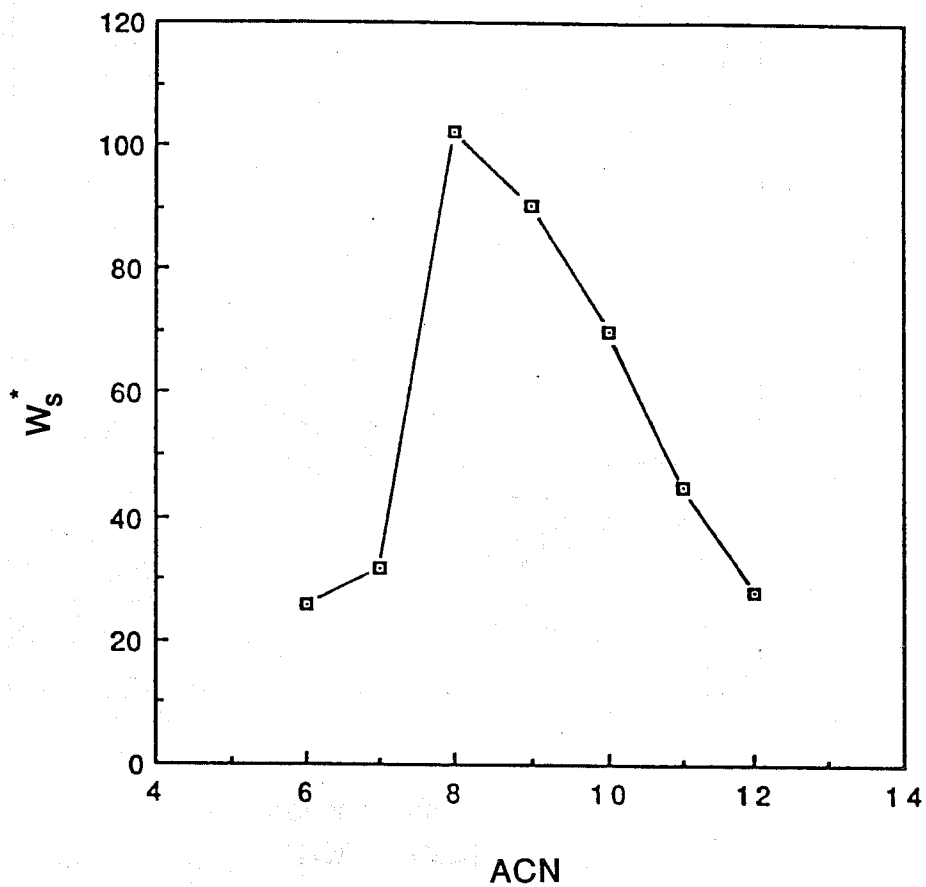


Fig. C.4. The maximum water-to-AOT molar ratio (W_s^*) in a series of alkanes; ACN = 6 to ACN = 12.

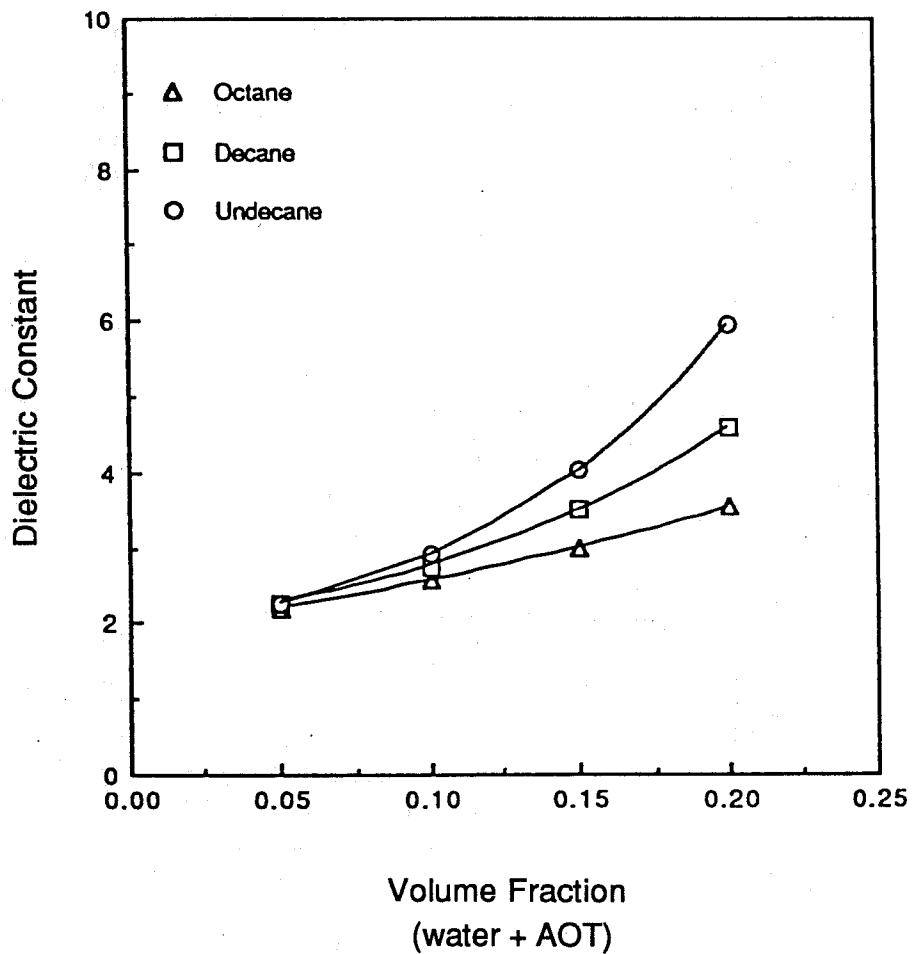


Fig. C.5. Dielectric constant versus the volume fraction of water-plus-AOT for octane, decane, and undecane solutions at 25°C; $W_s = 25$ and $f_w = 0.536 \phi_d$.

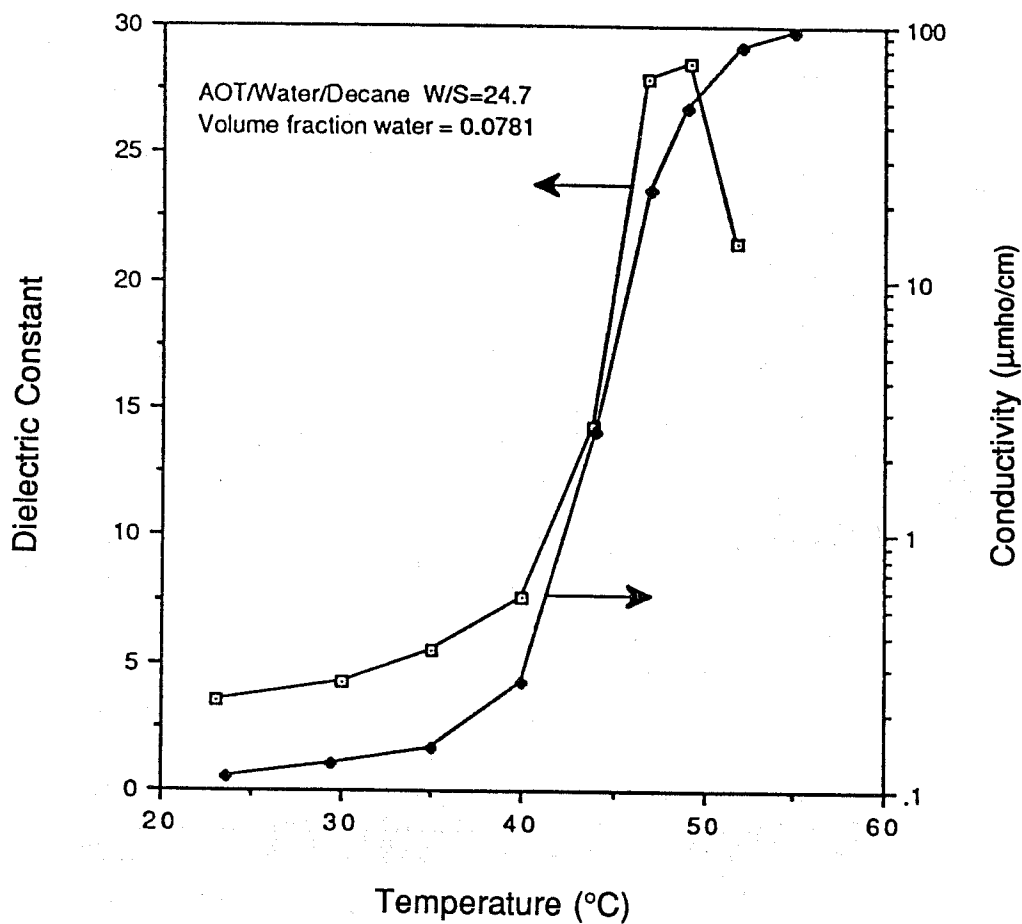


Fig. C.6a. Dielectric constant and conductivity versus temperature of AOT/water/decane solutions at 25°C; $\phi_d = 0.0781$ and $W_s = 24.7$. Note: the dielectric constants at 49 and 52°C are experimental artifacts and not the true values.

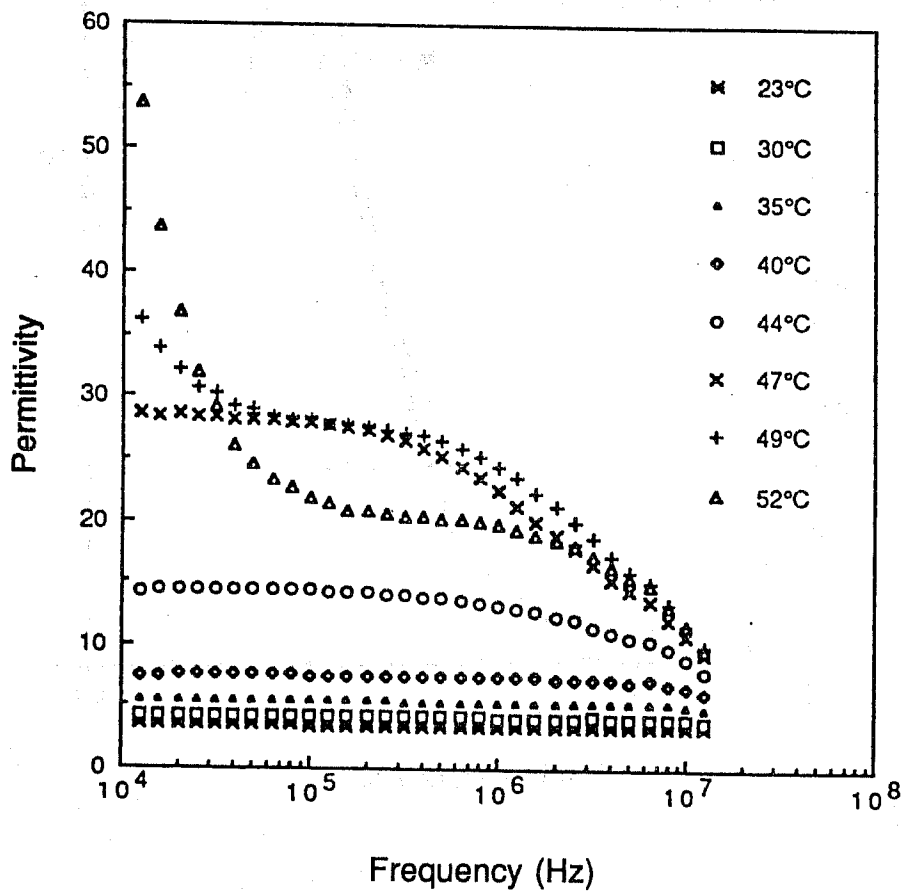


Fig. C.6b. Permittivity versus frequency of AOT/water/decane solutions at 25°C; $\phi_w = 0.0781$ and $W_s = 24.7$.

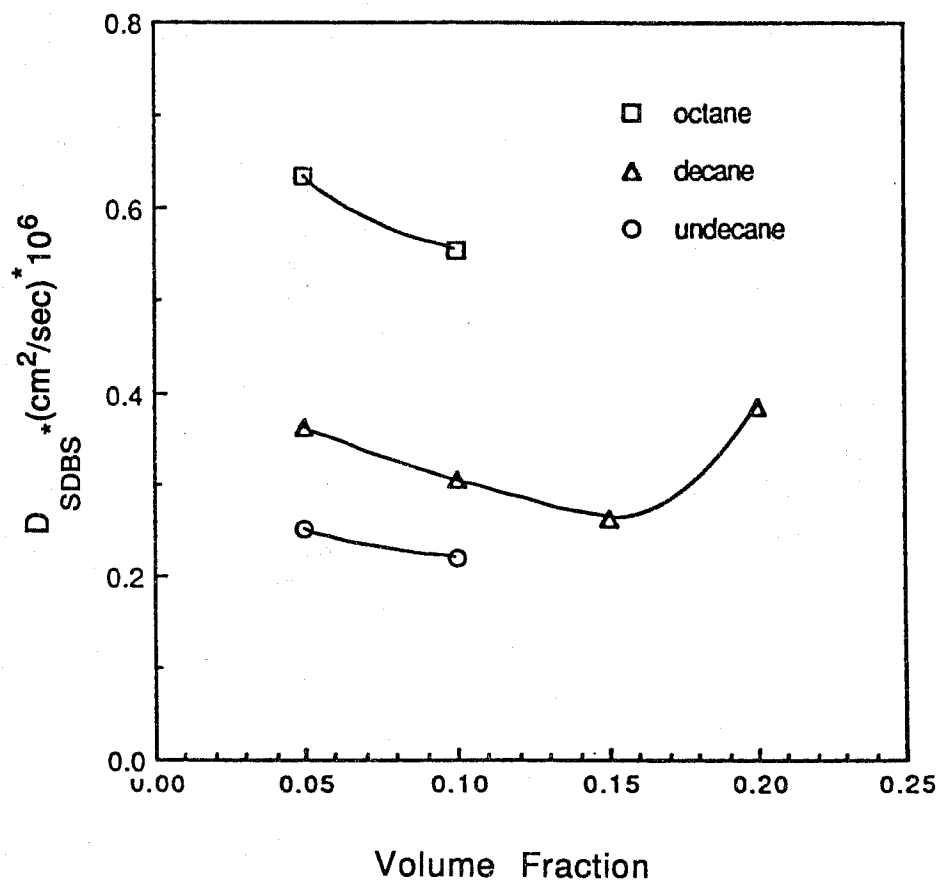
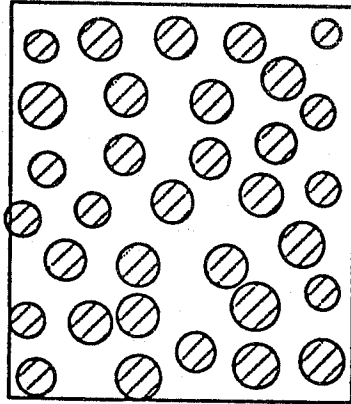
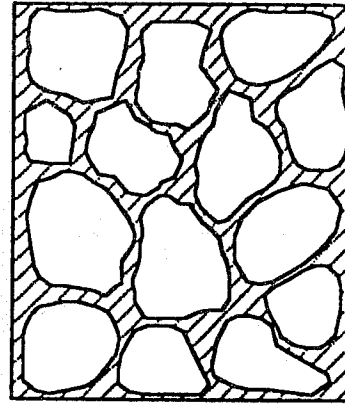


Fig. C.7. Diffusion coefficient of radioactively-tagged benzene sulfonate ion AOT/water/alkane solutions versus volume fraction of water-plus-AOT solutions at 25°C; $W_s = 25$ and $\phi_w = 0.536 \phi_d$.



Domain A



Domain B

 water domain

Fig. C.8a. Illustration of an oil-continuous domain (A) and a water-continuous domain (B) having the same compositions.

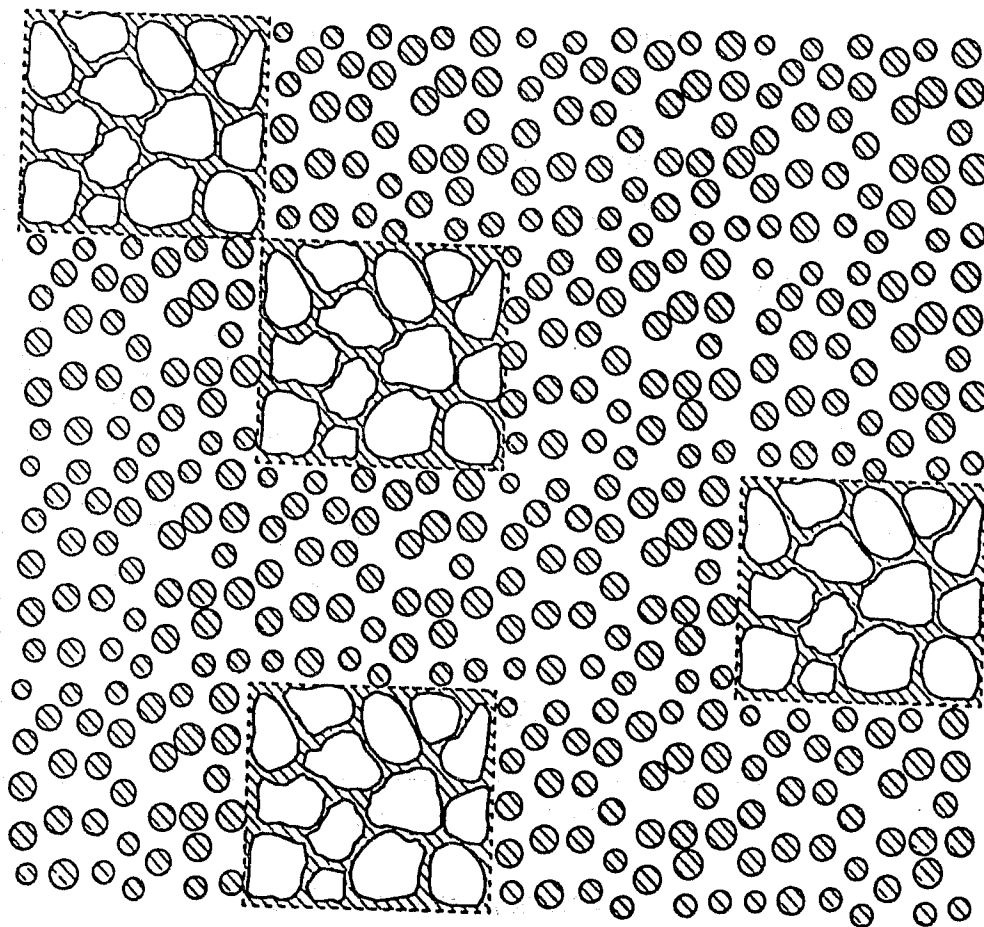


Fig. C.8b. Model of microemulsion 25% water-continuous domains in a continuum of oil-continuous domains.

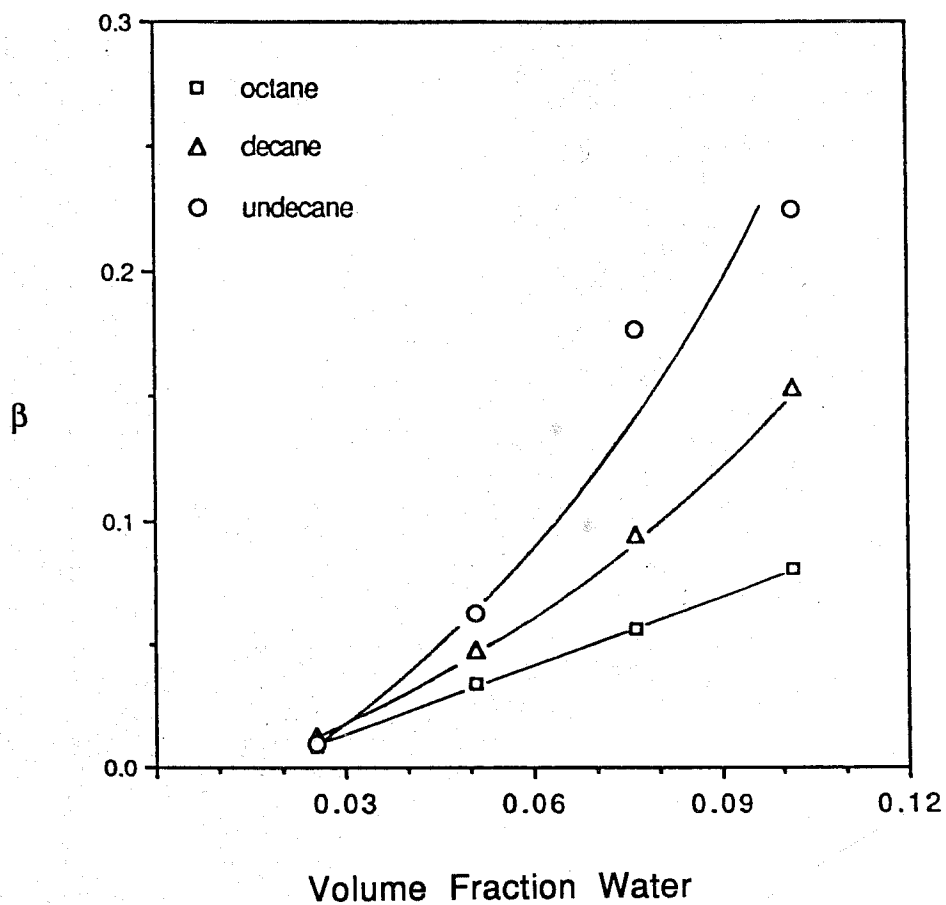


Fig. C.9. Fraction of domains that are water continuous (β) versus volume fraction of water as determined from the model for the AOT/water/alkane experiment reported in Fig. C.5.

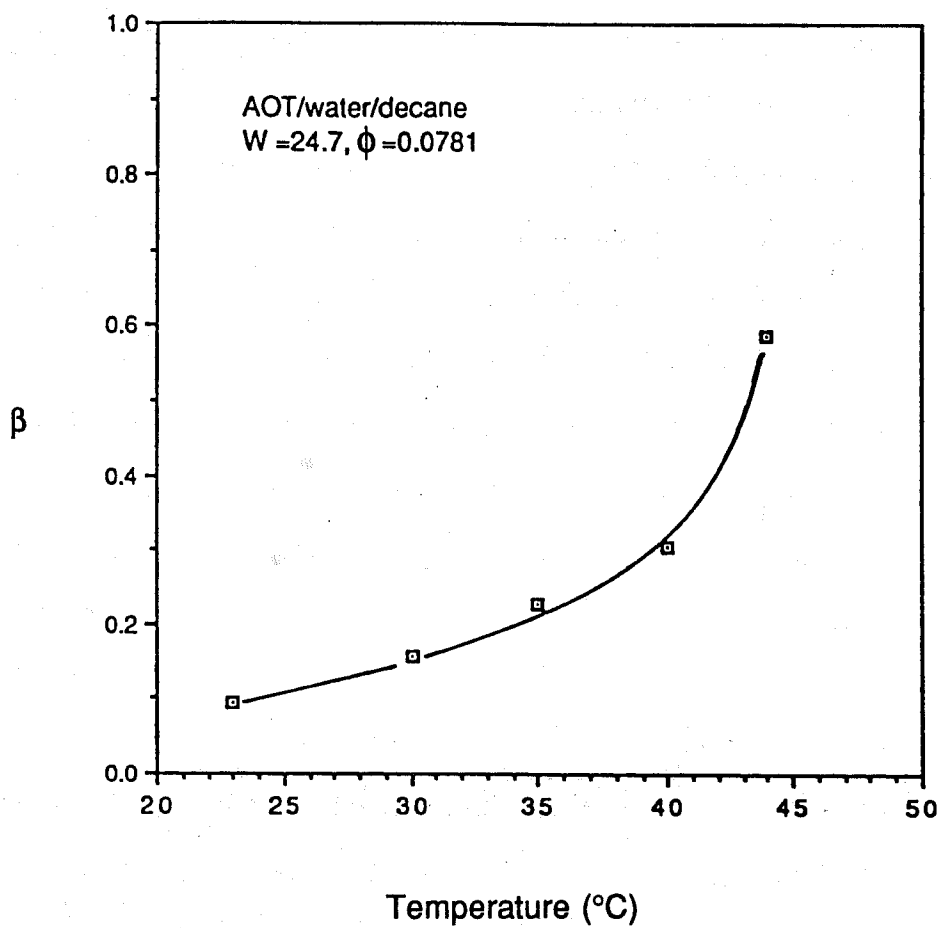


Fig. C.10. Fraction of domains that are water continuous (β) versus temperature as determined from the model for the AOT/water/decane system reported in Fig. C.6a.

D. Microemulsion Structure: The Role of Alcohols

The relationship of the micellar size and shape, as a function of alcohol concentration, is an important issue since most, if not all, microemulsions suitable for use in enhanced oil recovery include alcohol as one of the components. Those alcohols that are favored are the ones that partition in significant quantities into both oil and water. Isobutanol, butanol, amyl alcohol, and pentanol have all been used in formulating stable microemulsions. It has been long suspected that the alcohols bind to the micelles within the interfacial or palisade layer to reduce the electrostatic free energy resulting from the interaction of the charged head groups of the surfactant molecules. There has, however, been no systematic study in which the amount of alcohol actually in the palisade layer has been correlated to the physical properties of the micelles. The difficulty being, of course, that part of the alcohol added to a micellar solution will remain in a molecularly dispersed form in the water, while another part may be solubilized within the central core mixed with the lipophilic chains. Thus, of the total quantity of alcohol added to the solution, only a fraction is bound to the micelles within the palisade layer.

The binding of phenol to ionic surfactant (dodecyltrimethylammonium bromide) is studied here. This system has been selected because all components other than the phenol are transparent to ultraviolet radiation. To compare the influence of the phenol on micellar structure, parallel studies have been carried out with benzene instead of phenol.

These additives provide an instructive focus for comparison because, while their molecular structure is similar, phenol is much more soluble in water and would be expected to partition between aqueous and micellar phases, while benzene is almost completely solubilized inside the micelles. Furthermore, while benzene is almost certainly solubilized into the interior core of the micelle, the site of phenol binding is far from established. Recently, it has been suggested that

phenol may, in fact, be positioned at any one of three possible sites.^(D.1) Based on this work, it is possible to conclude that the mode of solubilization changes rather abruptly when the phenol to surfactant ratio is unity. This interesting transition has not been observed because previous studies have not considered the proportion of the added phenol that remains as the monomer in the aqueous phase.

Tracer Diffusion and Partitioning of Components

The effective tracer diffusivity denotes the movement of labeled surfactant and additive in both the monomeric and micellar forms. Assuming local equilibrium, the effective tracer diffusivity for a tagged surfactant can be represented as^(D.2)

$$D_{\text{eff}}^{\text{S}} = \alpha_{\text{s}} D_{\text{f}}^{\text{S}} + (1 - \alpha_{\text{s}}) D_{\text{m}} \quad [\text{D.1}]$$

where α_{s} is the fraction of tagged surfactant existing in the monomeric form, D_{f}^{S} is the tagged surfactant monomeric diffusivity, and D_{m} is the diffusivity of the micelles. A similar expression exists for the observed movement of radioactively labeled phenol

$$D_{\text{eff}}^{\text{P}} = \alpha_{\text{p}} D_{\text{f}}^{\text{P}} + (1 - \alpha_{\text{p}}) D_{\text{m}} \quad [\text{D.2}]$$

where α_{p} is defined as the fraction of tagged phenol residing in the monomeric form and where D_{f}^{P} and $D_{\text{eff}}^{\text{P}}$ are defined in the same manner for phenol as the above nomenclature is for a tagged surfactant. The experimental values for D_{f}^{S} and D_{f}^{P} , the monomeric diffusion coefficients of labeled surfactant and phenol in water, have been determined as $4.7 \times 10^{-6} \text{ cm}^2/\text{sec}$ and $7.5 \times 10^{-6} \text{ cm}^2/\text{sec}$, respectively. The objective of using tracer diffusion experiments is to calculate the parameter (α_{p}) that expresses the relative partitioning of the phenol additive between the

aqueous and micellar phases. Thus, tracer diffusion experiments provide a means of calculating partition coefficients for additives in micellar solutions.

In order to calculate the partitioning factor for α_p as a function of added phenol concentration in DTAB solutions, it is first necessary to calculate the dependence of the micellar diffusion coefficient (D_m) on concentration of additive. The determination of D_m requires the labeled surfactant partitioning factor (α_s) also as a function of additive concentration. A method for calculating tracer surfactant partitioning in micellar solutions in the presence of additives is given in McGreevy and Schechter^(D.3) involves the assumption of ideal mixing of the tracer species between the aqueous and micellar phases.^(D.4) However, the ideal mixing assumption used in that paper is not valid here because the labeled surfactant is anionic, while the bulk species DTAB is cationic. Because of ionic attractive effects between labeled and bulk surfactant, it is expected that essentially all of the labeled species partitions into the micelles in the solutions used for this study, which makes the partition factor (α_s) equal to zero for all additive concentrations studied.

The validity of this reasoning was confirmed by diffusion measurements in which trace amounts of ^{14}C -labeled hexadecane solubilizate were added to aqueous DTAB solutions. The observed tracer diffusion coefficients for labeled hexadecane and surfactant are nearly identical, confirming that both species are completely within the micellar phase. Thus, for each additive concentration used in this study, the observed surfactant diffusion coefficient (D_{eff}^p) and micellar diffusion coefficient (D_m) are equal. With these simplifications to the above equations, the fraction of phenol partitioning in DTAB solutions can be calculated knowing the observed tracer diffusivities of surfactant and phenol.

Determination of Aggregation Number of DTAB Micelles Based on Electrical Conductivity and Degree of Micellar Dissociation

Analysis in this section concerns the surfactant aggregation number in the micelles as a function of additive present in solution. A method will be presented for calculating changes in the aggregation number for ionic surfactant systems containing additives by means of electrical conductivity measurements when used together with diffusion data on the same system. When surfactant concentration is above the CMC, the material balance for surfactant is

$$C_S = \text{CMC} + nC_m \quad [\text{D.3}]$$

where C_S and CMC are defined as above, and n and C_m represent the surfactant aggregation number and the number concentration of micelles in solution, respectively.

The electrical conductivity of dispersed ionic surfactant systems has been shown to be^(D.5)

$$k = \frac{e^2}{k_B T} \left(\sum Z_i^2 D_i C_i + Z_m^2 D_m C_m \right) \quad [\text{D.4}]$$

where e is the fundamental unit of charge, k_B is Boltzmann's constant, Z_i is the valence of ionic species i , Z_m is the net valence of the aggregates, C_i is the concentration of species i in the continuous phase, and D_i is the molecular diffusivity of component i in the continuous phase. Our scheme for determining the surfactant aggregation number by conductivity measurements centers on the elimination of all unknown terms in Eq. [D.4] except C_m , which can be related to the aggregation number (n) through the mass balance (Eq. [D.3]).

For varying amounts of added phenol, electrical conductivity measurements that are made on solutions where the surfactant concentrations are below the CMC show that $\sum Z_i^2 D_i$ is constant and equal to $1.161 \times 10^{-5} \text{ cm}^2/\text{sec}$. This term can then

be inserted into the right-hand side of Eq. [D.4] to eliminate an unknown. The micellar diffusion coefficient (D_m) is determined from surfactant diffusion measurements and is known for all concentrations of added phenol. The only unknown term left in Eq. [D.4] is the net valence (Z_m) defined as

$$Z_m = n - q \quad [D.5]$$

where q is the number of counterions (Br^- in this case) bound to the micelle. Z_m can also be related to the aggregation number (n) by the degree of micellar dissociation (α) the value of which has been determined for aqueous solutions of DTAB by a variety of methods.^(D.6)

Other measurements of dissociation in trimethylammonium bromides^(D.7,D.8) show that the effect of additives on the value of α are small, being within $\pm 10\%$ in most cases. For this analysis, we assume α to be constant and equal to 0.24 over the range of additive phenol concentrations. Our expression for net valence of the aggregate is

$$Z_m = 0.24 n \quad [D.6]$$

Finally, the mass balance (Eq. [D.3]) can be inserted into the conductivity (Eq. [D.4]); and an expression for electrical conductivity (k) is obtained for ionic surfactant systems in terms of the aggregation number (n) with all other factors known. Calculated values of the surfactant aggregation number for various concentrations of additives are shown in the next section.

Results

A summary of experimental results and calculations can be found in Figs. D.1 to D.6. Measurements of electrical conductivity and viscosity for DTAB solutions with phenol and benzene additives are plotted in Figs. D.1 and D.2. The

abscissae used in these plots is the moles of additive contained in the micelles (equal to total moles of additive multiplied by $1 - \alpha_a$) relative to the total moles of surfactant. Phenol addition causes a slight initial decrease in electrical conductivity followed by a significant increase at higher concentrations. With benzene addition, a gradual decrease in conductivity was measured across the range of solubilize concentrations. In Fig. D.2, benzene solubilize causes a monotonic increase in solution viscosity but the effect of phenol is quite different. An initial sharp increase and a maximum in viscosity are the result of increasing phenol solubilization in the micelles.

Tracer diffusion coefficients for the system obtained from Taylor dispersion are given in Fig. D.3. The notation D_m refers to observed surfactant diffusion as a function of additive, which has been demonstrated to be the diffusion coefficient of the micelles. Tracer diffusion coefficients of labeled phenol additive in solution are given as D_{eff}^p . As benzene is solubilized inside DTAB micelles, the micellar diffusion coefficient gradually decreases across the range of benzene concentrations. For the case of phenol addition to DTAB solutions, labeled phenol diffusion coefficients monotonically increase with increasing solubilize concentration. The most interesting feature of this plot, however, is the minimum observed for D_m in the presence of phenol solubilize. This phenomenon of micellar diffusion occurs at the same phenol concentration as the dramatic changes in electrical conductivity and viscosity for the DTAB/phenol systems shown in Figs. D.1 and D.2. We will return to this point in the discussion section.

The calculated partitioning factor (α_p) for phenol in this system is plotted in Fig. D.4. It can be understood from this figure that, while the amount of phenol solubilize increases with total phenol added, the fraction existing in the micelles decreases due to the considerable solubility of phenol in bulk water. Figure D.5 shows calculated surfactant aggregation numbers with increasing additive

solubilization, which are obtained from conductivity and diffusion measurements. At zero additive concentration the aggregation number (n) is equal to 67.1, which is in excellent agreement with the value of 65 found in the literature.^(D.9) Phenol has the largest effect on both properties and a transition occurs at the same phenol concentration noted previously for the experiments in Figs. D.1 to D.3.

Finally, a set of comparative calculations for the micellar core^(D.10) with phenol addition is given in Fig. D.6. The bottom set of points gives the volume calculated when assuming that the chain length of surfactant is equal to the core radius and that the core is spherical in shape. The upper set of points gives the volume calculated, using surfactant aggregation numbers presented in Fig. D.5 and assuming a known volume per surfactant molecule of 323.3 \AA^3 . The disparity between the volumes predicted by these two methods shows the extent to which DTAB micelles are nonspherical.

Discussion

These experimental data and calculations for the DTAB system in the presence of phenol and benzene can be used to explain the changes in the micellar structure that occur at varying additive or solubilizate concentrations. Before discussing changes in the nature of the aggregates, let us first consider the site of solubilization for these additives within the micelles that can be established by UV spectrometry measurements performed in this study. Absorbance of benzene was measured in three solvents, while scanning over wavelengths ranging from 230 to 300 nm. Absorbance peaks were found for benzene dissolved in water, decane, and 0.1 M DTAB in water. Four different benzene peaks were found for the latter two solvents and their wavelengths at 242.6, 248.2, 253.8, and 259.8 nm were the same. In the former case, benzene and water were mixed and separated into two phases. The saturated water phase absorbance was measured and found to contain trace amounts of benzene. Four benzene peaks were

observed in the water solvent but their wavelengths were smaller than for the case of benzene absorbed in the decane and surfactant solutions. From these results, we conclude that, in DTAB, solutions, benzene is solubilized in the core or center portion of the micelles since this oil-like environment gives the same absorbance peaks as found in decane.

Phenol was dissolved in the same three solvents at a concentration of 0.01 vol% and its absorbance was measured over the same scan. The number of peaks and the wavelengths observed for phenol absorbance differed in each solvent and from this we infer that phenol is solubilized in a location within the DTAB micelles that is neither completely hydrophobic nor hydrophilic. Jacobs et al.^(D.11) used ^1H NMR chemical shift measurements to investigate the solubilization of phenol in SDS micelles. The conclusion of these investigators was that phenol was oriented in the micelles in such a manner that the hydroxyl group was close to the polar micellar surface. Bunton and Cowell^(D.1) also observed NMR shift spectra for phenol added to aqueous solutions of CTAB, which is very similar to DTAB used in this study. They concluded likewise that for cationic micelles, phenol is bound near the surface. When our observations of phenol absorbance are considered in this light, it appears that, in DTAB micelles, the solubilization of phenol molecules in the hydrophobic core can be ruled out.

In order to demonstrate more fully the effect of the additives on micellar structure, let us first examine the case of benzene addition, referring to Figs. D.1 to D.3. The addition of increasing amounts of benzene to the DTAB system results in a monotonic decrease in electrical conductivity and micellar diffusion coefficient and an increase in solution viscosity. As benzene is solubilized, it seems reasonable that the aggregates will become swollen and increase in size. The diffusion data in Fig. D.3 support this claim. Referring to the right-hand side of the expression for electrical conductivity in Eq. [D.4], it is evident that k is proportional

to D_m so a drop in electrical conductivity is consistent with larger swollen micelles; and this is, in fact, observed in Fig. D.1. Figure D.5 illustrates that benzene addition has little effect on the surfactant aggregation number, except at the highest concentrations. One can conclude from these data and calculations that the primary effect of benzene solubilization on the DTAB system is to increase the size of the micelles.

Now the effect of phenol addition must be considered. The low concentration region of phenol on the left-hand side of Figs. D.1 to D.3 ranges up to one mole of phenol solubilization per mole of DTAB. While the viscosity of the system increases sharply over this region, a gradual increase was observed for both electrical conductivity and the micellar diffusion coefficient. These results correspond to an increase in the uptake of phenol by the micelles and an increasing hydrodynamic radius. The increase in micellar size seems to be particularly great for phenol addition compared to benzene addition, if the D_m for each case is considered. This difference could be related to the site of solubilization within the micelles and suggests that solubilization of the additive in the palisade layer results in a greater aggregate size increase than solubilization in the core.

With further phenol addition to DTAB solutions, a dramatic change in properties was observed beginning at a solubilization concentration of approximately one mole of phenol per mole of DTAB. The electrical conductivity and diffusion measurements go through a minimum and then increase as more phenol is solubilized. Over the same concentration range a maximum is observed for viscosity that drops slightly at higher concentrations of phenol. Using the same reasoning as given above for the dilute phenol region, these experimental measurements are all consistent with each other in the concentrated region and lead to the conclusion, that in the concentrated phenol region (near one mole of

phenol solubilized per mole of surfactant), the hydrodynamic radius of the aggregates reaches a maximum; and then with further addition of phenol, the decrease begins.

The reason for this unusual change in the size of micelles in this system is far from obvious. Calculations of the phenol partitioning factor (α_p) and the surfactant aggregation number (n) shown in Figs. D.4 and D.5 can be used to help explain these phenomena. Concerning Fig. D.4 it was observed in the previous section that, as more phenol is added to the system, the fraction of phenol partitioned into the micelles ($1 - \alpha_p$) steadily declines, suggesting that increasing amounts of phenol are present in the aqueous phase. In Fig. D.5, the trend in the calculated aggregation number levels off abruptly at a saturation point where there is one mole of phenol solubilized per mole of surfactant. This is, in fact, the transition concentration noted previously, and it appears that the palisade layer inside the micellar surface is saturated with additive. Further phenol solubilization by DTAB micelles must occur at a different location. Bunton and Cowell^(D.1) suggested three possible modes or sites of solubilization of phenols near the surface of a cationic micelle. The first two possibilities involve solubilization inside the micelle, wedged between surfactant molecules. This appears to be the mechanism in our system at low concentrations of added phenol. The other mode of phenol solubilization occurs by binding to the exterior of the micelle and we hypothesize this mechanism of binding to occur at high phenol concentrations above the transition point.

Refer now to Fig. D.6, which gives the volume of the micellar core calculated from aggregation numbers (upper set) compared with the case of spherical aggregates (lower set). The interpretation of this figure is, that if DTAB micelles are completely spherical, the volume calculated from aggregation numbers would equal that calculated from surfactant tail lengths and all points would fall on the

bottom line. However, as phenol solubilization in this system increases, the micelles become more and more nonspherical up to the transition point. The exact shape cannot be determined by our measurements. The change of the core away from spherical shape levels off as phenol is added beyond the transition point and its shape appears not to be affected further.

This evidence presented for phenol solubilization in DTAB solutions allows a greater understanding of the changing structure of the micelles than was previously possible. As phenol is solubilized in low concentrations up to the transition point, phenol binding occurs in the palisade layer, the micelles become more rod-like and less spherical in shape, and the surfactant aggregation number increases. Further solubilization beyond the transition point results in phenol binding to the micelle exterior while the shape of the core and the aggregation number remain unchanged under these conditions. Increasing phenol addition also affects the aqueous phase by decreasing its dielectric constant, causing it to be more hydrophobic. Under these circumstances, we would expect the hydration layer surrounding the micelles to shrink in thickness. Such an effect would give rise to smaller hydrodynamic radii and increased micellar diffusion and electrical conductivity. This is, in fact, observed for the high concentration region of phenol in Figs. D.1 to D.3.

Conclusions

Based on the experiments and calculations performed in this study, we make the following conclusions concerning the addition of phenol and benzene to aqueous solutions of DTAB:

- (1) Partition coefficients for additives to surfactant solutions can be calculated by means of tracer diffusion experiments where the additive and amphiphilic components are radioactively labeled. Partition results for phenol in the

DTAB system reveal that the fraction of phenol residing in the micelles declines as its concentration in solution increases.

- (2) Ionic surfactant aggregation numbers can be calculated by means of electrical conductivity and micellar diffusion measurements for a given surfactant system. Aggregation numbers calculated by this method were found to be in excellent agreement with those in the literature.
- (3) Both of the additives used in this study, phenol and benzene, are solubilized by the micelles in DTAB solutions and cause them to swell in size with increasing additive concentration. This effect seems to be more pronounced for the case of phenol and probably is due to the fact that phenol solubilizes in the palisade layer and not in the micellar core.
- (4) Phenol addition has a much greater effect on the surfactant aggregation number than does benzene. The site of phenol solubilization by the micelles changes at a transition concentration of one phenol molecule per surfactant molecule, which has a dramatic effect on the physical properties of this surfactant system.
- (5) Phenol solubilization below the transition point occurs in the palisade layer between surfactant molecules; further addition above the transition point results in phenol binding to the exterior of the micelle.
- (6) Phenol addition up to the transition point causes DTAB micelles to be more rod-like and less spherical and causes surfactant aggregation to increase; solubilization beyond the transition point does not have any further effect on the shape or aggregation number.
- (7) Increasing phenol solubilization in the bulk water makes the aqueous phase more hydrophobic and causes the hydration layer surrounding the micelles to shrink at high phenol concentration. This effect leads to smaller hydrodynamic radii of aggregates at high phenol concentrations.

References

- (D.1) Bunton, C. A., and Cowell, C. P., J. Colloid Interface Sci. **122**, 154 (1988).
- (D.2) Kamenka, N., Lindman, B., and Brun, B., Colloid and Polym. Sci. **252**, 144 (1974).
- (D.3) McGreevy, R. J., and Schechter, R. S., J. Colloid Interface Sci. (in press).
- (D.4) Scamehorn, J. F., Schechter, R. S., and Wade, W. H., J. Colloid Interface Sci. **85**, 463 (1982).
- (D.5) Lam, A. C., Ph.D. dissertation, The University of Texas, Austin (1986).
- (D.6) Attowood, D., and Florence, A. T., Surfactant Systems. Their Chemistry. Pharmacy and Biology, Chapman and Hall (1985)
- (D.7) Pearson, J. T., and Humphreys, K. J., J. Pharm. Pharmacol. **22**, 126 (1970).
- (D.8) Briggs, J., Dorshow, R. B., Bunton, C. A., and Nicol, D. E., J. Chem. Phys. **76**, 775 (1982).
- (D.9) Milliaris, A., Le Moigne, J., Strum, J., and Zana, R., J. Phys. Chem. **89**, 2709 (1985).
- (D.10) Tanford, C., The Hydrophobic Effect: Formation of Micelles and Biological Membranes, John Wiley & Sons, New York, 51 (1980).
- (D.11) Jacobs, J. J., Anderson, R. A., and Watson, T. R., J. Pharm. Pharmacol. **23**, 148 (1971).

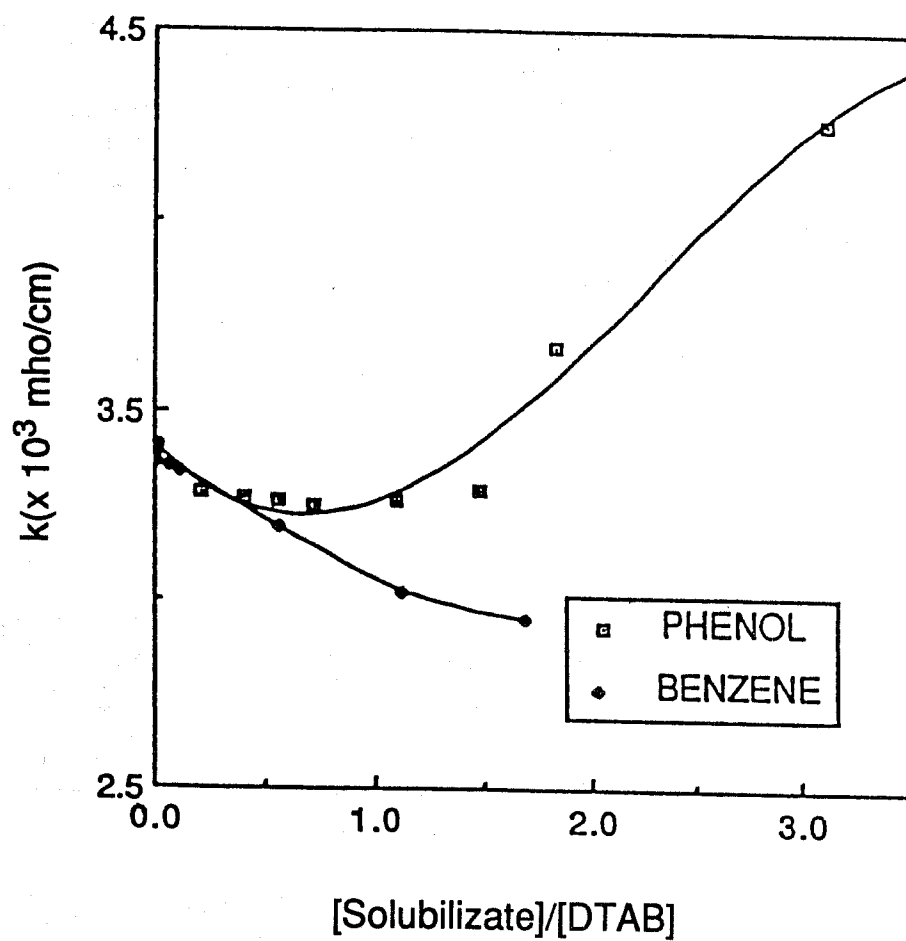


Fig. D.1. Effect of solubilizates on electrical conductivity.

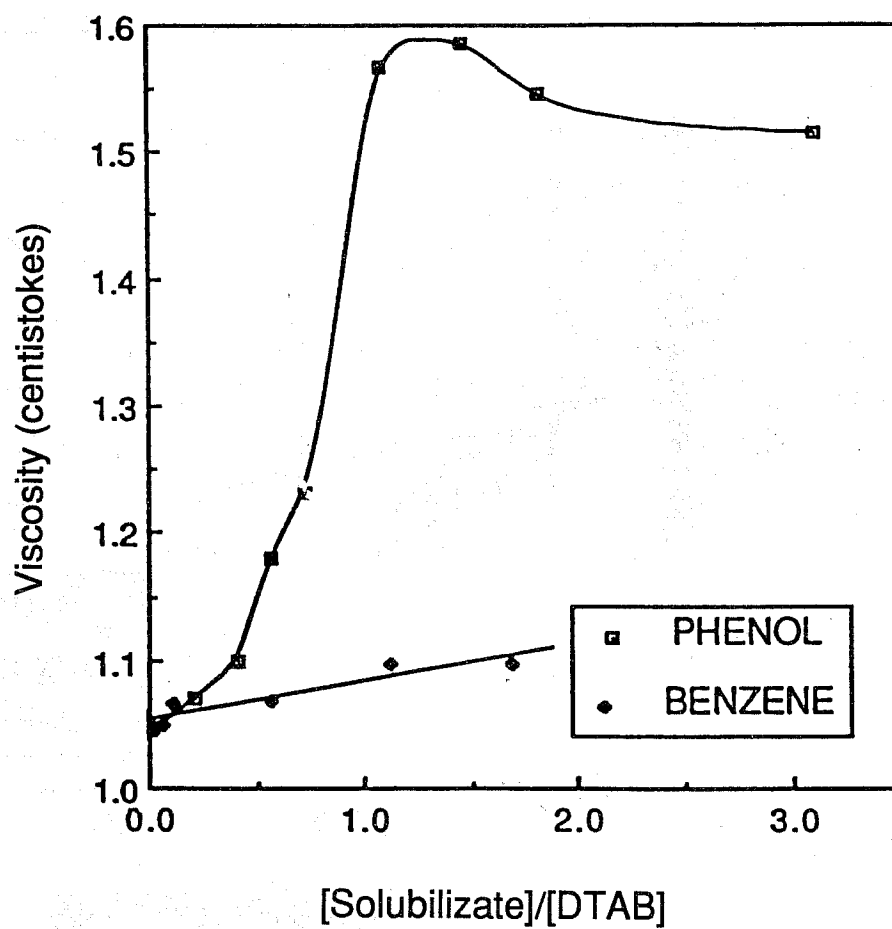


Fig. D.2. Effect of solubilizates on viscosity.

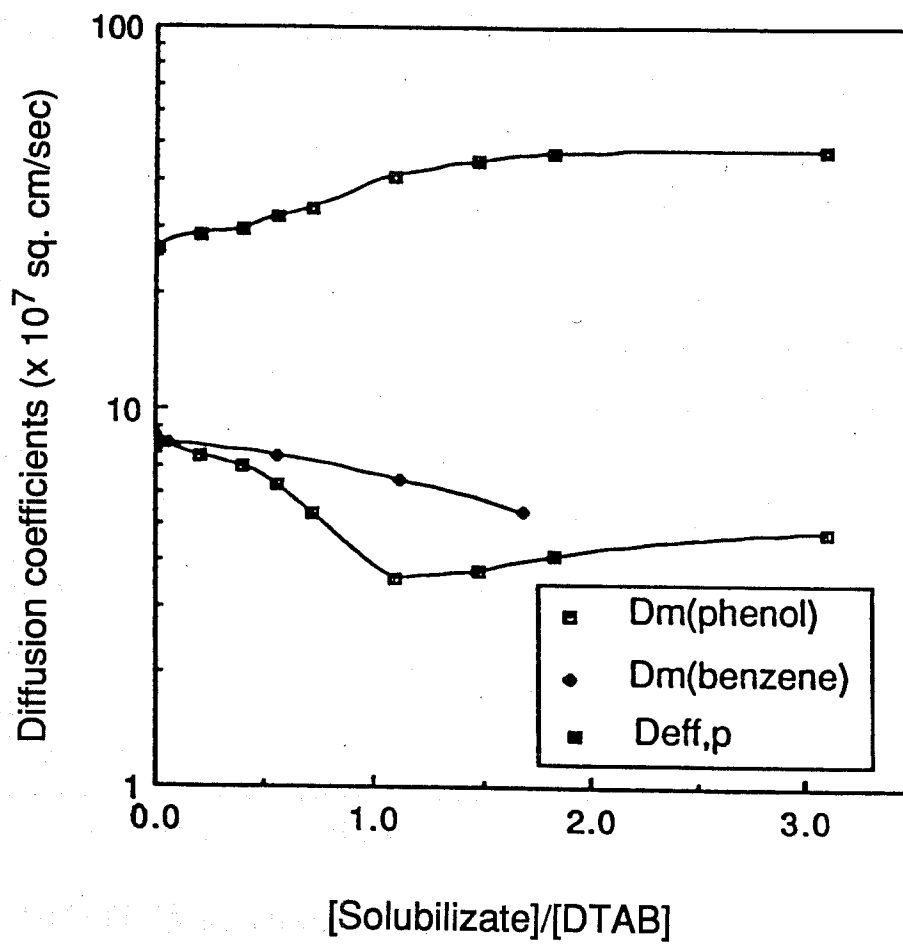


Fig. D.3. Effect of solubilizates on tracer diffusion coefficients.

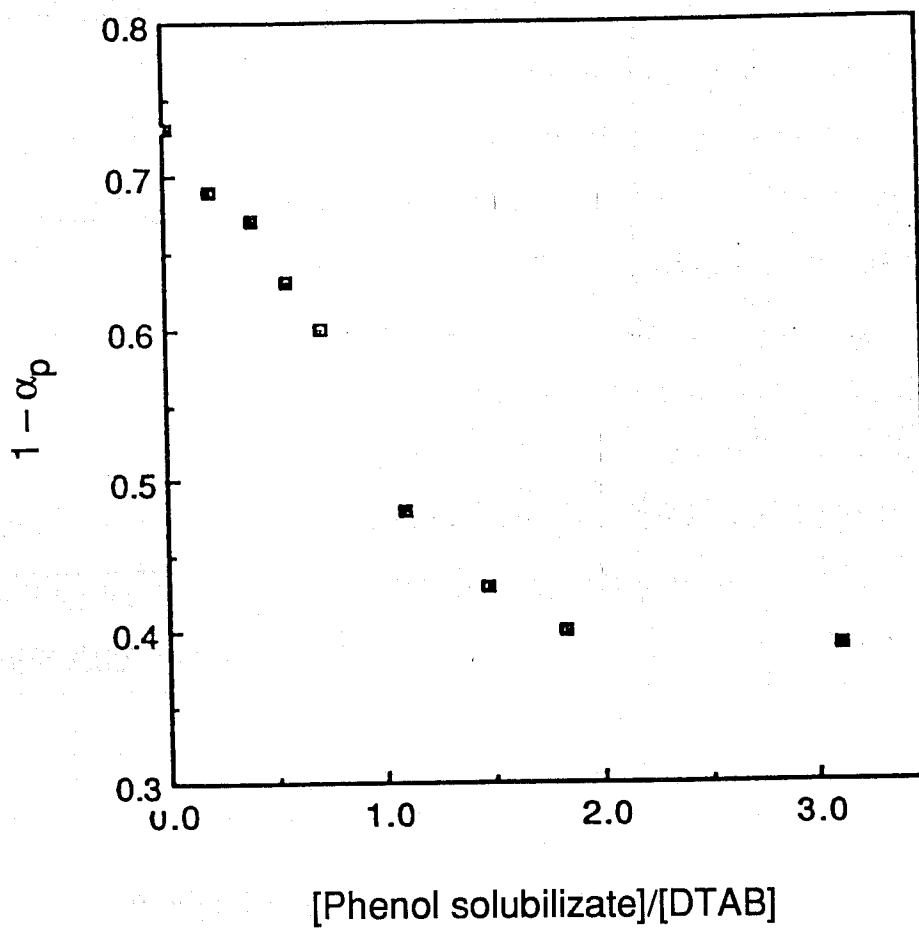


Fig. D.4. Change in micellar partitioning of phenol.

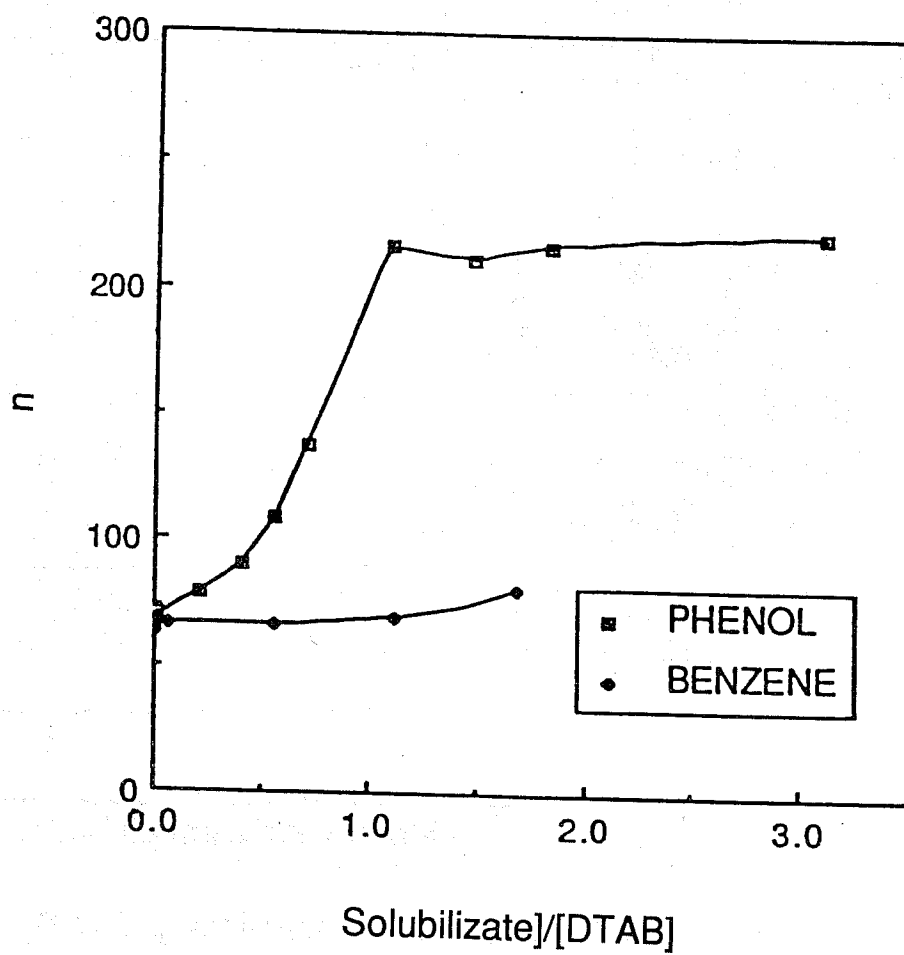


Fig. D.5. Effect of solubilizates on the surfactant aggregation number.

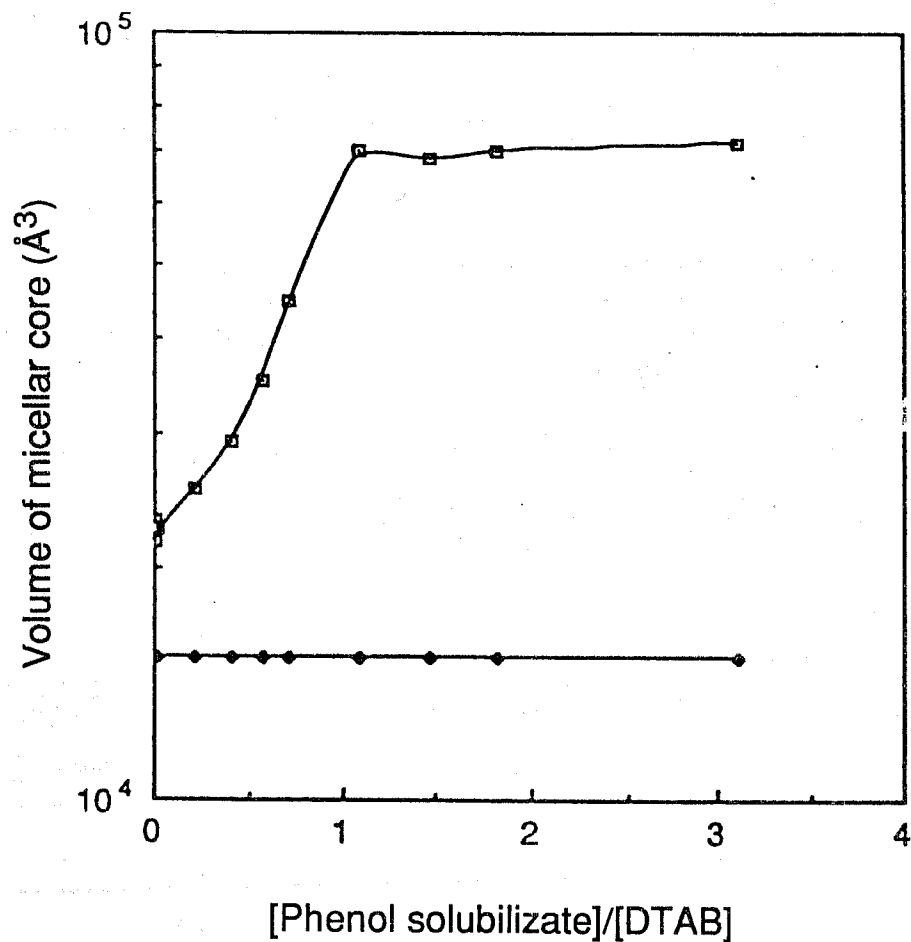


Fig. D.6. Calculated volumes of micellar core using two different methods.
 □ Calculated from the aggregation number and known volume per surfactant.
 ◆ Calculated from the known surfactant tail length, assuming spherical shape.

